Dissertation zur Erlangung des Doktorgrades

der Fakultät für Chemie und Pharmazie

der Ludwig-Maximilians-Universität München

Structural biochemistry of actin-related protein 8 within its INO80 chromatin remodeler environment

Christian-Benedikt Franz Gerhold

aus

Neustadt an der Weinstraße in Rheinland-Pfalz, Deutschland

2012

Erklärung

Diese Dissertation wurde im Sinne von §7 der Promotionsordnung vom 28. November 2011 von Herrn Prof. Dr. Karl-Peter Hopfner betreut.

Eidesstattliche Versicherung

Diese Dissertation wurde eigenständig und ohne unerlaubte Hilfe erarbeitet.

München, am 31.10.2012

……

Christian-Benedikt Franz Gerhold

Dissertation eingereicht am 02.11.2012

1. Gutachter: Herr Prof. Dr. Karl-Peter Hopfner

2. Gutachter: Herr Prof. Dr. Roland Beckmann

Mündliche Prüfung am 07.12.2012

This thesis has been prepared from February 2008 to October 2012 in the laboratory of Prof. Dr. Karl-Peter Hopfner at the Gene Center of the Ludwig-Maximilians-University of Munich (LMU).

Parts of this thesis have been published in scientific journals:

Structure of Actin-related protein 8 and its contribution to nucleosome binding.
Gerhold CB, Winkler DD, Lakomek K, Seifert FU, Fenn S, Kessler B, Witte G, Luger K, Hopfner KP.
Nucleic Acids Res. 2012 Sep 12.

Structural biochemistry of nuclear actin-related proteins 4 and 8 reveals their interaction with actin.
Fenn S, Breitsprecher D, **Gerhold CB**, Witte G, Faix J, Hopfner KP.
EMBO J. 2011 Jun 1;30(11):2153-66.

Reviews published in the course of this thesis:

Swi2/Snf2 remodelers: hybrid views on hybrid molecular machines.
Hopfner KP, **Gerhold CB**, Lakomek K, Wollmann P.
Curr Opin Struct Biol. 2012 Apr;22(2):225-33. Review.

Nuclear actin-related proteins take shape.
Fenn S, **Gerhold CB**, Hopfner KP.
Bioarchitecture. 2011 Jul;1(4):192-195.

Parts of this thesis have been presented at international conferences:

Poster presentation at the 43rd Annual Meeting of the German Genetics Society "Chromatin and Epigenetics", Essen, Germany, 5th-7th of September 2012

Talk at the Cold Spring Harbor Meeting "Epigenetics and Chromatin", Cold Spring Harbor, USA, 11th – 15th of September 2012

1. Introduction

1.1 Genome Compaction

Chromatin is a highly condensed form of DNA in the eukaryotic nucleus held in place by various proteins, such as histones and structural maintenance of chromosomes (SMC) proteins and enables packaging of a large amount of nucleic acids into single cell nuclei. Moreover, the structure of chromatin is inherently stable, which is a prerequisite to maintain genomic integrity.

However, since accessibility of the genomic material is a necessity for the elementary processes of life, such as replication or transcription, the cell must arrange for a dynamic and regulated access to its DNA. The temporary and spatial control of gene activity is largely accommodated by epigenetic mechanisms that influence the development of an organism and are independent from its DNA sequence [1].

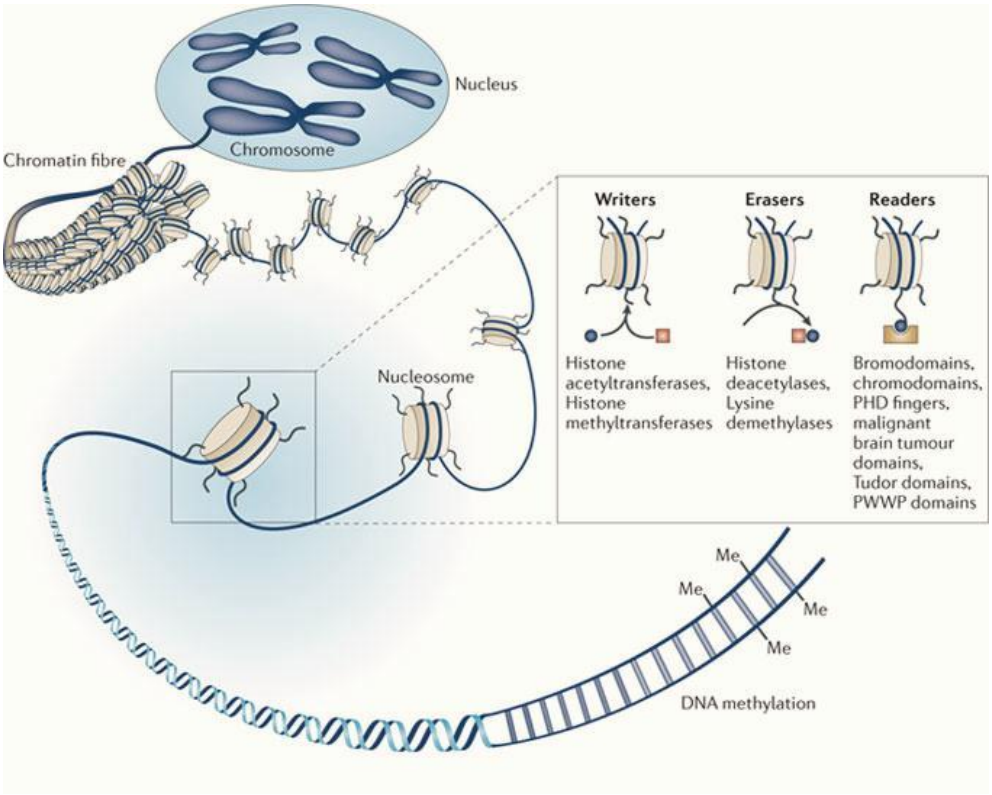

Figure 1: Organization of DNA in the eucaryotic nucleus
DNA is wrapped around histone octamers to form nucleosomes, which are packaged into higher order structures to eventually form the chromosomes.
Epigenetic writers, readers and erasers modify nucleosomes and hence the accessibility of chromatin.
Figure adapted from Arrowsmith *et al.*, 2012 [2].

1.2 Epigenetic readouts

So far, four main regulatory mechanisms have been discovered to inter-dependently modulate the state of chromatin, namely DNA methylation, post-translational modification or exchange of histones and histone variants, ATP-dependent chromatin remodeling and large intervening non-coding RNAs (ncRNAs) [3]. Please find a short discussion of these concepts in the attachment of this thesis (see chapter 7). These mechanisms are responsible for the degree of chromatin compaction, which can differ from six nucleosomes per 11 nm in euchromatin opposed to 12-15 nucleosomes per 11 nm in heterochromatin, largely accounting for the accessibility of the genetic material [4]. Epigenetic alterations can be dynamically modified as distinct enzymatic machineries not only implant or specifically interact with these marks, but are also capable of removing them. Hence according to their mode of action, these protein complexes are referred to as epigenetic writers, readers or erasers [5], which play pivotal roles in the regulation of gene expression. Chromatin remodelers are part of this epigenetic machinery and could be classified to be readers and writers as they appear to recognize distinct chromatin states and are able to eventually alter these to orchestrate DNA accessibility.

1.3 Chromatin remodelers

Remodelers are sophisticated and diverse molecular machines that disrupt or remodel protein : nucleic acid interactions at nucleosomes but also transcription factors or polymerases using ATP hydrolysis as energy source. Hence, the engine of these remodelers is a swi2/snf2 ATPase, which generally is the catalytic domain of a scaffold protein that harbors several domains to couple the ATPase with auxiliary domains or additional subunits (Figure 2). This ensures a highly precise and tightly regulated mechanism for each remodeler and its specific substrates [6].

According to recent structural models, the remodeler moves along the minor groove of DNA. When the remodeler binds to its nucleosomal substrate and the ATPase domain is anchored at a fixed position, the torque required for the remodeling process may be generated [7, 8]. The ATPase dependent DNA translocation creates a DNA loop, which loosens the interaction between DNA and the histone octamer. This in turn gives leeway for a plethora of different subsequent events, depending on additional domains of the remodeler or accompanying subunits. Possible outcomes of the remodeling reaction are a positional shift or complete eviction of the nucleosome or the exchange of histone variants. [9, 10]

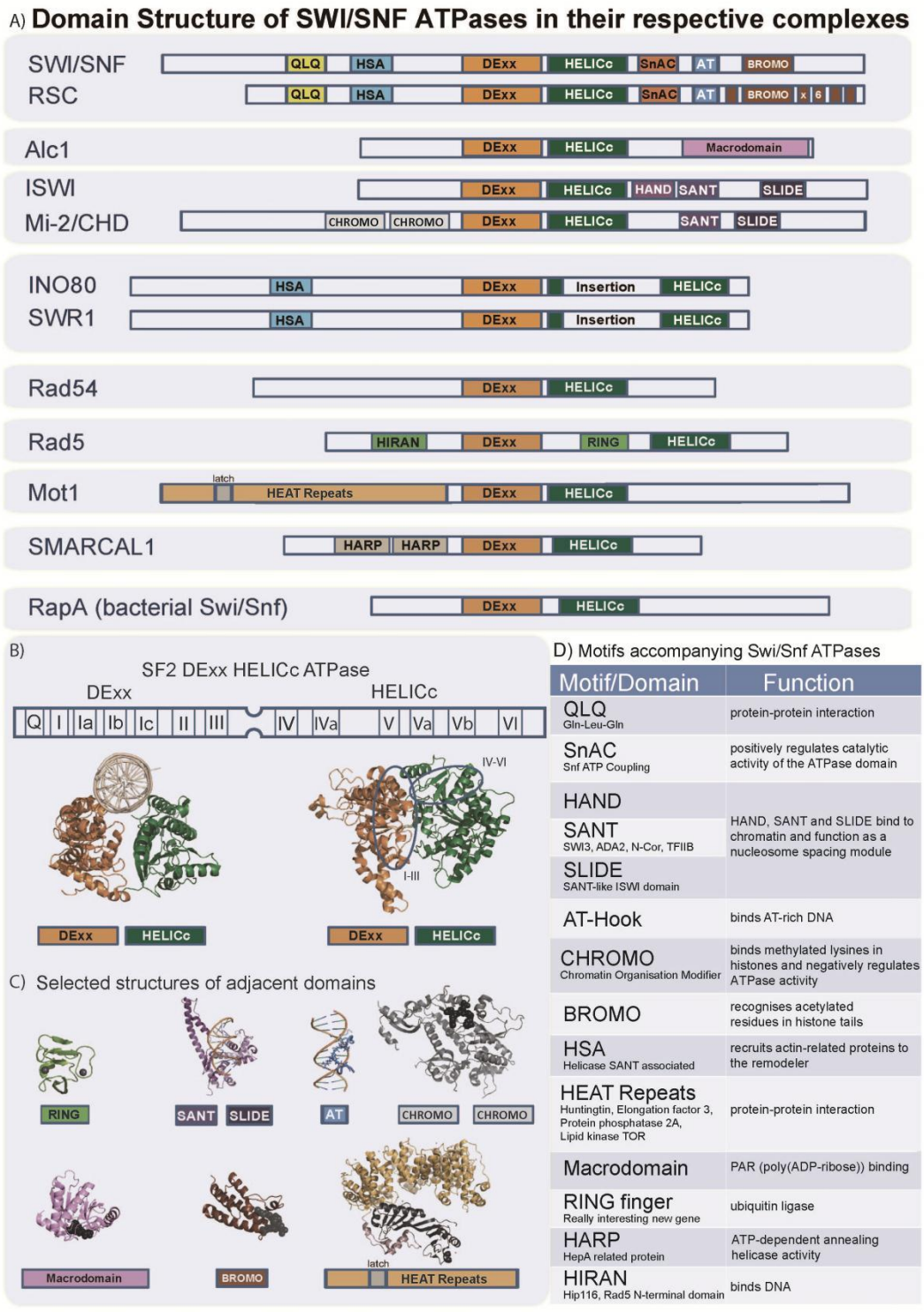

Figure 2: Overview of the modular composition of chromatin remodelers

A) Domain architecture of several chromatin remodeling enzymes. The CHD and ISWI families are suggested to be one structural family. B) The core Swi/Snf ATPase consists of a DEXX and a HELICc domain. C) Several adjacent domains of the SF2 (superfamily 2) ATPase have been structurally elucidated. D) Summary of adjacent domains with annotated function.

Figure adapted from Hopfner *et al.* 2012 [6].

Classification based on the similarity in sequence over the helicase-like region results in six different families [11], but generally remodelers are classified into four main families: SWI/SNF, INO80, ISWI and CHD [9]. One could argue, that the latter two comprise just one structural family due to the similarity of their SANT-SLIDE nucleosomal spacing module [6] and their helicase domain [11].

Remodelers of the SWI/SNF family are composed of 8 to 14 subunits, including a pair of actin related proteins (Arps), which bind to the adjacent HSA (helicase-SANT) domain of the ATPase [12]. Their unique characteristic feature is a C-terminal bromodomain (Figure 2A)[13]. The most prominent family members SWI/SNF (Switch/sucrose-non-fermenting) and RSC (Remodeling the state of chromatin) disrupt nucleosomes either through repositioning or dissociation. Thereby these complexes execute a broad spectrum of sophisticated catalytic reactions in modifying the state of chromatin, which play important roles in several cellular processes like replication or transcription [14, 15].

Chd1 (chromodomain-helicase-DNA-binding protein 1) and ISWI (imitation switch) catalyze nucleosome spacing. While ISWI family remodelers contain 2 to 4 subunits, CHD remodelers are composed of 1 to 10 subunits. Characteristic domains include a SANT domain (y<u>S</u>WI3, y<u>A</u>DA2, h<u>N</u>CoR, h<u>T</u>FIIIB) adjacent to a SLIDE domain (SANT-like ISWI) at the C terminus of the ATPase and are important for nucleosomal spacing [16, 17]. More recently, the structural equivalent of SANT-SLIDE has been recognized in Chd1, which has previously escaped notice due to little sequence homology [18].

Chd1 additionally harbors a double chromodomain unit that blocks the DNA binding site of the ATPase and functions like an internal repressor, which adds another level of regulation complexity [19, 20]. This regulatory domain could be involved in augmented functional versatility, as the CHD family seems to have roles in activating as well as repressing transcription [21-23]. INO80 and SWR1 on the other hand are involved in exchanging histone variants amongst other tasks and will be discussed in more detail below.

The variability of processes catalyzed by these molecular machines that all share the same motor are most likely explained by a unique domain structure accompanying the conserved swi2/snf2 ATPase across and even within families, which serves as chromatin binding and complex assembling scaffold protein (Figure 2A). Hence, specific substrate recognition of the swi2/snf2 ATPase can be facilitated either by a combination of accessory domains that bind to specifically modified nucleosomes or by the unique compilation of the resulting complex in which specific subunits also bind to histones (Figure 2D).

Considerable progress has been made over the past few years in structurally elucidating the interplay between the swi2/snf2 ATPase with adjunct domains or subunits and their interactions with the epigenetic code of nucleosomes. For instance, in the human ISWI homologue NURF (nucleosome

remodeling factor), subunit BPTF (bromodomain PHD finger transcription factor) contains a PHD finger with an adjacent bromodomain. This combination specifically recognizes nucleosomes that are trimethylated at H3K4 and also bear an acetyllysine in their H4 histone tail [24] and it can be easily envisaged that the complex structures of multisubunit remodelers generally provide various combinations of nucleosome binding platforms. Hence, accessory domains of remodeling enzymes recruit additional subunits, recognize the chromatin substrate partially with help of these subunits and also regulate the activity of the swi2/snf2 ATPase. For example, a newly identified SnAC domain influences the catalytic activity of ATP hydrolysis in swi2/snf2 ATPases [25].

Overall, chromatin remodeling complexes are capable of reading epigenetic marks and remodel the state of chromatin according to the epigenetic code in a highly regulated manner.

1.3.1 The INO80 family of remodelers

Recently, it has become clear that the INO80 family of chromatin remodelers (SWR1 and INO80) is responsible for the incorporation and eviction of histone variant H2A.Z. While SWR1 deposits H2A.Z into chromatin, preferentially into euchromatin at regions flanking silent heterochromatin [26-28], INO80 antagonistically removes H2A.Z in case it remains unacetylated [29].

Both remodeling complexes contain more than 10 subunits and have been originally purified and characterized from *Saccharomyces cerevisiae* [26, 30] but have counterparts in higher eukaryotes that all have a conserved basic framework of a core remodeler and species specific subunits (table 1) [31-33].

Table 1: conserved and species specific INO80 subunits.
Table adapted from Conaway and Conaway 2012 [31].

Yeast[a]	Human[a]	*D. melanogaster*[a]	Domain structure
Ino80p	INO80[c]	dIno80	Snf2-like ATPase
Actin	β-actin[b] (ACTB[c])	Actin 5C	
Arp4p	Baf53a (Arp4, ACTL6A[c])	ND[d]	Actin-related protein
Arp5p	Arp5 (ACTR5[c])	Arp5	Actin-related protein
Arp8p	Arp8 (ACTR8[c])	Arp8	Actin-related protein
Rvb1p	RuvB-like 1 (Tip49a, RUVBL1[c])	Pontin	AAA+[e] ATPase
Rvb2p	RuvB-like 2 (Tip49[c], RUVBL2b)	Reptin	AAA+[e] ATPase
Ies2p	Ies2 (INO80B[c], PAPA-1)	ND[d]	Zinc finger-HIT[e] domain
Ies6p	Ies6 (INO80C[c], c18orf37)	ND[d]	
Nhp10p	–	–	HMG[e] type-II domain
Taf14p	–	–	
Ies1p	–	–	
Ies3p	–	–	
Ies4p	–	–	
Ies5p	–	–	
–	YY1[c]	Pho	Gli[e]-Kruppel zinc finger transcription factor
–	Uch37 (UCHL5[c])	Uch37 (Uch-L3)	UCH[e] family deubiquitylating enzyme
–	NFRKB[c] (INO80G)	Nfrkb (CG11970)	
–	MCRS1[c] (MCRS2, MSP58, INO80Q)	ND[d]	FHA[e] domain
–	TFPT[c] (Amida, INO80F)	ND[d]	
–	INO80D[c] (FLJ20309)	ND[d]	
–	INO80E[c] (CCDC95, FLJ90652)	ND[d]	Coiled-coil domain

Unlike other swi2/snf2 ATPases, Ino80p and Swr1p have a large insertion to their HELICc domain, which is the characteristic feature of the INO80 family of remodelers [34].

SWR1-C and INO80 share a conserved set of subunits, namely the AAA+ (ATPases associated with a variety of cellular activities) ATPases RvB1/RvB2, and the actin-related protein Arp4 as well as actin. Interestingly, the ATPase insertion recruits RvB1/2 to the remodelers [35], which in turn recruit Arp5 to INO80 and putatively Arp6 to SWR1 [35, 36].

A few more interactions between proteins within INO80 or SWR1 are known [37, 38] but the overall architecture and topology still need to be elucidated. It has become clear, however, that both remodelers consist of functional modules as the loss of one subunit often results in the loss of other accompanying subunits as well [36, 39].

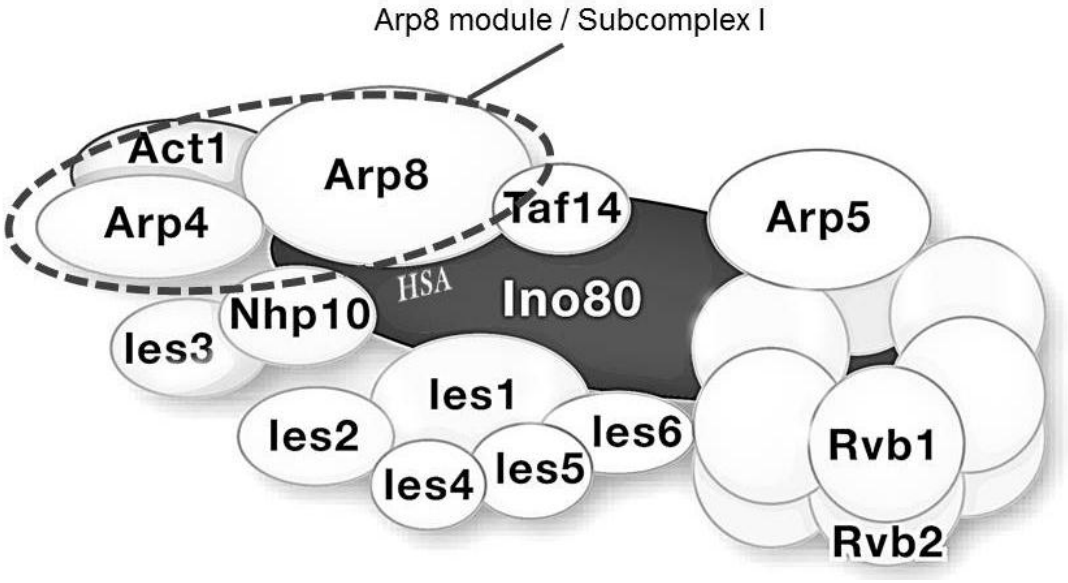

Figure 3: The INO80 complex of *Saccharomyces cerevisiae*
The yeast INO80 complex consists of 15 subunits and the knowledge on the overall architecture is limited. The subcomplex I consisting of Arp8, Arp4 and actin bound to the HSA domain was identified in 2008 [12]. Image adapted from [40].

1.3.2 INO80 functions largely depend on Actin-related proteins

One important module of INO80 is the Arp8-Arp4-actin subcomplex that assembles at the HSA domain of the swi2/snf2 ATPase (Figure 3) [12]. Actin related proteins (Arps) all share the basic actin fold and there are 10 different Arps in *Saccharomyces cerevisiae*, which are conserved from yeast to man with the exception of Arp7 and Arp9. Their classification is based on the sequence similarity to actin with Arp1 being the most akin and Arp10 the least [41]. The rigid partitioning of Arp1 to 3 and 10 to be cytoplasmic while Arp4 to 9 are present in the nucleus [42] has recently been extenuated as for instance

the Arp2/3 complex also affects transcription by RNA polymerase II [43, 44]. Nuclear ARPs4-9 associate with the multi-subunit chromatin remodeling complexes INO80 [30], SWR1 [28], SWI/SNF [45], RSC [46] and the histone actetyl transferase HAT [47] in yeast and their accordant homologues [48].

Table 2: Arp-containing chromatin modifiers in budding yeast and human.
The table is adapted from Dion *et al.* 2010 [48].

Organism	Remodeling complex	Full name	Catalytic subunit	ARPs included
Budding Yeast	INO80.com	Inositol requiring mutant 80	Ino80	Actin, Arp4, Arp5, Arp8
	SWR1-C	Swi2/Snf2-Related 1 complex	Swr1	Actin, Arp4, Arp6
	RSC	Remodel the Structure of Chromatin	Sth1	Arp7, Arp9
	SWI/SNF	Switch/Sucrose Non-Fermentable	Snf2	Arp7, Arp9
	NuA4	Nucleosome Acetyltransferase of histone H4	Esa1	Actin, Arp4
Human	INO80	Inositol requiring mutant 80	hIno80	Actin, Baf53a, hArp5, hArp8
	SRCAP	SNF2-related CREB-activator protein	Srcap	Baf53a, hArp6
	BAF	Brahma (BRM) or Brahma related gene (BRG) associated factors	Brm1 or Brg1	Actin, Baf53a or b
	PBAF	Polybromo-associated BAF	Brg1	Actin, Baf53a or b
	TIP60/TRRAP	HIV-1 Tat interactive protein 60 kDa/transformation/transcription domain-associated protein	p400, Tip60	Actin Baf53a

Notably, whenever Arp4 is a member of the complex, actin is also recruited to the HSA domain, which is the conserved binding platform for most Arps and actin in chromatin modifying complexes [12]. INO80 comprises actin and the three different actin-related proteins Arp4, Arp5 and Arp8, being the only complex harboring as many as four members of the actin family.

Arp5 and Arp8 are the largest nuclear Arps with usually 600-900 amino acids, due to very large insertions emanating from the actin fold [49] and they are indispensable for INO80 complex function as *arp5*Δ and *arp8*Δ mutants mimic the *ino80*Δ phenotype [39]. Especially Arp8 has been shown to play a plethora of structural and functional roles as an *arp8*Δ INO80 also lacks Arp4 plus actin and the complex, now deprived of this submodule, loses DNA binding capacity as well as ATPase activity [39]. Therefore, it is not surprising that Arp8-defective mutants are intensely hampered in DNA repair and cell cycle progression [50], since INO80 is involved in these processes [30]. More specifically, yeasts with mutant Arp8 are defective in end-processing of gamma radiation induced DNA double-strand breaks (DSBs) [51] as well as in sister chromatid and also heteroallelic interchromosomal recombination induced by DNA damage [52]. Moreover, Arp8 significantly contributes to the recruitment or retention of Mre11, Ku80 and Mec1 at a DSB [51].

While INO80 in *Saccharomyces cerevisiae* is recruited to DNA damage sites via Arp4 and Nhp10 in a H2A P-Ser129 dependent manner [53, 54], mammalian INO80 seems to be targeted to γ-H2AX foci by its Arp8 subunit and not by Arp4, suggesting that the recognition of DNA damage marker by INO80 might differ across species [55].

The INO80 complex contributes to genome stability via the removal of unacetylated H2A.Z from chromatin. Here, the Arp4-Arp8-actin-HSA submodule plays an important role in this regulatory process, as the collapsed replication fork phenotype in an *arp8* mutant is extenuated via expression of the H2A.Z panacetyl mimic H2A.Z-K3, 8, 10, 14Q under conditions that promote replication stress [29].

Furthermore, Arp8 binds all four core histones preferring H3 and H4 over H2A and H2B, possibly acting as a chaperone for the $(H3/H4)_2$ tetramer [39]. This is strongly corroborated by the finding that the *arp8*Δ phenotype in stress gene induction resembles loss-of-function mutations of the histone chaperones Asf1 and Spt6 phenotypes under hyperosmotic stress [56].

It was previously thought that Arps only play functional roles within their respective complexes [57], but human Arp8 was shown to be enriched on mitotic chromatin and its silencing caused misalignment of metaphase chromosomes, while knock down of Arp5 or Ino80 homologs did not [58]. Moreover, yeast Arp8 concomitantly supports Arp4's inhibitory effect on actin filaments *in vitro* [59] and might therefore aid in regulating the state nuclear actin, which can be monomeric or also polymeric [60]. These data suggest novel functions for Arps independent of their remodeling complex hosts.

The Arp submodule assembled at remodelers' HSA domain together with the post-HSA domain also appears to play an intrinsic regulatory role. In Sth1, the ATPase of RSC, several *mra* (modify the requirement for Arps) mutations are able to suppress Δ*arp* phenotypes [12]. Interestingly, these mutations cluster in the PTH (post-HSA) domain, located next to the actin-related protein recruiting HSA domain, and in protrusion1, a short insertion in the swi2/snf2 ATPase sequence between motif III and IV. Therefore, Arps appear to be regulators of the swi2/snf2 ATPase via the antagonistic interplay with adjacent domains.

Before completion of this thesis, only one structure of a nuclear Arp was available [59] and insights on the exact nature of their histone binding properties remained to be elucidated just like the enigmatic role of nuclear monomeric actin accompanying Arp4 in SWR1, INO80 and NuA4.

1.4 Actin biochemistry

In order to comprehend the function of actin within chromatin remodelers it is important to understand the basic properties of actin, which have been assessed since its first biochemical description in the 1940s [61].

Actin is a versatile protein building block of the cytoskeleton and implicated in intracellular motility, cell adhesion and locomotion and also signaling on the cellular level [62, 63] but also important for the

function of muscles in multi-cellular organisms [64]. It is structurally and functionally highly conserved [65, 66] and one of the most abundant proteins in the cell of eukaryotes, yet still not completely understood [67].

The X-ray structure of actin has been solved in 1990 and comprises a characteristic fold, where four subdomains encircle a single nucleotide [68]. A nucleotide binding cleft separates subdomain 2 from 4 at the "pointed end" of the molecule, while a target-binding cleft is situated at the "barbed end" between subdomains 1 and 3 (Figure 4A).

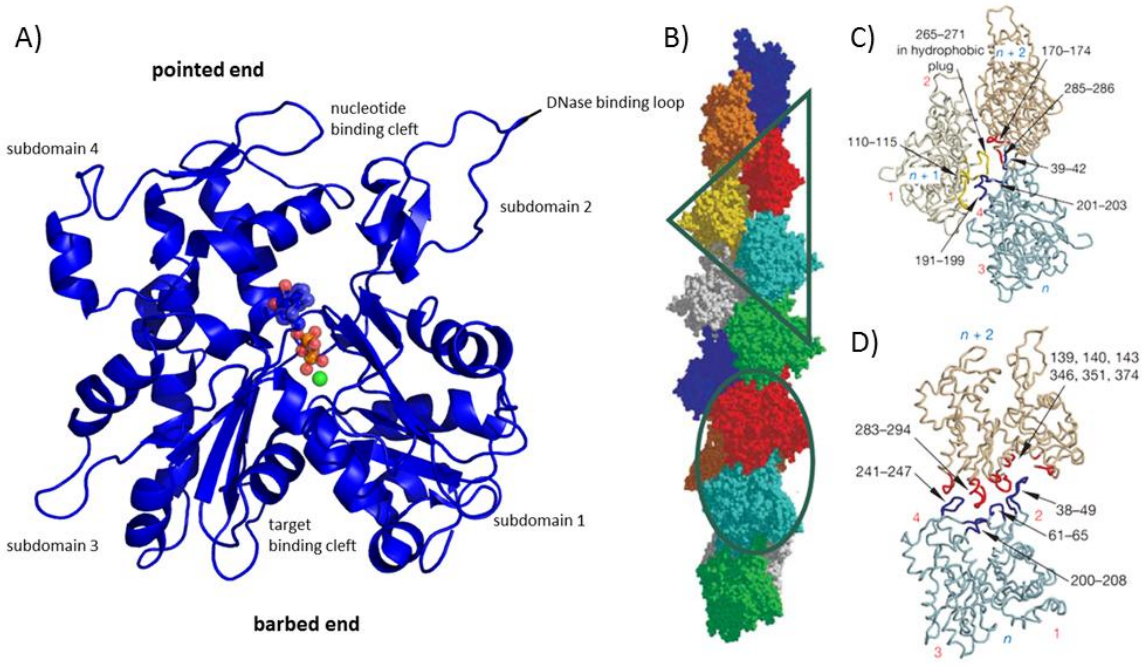

Figure 4: actin structure and also the filament.
A) The actin monomer comprises the actin fold with 4 subdomains engulfing the nucleotide. Distinct ends termed pointed and barbed end are important for filament contacts. B) Structural model of the actin filament according to Oda *et al.* C) The smallest repetitive unit of the filament is the actin trimer. D) Pointed to barbed end binding of adjacent actin building blocks reveal the importance of the DNase binding loop and the target binding cleft.
Figure adapted from Oda *et al.* [69].

Both ends are important for filament contacts as one pointed end interacts with an adjacent actin's barbed end (Figure 4D). A third actin molecule binds to these two actins with its hydrophobic plug at their interface to form an actin trimer, which is the smallest repetitive unit of the actin filament (Figure 4B,D). Basically, all actins in the filament have the same pointed to barbed end configuration and therefore the actin filament also possesses these two distinct ends. In the early filament however, appearance of a lower dimer of anti-parallel configuration has been reported [70, 71].

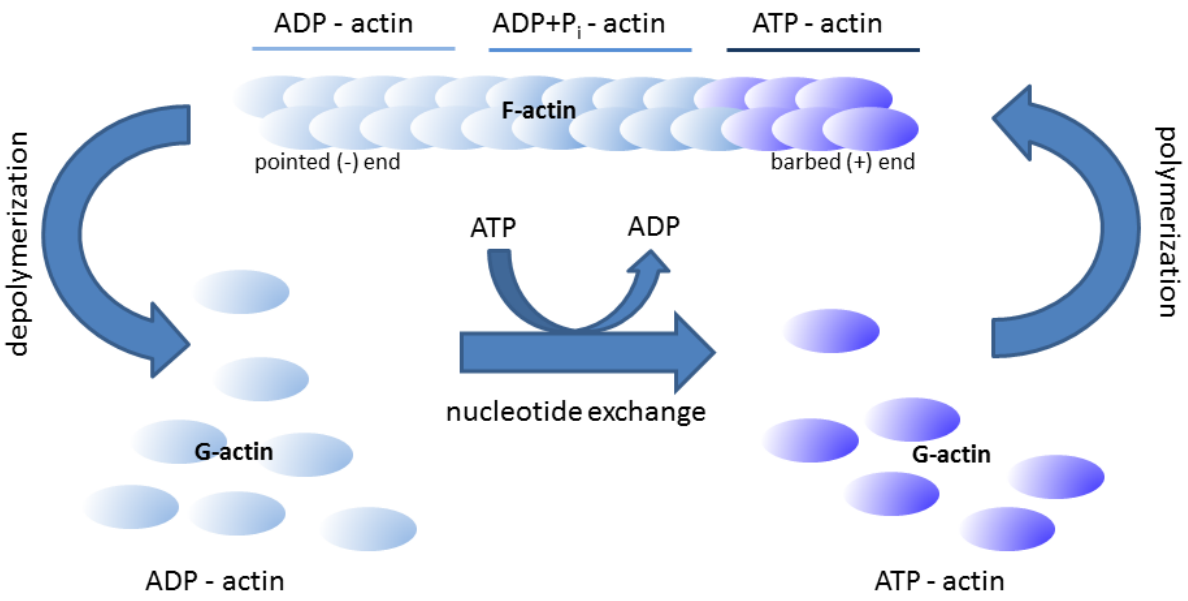

Figure 5: actin (de-) polymerization cycle
The transition between G-actin and F-actin is called actin dynamics. Actin filaments grow by incorporation of ATP-actin to the barbed end. Within the filament, ATP is hydrolyzed and subsequently the inorganic phosphate is released. The ADP-actin filament eventually depolymerizes into ADP-G-actin and nucleotide exchange occurs to poise ATP-G-actin for polymerization.

The transition between monomeric G-actin (globular-actin) and polymeric F-actin (filamentous actin) is the major property of actin and the basis of actin dynamics, which gives rise to its multitude of functions. A plethora of actin-binding proteins influence and fine-tune the properties of actin and hence regulate actin dynamics [72]. One key factor in actin dynamics is actin's nucleotide state. A bound nucleotide appears to be essential for the structural integrity of the actin molecule [73], nonetheless actin is a filament stimulated ATPase [74]. ADP containing F-actin is less stable and will eventually depolymerize. The resulting G-actin can exchange ADP by ATP and reenter the polymerization cycle (Figure 5). Physiological actin filament growth occurs at the barbed end side of actin filaments, which has a lower critical concentration for polymerization (0.1 µM) compared to the pointed end (0.7 µM) [75]. Yet, actin polymerization is no spontaneous reaction as filament nucleation requires stable actin dimers or trimers, which are kinetically unfavorable [76]. In this respect, it is interesting to note that actin is always accompanied by Arp4 to form heterodimers within chromatin modifying complexes [77].

1.5 The relationship of nuclear Arps and nuclear actin

It is indeed a puzzling fact that several multi-subunit remodeling complexes have Arps (actin-related proteins) and sometimes even actin among their entourage. Actin and Arps have long been known as critical components of the cell's dynamic cytoskeleton, but only for the last two decades a growing body of evidence indicates that actin together with Arps is implicated in many nuclear processes as well.

Polymeric actin has important functions in transcription of polymerases I-III [78-80], which might be assisted by the Arp2/3 complex or other actin binding factors [43, 81]. In a recent study, nuclear actin filaments (F-actin) are important for pluripotency gene *Oct4* (octamer-binding transcription factor 4) transcription and hence appear to play a role in reprogramming after nuclear transfer [82].

Moreover, actin together with nuclear myosin I seems to be implicated in long-range chromatin movement [83] and reposition of chromatin loci are linked to altered transcription rates [84]. DNA double strand breaks also undergo putatively active transportation as they are redirected to the nuclear lamina, if they remain unrepaired [85].

Interestingly, lamins, which sit at the inner nuclear membrane, have actin binding sites and are capable of polymerizing actin filaments *in vitro* [86]. These lamins interact via nesprins with nuclear envelope lamina spanning complexes (NELSCs) and emerin [87]. As NELSCs such as the LINC (linker of nucleoskeleton with cytoskeleton) complex are putatively capable of transducing mechanical force via the nuclear envelope [88, 89] and emerin binds pointed ends of actin filaments [90], it is quite conceivable that actin on both sides of the nuclear envelope plays an important role to transmit stimuli to the nucleus to affect transcription via the nucleoskeletal network [91].

Despite considerable and mounting evidence, that actin is an important factor in transcription it still remains enigmatic how actin directly interacts with chromatin. As the primordial nuclear Arp, Arp4 is accompanied by monomeric actin in these molecular machines and capable of binding histones, it is interesting to probe for the chromatin binding properties and participation in actin dynamics of actin and Arps in a remodeler associated subcomplex.

1.6 Aims of the project

The understanding of the versatile cellular functions of INO80 increases constantly, even though not every subunit of INO80 could be assigned to distinct roles yet. The understanding of detailed

mechanistic functions goes hand in hand with the availability of structural information on the complex, which up to date remains scarce within the literature.

In order to understand the versatile functions of INO80 mechanistically on a molecular level, it is therefore indispensable to acquire more structural information on all parts of this chromatin remodeler. Of special interest within INO80 but also other chromatin remodeling complexes are the Actin-related proteins and actin itself. Working together as a functional module in case of Arp8-Arp4-actin or possibly independent from other Arps like Arp5, they represent a very important group of proteins within INO80. Arp4 and of course actin are essential, while Δ*arp8* and Δ*arp5* mutants show similar phenotypes as a Δ*ino80* mutant, which is viable in some yeast strains but hypersensitive to genotoxic agents.

Especially the role of actin within the remodeler remains enigmatic. Whether it is a structural switch dependent on ATPase activity that fine-tunes Arp properties or if it is involved in processes that require actin's capability to polymerize has not been elucidated. This is at least in part due to the complicated handling of chromatin remodeler per se on the one hand and actin itself on the other hand. The nature of nuclear actin within chromatin remodeling complexes however will be important to assess in order to understand the function of Arp and actin containing remodelers.

Therefore this thesis deals with the determination of structural and biochemical features of actin-related proteins as well as actin in chromatin remodeling and actin dynamics.

2. Materials and Methods

2.1 Chemicals, Oligos, Enzymes

Common chemicals were obtained from either Merck (Darmstadt, Germany), Sigma (Deisenhofen, Germany) or Roth (Karlsruhe, Germany) unless otherwise stated. Oligonucleotides for cloning were bought in HPLC purified grade from Thermo Electron Corporation (Ulm, Germany), Eurofins MWG (Ebersberg, Germany) or Metabion (Martinsried, Germany). Enzymes and nucleotides for molecular biology were purchased from Fermentas (St- Leon-Rot, Germany), or New England Bioscience (Frankfurt, Germany). Chromatographic media and columns that were used for purification were acquired from GE Healthcare (Freiburg, Germany).

Crystallization screens and crystallization tools were obtained from Jena Bioscience (Jena, Germany), Hampton Research (Aliso Viejo, USA) or Nextal Biotechnologies (QIAGEN, Hilden, Germany).

2.2 Molecular Biology

Within this project a lot of constructs of protein encoding genes have been cloned into different vectors. Genes were amplified from genomic DNA or cDNA libraries from various organisms with suitable primers (table 3) in a polymerase chain reaction (PCR). For PCR reactions the Phusion Mastermix was used (Finnzymes/Thermo, Ulm) and reactions were performed according to the user's manual. For several constructs, overlap-PCRs were required to yield the nucleotide sequence of interest. Hereby, primers were designed that amplify fragments of the gene of interest and also partially hybridize with one another at the desired gene junctions. A suitable melting temperature of primers for efficient PCRs is around 60-70°C, which is achieved with roughly 20 complementary DNA bases. The PCR reaction then yields two oligonucleotide fragments that can be tethered together in a subsequent PCR reaction with the flanking primers. The primers are added in approximately 0.5 µM concentrations, after the first three cycles of the PCR in which the two fragments first serve as mutual primers to yield the tethered oligonucleotide that is amplified afterwards. Overlap PCR is a powerful tool to insert point mutations into a gene, a cleavable affinity tag or to generate nucleotide sequences that code for fusion proteins. For every construct to be cloned, the final 5' and 3' primers contained a suitable restriction enzyme recognition site and a polyA overhang to facilitate restriction.

The accordant PCR products were separated from primers and unspecific PCR products on a 1% agarose TAE (40 mM Tris, 20 mM acetic acid, 1 mM EDTA) gel via gel electrophoresis in TAE buffer. 6x loading

dye x6 (0.15 g/l bromphenol blue, 0.15 g/l xylene cyanol and 50% v/v glycerol) was added to load the PCR product on the gel and indicated the running length. PCR products were purified from agarose gels using gel extraction kits (Metabion, Martinsried or Macherey-Nagel, Düren/Germany). DNA digestion with the accordant restriction enzymes in suitable buffers were performed as recommended by the manufacturer and subsequently purified via agarose gels. The plasmids that serve as vectors for the transfection of the cloned genes were treated with the same restriction enzymes and additionally with alkaline phosphatase to dephosphorylate the restricted plasmid, which prevents re-ligation. Two- or three-fold molar excess of the digested PCR product was incubated with the linearized vector in presence of T4 DNA ligase and the accordant supplied buffer (Fermentas, St. Leon-Rot, Germany).

Table 3: Oligonucleotides used for cloning

primer name	5' - 3' sequence	purpose
Fw_HisPreSci_Nhe_Nco_Nde	AAA AAA GCTAGCCATGGCGCAT ATG CAT CAT CAT CAT CAT CAT CAT CAT CTG GAA GTT CTG TTC CAG GGG	Overlap PCR to include cleavable His-Tag
Fw_HisPreSci_Sal	AAA AAA GTCGAC ATG CAT CAT CAT CAT CAT CAT CAT CAT CTG GAA GTT CTG TTC CAG GGG	Overlap PCR to include cleavable His-Tag
Fw_HisPreSci_Xho	AAA AAA CTCGAG ATG CAT CAT CAT CAT CAT CAT CAT CAT CTG GAA GTT CTG TTC CAG GGG	Overlap PCR to include cleavable His-Tag
hArp8_SalI_for	AAAAAA GTCGAC ATG ACC CAG GCT GAG AAG GG	Rv primer full-length human Arp8 for pFBDM
hArp8_NotI_rev	AAAA GCGGCCGC TCA CCA CAC AAA CGC AGC	Rv primer full-length human Arp8 for pFBDM
hArp8His_SalI_for	AAAAAA GTCGAC ATG CAT CAT CAT CAT CAT CAT ATG ACC CAG GCT GAG AAG GG	Fw primer for full length human Arp8 and N-terminal His-Tag
Fw_PrSc_hA8_L33	GAAGTTCTGTTCCAGGGGCCC CTG GTG CCG GAG TCG CTG CAA	Fw primer N-terminally truncated human Arp8 for hybridization with cleavable His-tag
Rv_hArp8_NheI	AAAAA GCTAGC TCA CCA CAC AAA CGC AGC	Rv primer full length human Arp8 for pET
Arp8_SalI_His6_TAGzyme_for	AAAAA GTCGAC ATG AAA CAT CAT CAT CAT CAT CAT AAA ATG TCG CAA GAA GAA GCA GAA TCC AGT ATT ATT	Fw primer N-terminal His tag – TAGzyme cleavage of full-length yeast Arp8 for pFBDM
Arp8_NotI_Stop_bac	AAAAA GCGGCCGC CTA GTA CGT GAA AAT ACA TTT ATA TTG TAA GAT TCT	Rv primer full-length yeast Arp8 for pFBDM
Arp4_SalI_His6_TAGzyme_for	AAAAAGTCGACATGAAACATCATCATCATCATCATAAA ATGTCCAATGCTGCTTTGCAAGTT	Fw primer N-terminal His tag – TAGzyme cleavage of full length yeast Arp4 for pFBDM
Fw_Arp4_SalI	AAAAAGTCGACATGATGTCCAATGCTGCTTTGCAAGTT	Fw primer full length yeast Arp4 for pFBDM
Arp4_NotI_Stop_bac	AAAAAGCGGCCGCCTATCTAAACCTATCGTTAAGCAATCT	Rv primer full length yeast Arp4 for pFBDM
yArp4QC-BstZ_for	CCAGTCATGGCTTGGCGGTAGCATACTTACAAGTCTGGGAACATTTCACC	Elimination of BstZI resriction site in yeast Arp4 for pFBDM cloning
yArp4QC-BstZ_rev	GGTGAAATGTTCCCAGACTTGTAAGTATGCTACCGCCAAGCCATGACTGG	Elimination of BstZI resriction site in yeast Arp4 for pFBDM cloning
Fw_act1_SmaI	AAAAACCCGGGATGGATTCTGAGGTTGCTGCTTTGG	Fw primer to eliminate actin intron and full length yeast actin cloning in pFBDM
Rv_act1_Nco	AAAAACCATGGTTAGAAACACTTGTGGTGAACG	Rv primer full length yeast actin for pFBDM
Fw_yHSA_NdeI	AAAAAACATATG GCC CGT GCT ATC CAG AGG	Fw primer HSA domain (INO80 A462)
Rv_yHSA_XhoI	AAAAAACTCGAG TTA CCT TCC AAT GAA ATG CG	Rv primer HSA domain (INO80 K598)
Rv_HSAX_NheI	AAAAAAGCTAGCTTAGAAGTTCAACTCATCTTCCTCCTC	Rv primer HSA/postHSA (INO80 F685)
Fw QC yA4 3xmut	GGTAGTATACTTACAAGTGAGGGAACATATCACCAAGAGTGGGTTGGGAAAAAGG	L462E; F465Y; L468E mutations for Arp4
Rv QC yA4 3xmut	CCTTTTTCCCAACCCACTCTTGGTGATATGTTCCCTCACTTGTAAGTATACTACC	L462E; F465Y; L468E mutations for Arp4
yArp4_3xQC_E_f	GGTAGTATACTTACAAGTGAGGGAACAGAGCACCAAGAGTGGGTTGGGAAAAAGG	L462E; F465E; L468E mutations for Arp4
yArp4_3xQC_E_r	CCTTTTTCCCAACCCACTCTTGGTGCTCTGTTCCCTCACTTGTAAGTATACTACC	L462E; F465E; L468E mutations for Arp4
yArp4_L462R_f	GGTAGTATACTTACAAGTCGTGGAACATTTCACCAACTGTGG	L462R mutation for Arp4
yArp4_L462R_r	CCACAGTTGGTGAAATGTTCCACGACTTGTAAGTATACTACC	L462R mutation for Arp4
yArp4_F465R_f	CTT ACA AGT CTG GGA ACA CGT CAC CAA CTG TGG GTT GGG	F465R mutation for Arp4
yArp4_F465R_r	CCCAACCCACAGTTGGTGACGTGTTCCCAGACTTGTAAG	F465R mutation for Arp4
yArp4_L468R_f	GGA ACA TTT CAC CAA CGT TGG GTT GGG AAA AAG G	L468R mutation for Arp4
yArp4_L468R_r	CCTTTTTCCCAACCCAACGTTGGTGAAATGTTCC	L468R mutation for Arp4
Fw_QC_Act G13R	GGT TAT TGA TAA CCG TTC TGG TAT GTG TAA AGC	polymerization defective actin
Rv_QC_Act G13R	GCT TTA CAC ATA CCA GAA CGG TTA TCA ATA ACC	polymerization defective actin
Fw_QC_Act S14C	GGT TAT TGA TAA CGG TTG TGG TAT GTG TAA AGC	polymerization enhanced actin
Rv_QC_Act S14C	GCT TTA CAC ATA CCA CAA CCG TTA TCA ATA ACC	polymerization enhanced actin

Primer Name	5' - 3' sequence	purpose
Rv_Act_A4-300	CAACAACGTTTTCTATTC TTA GAA ACA CTT GTG GTG AAC G	Reverse primer to hybridize actin sequence with downstream genomic sequence of Arp4
Rv yA4 Strep PreSci	TGGACCTTGGAATAAGACTTCCAATTTTTCGAATTAGGATGTGACCATTAAACCTATCGTTAA GC	Rv primer Arp4 no stop codon Strep, hybridizes with PreSci sequence
Fw_Actin_GSA	GGCTCTGCGGGTTCCGCAGGCAGCGCG ATGGATTCTGAGGTTGCTGC	Fw primer actin for fusion protein with N-terminal linker, actin C-terminal of Arp4
Rv_Actin_GSA	TGCGGAACCCGCAGAGCCGGCGCTACC GAAACACTTGTGGTGAACG	Rv primer actin no stop codon and C-terminal linker
up 500 yA4 Bam	AAA AAG GAT CCG CCA AGG CAC CAT CTG CTA CAT ATG C	Fw primer amplifies genomic sequence upstream of Arp4
dn 300 YA4 Not	AAA AAG CGG CCG CGC TAG CAG TTA TTA CAA CCA TCA TTT TTT CG	Rv primer amplifies genomic sequence downstream of Arp4

Cloning of multiple genes into one pFBDM vector for insect cell expression was achieved via the multiplication module according to a published protocol [92]. Here it is important to note that an additional SpeI recognition site is present in the multiple cloning site of the polyhedrin promotor, which needs to be eliminated for the multiplication module to work. Additionally, Bst17I digestion of the vector is recommended prior to SpeI digestion, since the recognition sequences partially overlap.

Plasmid transformation into 80 µl competent *E. coli* XL1 blue cells [93] (table 5) was performed via heat-shock at 42°C for 60 seconds. Addition of 500 µl of LB medium and incubation at 37°C for 45 minutes granted antibiotic resistance of cells that internalized the accordant plasmid and these cells were selected on LB agar plates with the appropriate antibiotics (table 4).

Table 4: Antibiotics

antibiotic	concentration (1000x)	solvent
Ampicilin	100 mg/ml	water
Kanamycin	50 mg/ml	water
Chloramphenicol	35 mg/ml	ethanol
Tetraycline	12.5 mg/ml	ethanol
Gentamycin	7.5 mg/ml	water

Plasmid DNA from these clones was isolated with a plasmid extraction kit (metabion, Martinsried) from 5 ml overnight cultures and test-digestions, with the same restriction enzymes that were used for cloning, were performed to probe for the successful incorporation of the gene of interest.

2.2 Protein Expression

Protein expression with yields required for crystallization can be a challenging task, especially for proteins that are eukaryotic and members of multi-subunit complexes. Therefore, next to the standard expression system in *E. coli*, expression in High Five Insect cells (Invitrogen, Karlsruhe) was necessary for some protein constructs. Protein expression in *Saccharomyces cerevisiae* was only qualitative and not preparative during this PhD project and was used to probe for the *in vivo* effects of mutant protein. Yeast strains were obtained from Euroscarf (EUROpean Saccharomyces Cerevisiae ARchive for Functional Analysis, Frankfurt, Germany).

2.2.1 Media and supplements

Standard protocols were used to prepare standard media LB (Luria Bertani), TB (Terrific broth), YPD (yeast extract peptone dextrose) and 1% (w/v) agar was added for the accordant plates [94]. The media were supplemented with the respective antibiotics using stock solutions in 1:1000 dilutions prior to use.
Insect cell media *Express Five* for High Five insect cell expression was purchased in powder form from Invitrogen (Karlsruhe, Germany). 321.9g powder was solved in 10l of water and 3.815g of $NaHCO_3$ was added prior to adjustment to pH 6.2. Subsequently, the medium was sterile filtered and stored at 4°C. Before use, the medium was supplemented with 50 ml of 200 mM L-glutamine (GIBCO/Invitrogen, Karlsruhe) as nitrogen source per liter of medium. In order to prevent bacterial contamination of the medium 200 µl of 10 mg/ml gentamycin were also added to the medium.
For yeast experiments, YPD (1% /w/v) yeast extract, 2% (w/v) peptone, 2% (w/v) dextrose) medium was generally used and supplemented with accordant reagents, if necessary (chapter 2.8). For the sporulation procedure, GNA (Glucose nutrient broth agar) plates (5% (w/v) glucose, 3% (w/v) Difco nutrient broth, 1% (w/v) yeast extract, 2% (w/v) agar) were used as presporulation plates and sporulation occurred in 0.005% (w/v) zinc acetate and 1% (w/v) potassium acetate liquid media. Plasmid shuffling occurs on plates containing 1% (w/v) FOA (5-fluoroorotic acid).

2.2.2 Protein expression in *Escherichia coli*

Protein expression in *E. coli* was performed according to standard methods [95]. Generally, bacterial expression of N-terminally truncated actin-related protein 8 originating from different species coded on

pET28 plasmids (Novagen/Merck, Darmstadt) could be expressed soluble in *E. coli*. Expression in strains Rosetta 2 (DE3) and BL21 (DE3) (table 5) resulted in reasonable yields of purifyable protein.

Table 5: *E. coli* strains used in this research project

***E.coli* strain**	**Genotype**	**Source**
XL1 Blue	recA1 endA1 gyrA96 thi-1 hsdR17 supE44 relA1 lac [F´proAB lacIqZΔM15 Tn10 (Tetr)]	Stratagene, Heidelberg
Rosetta 2 (DE3)	F– *ompT hsdS*B (rB– mB-) *gal dcm* (DE3) pRARE2 (CamR)	Novagen/Merck, Darmstadt
BL21 (DE3)	BL21CodonPlus(DE3)-RILB F- *omp*T *hsd*S (rB- mB-) dcm+ Tetr gal_(DE3) endA Hte [argU ileY leuW Camr], extra Copies of argU, ileY und leuW tRNA genes on ColE1-compatible plasmid (CmR)	Novagen/Merck, Darmstadt
DH10MultiBac	F– *mcr*A Δ(*mrr-hsd*RMS-*mcr*BC) Φ80*lac*ZΔ M15 *lac*X74 *rec*A1 *end*A1 *ara*D139 (*ara*, *leu*)7697 *gal*U *gal*K Δ– *rps*L *nup*G /pMON14272 / pMON7124	Imre Berger Redbiotech, Schlieren/ Switzerland

Several liters of LB medium were inoculated 1:100 (v/v) with overnight cultures of *E. coli* cells containing the gene of interest regulated by a lac operon controlled T7 promotor inducible by IPTG (isopropyl-β-D-thiogalactopyranosid). Cells were grown at 37°C, 200 rpm (INNOVA 44R Shaker) to an optical density OD_{600nm} of approximately 0.7, then chilled on ice and subsequently expression was induced by the addition of 0.5 mM IPTG. Cells were then kept on 18°C, 200 rpm overnight and harvested by centrifugation at 2000 x g for 15 min and the resulting cell pellet was flash frozen in liquid nitrogen and stored at -20°C until required.

2.2.3 Protein expression in insect cells

Expression in High Five insect cells depends on efficient infection with the baculovirus based vector. The yield of protein complexes decreases with increasing amount of different viruses. Therefore, the incorporation of all genes of interest into one single baculovirus vector is preferred. This is achieved via the multiplication module on the pFBDM vector, which theoretically is able to integrate an arbitrary amount of genes into one single vector. Via its Tn7 recombination sequence, the vector is then partially merged with bacmid DNA through transformation into *E. coli* DH10MultiBac (table 5). Bacmid DNA is propagated in *E. coli* DH10Bac like a large plasmid that confers resistance to kanamycin and tetracycline. The bacmid complements a genomic lacZ deletion, which results in blue colonies (Lac-) in the presence of IPTG and 100µg/ml chromogenic substrate X-gal (X-α-galactose). Transposition of the gene(s) of interest from the pFBDM donor plasmid into the bacmid disrupts the lacZ sequence enabling blue-white screening for recombination events in bacmids. Isolation of recombinant bacmid DNA was achieved with Midi Prep kits (Macherey-Nagel, Düren or Quiagen, Hilden). Subsequent transfection of approx. 2 µg bacmid DNA with 3 µl transfection agent FuGene (Promega, Mannheim) and 200 µl Sf-900 III serum-free medium (Gibco/Invitrogen, Karlsruhe) into 2ml of $0{,}4x10^6$ mio/ml Sf21 or Sf9 insect cells (table 6) in 6-well culture dishes led to the first generation of recombinant baculovirus particles (P0) that are amplified in successive rounds of infection.

Table 6: Insect cell lines used for virus generation and amplification as well as protein expression

cell line	origin	source
High Five insect cells	clonal isolate, derived from *Trichopulsia ni*	Invitrogen, Karlsruhe
Sf9 insect cells	clonal isolate, derived from *Spodoptera frugiperda*	Invitrogen, Karlsruhe
Sf21 insect cells	clonal isolate, derived from *Spodoptera frugiperda*	Invitrogen, Karlsruhe

After four days at 27.5°C, the supernatant of the suspension with the transfected cells is given to 10 ml of SF21 cells with a density of $1.0x10^6$ cells/ml. After another four days of shaking (85 rpm INNOVA 44R Shaker) at 27.5°C, cell density and viability was measured in a Vi-Cell counter (Beckmann-Coulter,

Sinsheim). If the density was below $3.0x10^6$ cells/ml, cells were centrifuged 10 min 3000 rpm in a Rotana centrifuge (Hettich, Tuttlingen) and the supernatant was sterile-filtered yielding the P1 baculovirus generation in suspension, which was kept at 4°C. A first test-expression was performed by infecting 50 ml High Five cells ($1.0x10^6$/ml) with 2ml of P1 virus. If the protein(s) of interest were detected on an SDS-PAGE gel (see below) after a short purification procedure, 200 ml of Sf21 cells ($0.4x10^6$/ml) were infected with 2 ml of P1 virus for a second amplification step and incubated for four days at 27.5°C and 85 rpm in an INNOVA 44R Shaker. After centrifugation, the supernatant containing the new P2 virus was filtered through a Stericup filter (Milipore/Merck, Darmstadt) and kept at 4°C in the dark until further usage.

Large scale expression in High Five insect cells was performed by incubating 1-3 l of freshly resuspended cells (1.0×10^6 cells/ml) with 1:50 (v/v) of P II virus. Cells were cultured in 5 l flasks at 27.5°C and 85rpm for 48-72hrs. Then, cells were harvested by centrifugation (15 min, 3500 rpm, 4°C), flash frozen in liquid nitrogen and stored at -20°C until further use.

2.3 Protein purification

2.3.1 Buffers and solutions

Generally, all proteins were purified and stored in buffer containing 20 mM Tris-HCl pH 7.8, 100 mM NaCl, 5 mM β-mercaptoethanol, 5% (v/v(glycerol. For purification on Ni-NTA resin different amounts of imidazole were added to yield washing buffer (20 mM or 35 mM imidazole) or elution buffer (200 mM imidazole). Elution buffer for gradient anion exchange chromatography contained 1 M of salt instead of 100 mM.

Purification of proteins subjected to lysine-specific cross-linking and also actin dynamics were performed in buffers containing EPPS-KOH pH 7.8 instead of Tris-HCl and KCl instead of NaCl.

Purity of protein samples were analysed via SDS-PAGE (sodium dodecyl sulfate polyacrylamide gel electrophoresis). Samples were denatured in 4x SDS loading dye (50% v/v glycerol, 250 mM Tris-HCl pH 6.8, 7.5% w/v SDS, 5 mM EDTA, 10 mM DTT, 0.5% w/v bromphenol blue) at 90°C for 2 minutes and separated according to their size on 15% acrylamide gels.

2.3.2 Purification of *Homo sapiens* Arp8 (Δ1-33)

Truncated human Arp8 amplified from human macrophage cDNA and cloned into pET28 was expressed in *E. coli* BL21 (DE3) cells. The cell pellet from 18l expression culture was resuspended in 100 ml Tris-HCl buffer supplemented with protease inhibitors (Roche, Penzberg/Germany). Cells were lysed by sonication and cell debris was removed by centrifugation (40 000 x g, 45 min, 4°C). The supernatant was incubated for 1 h with Ni-NTA resin (Qiagen, Hilden) at 8°C and subsequently purified using gravity flow with three wash steps of 3 column volumes of standard buffer containing 0, 20 and 35 mM imidazole. Bound protein was eluted with buffer containing 200 mM imidazole. The eluate was applied to a Q sepharose column (GE Healthcare, Heidelberg) and the flow-through containing the histidine-tagged protein was supplemented with PreScission Protease (GE Healthcare, Freiburg) to cleave off the N-terminal affinity tag and dialysed against Tris-HCl buffer overnight at 4°C. The protein solution was centrifuged (40 000 x g, 20 min., 4°C) and the supernatant was incubated with GSH sepharose (GE Healthcare) to remove GST-fused PreScission protease.

The flow-through was again applied to a Ni-NTA resin and the obtained flow-through was further purified via size exclusion chromatography with a Hiload Superdex-200 26/60 (GE Healthcare, Freiburg). The protein was concentrated up to 14 mg/ml in Amicon ultra centrifugal filters (Millipore/Merck, Darmstadt), flash-frozen in liquid nitrogen and stored at -80°C until required.

2.3.3 Purification of *Homo sapiens* full-length Arp8

The Arp8 coding gene was amplified from human macrophage cDNA with primers containing SalI and NotI restriction enzymes and coding for an N-terminal hexahistidine tag and cloned into the pFBDM vector (Redbiotech, Schlieren/Switzerland). Protein expression was achieved according to a published protocol [96]. The purification protocol was similar to that for the N-terminally truncated hArp8 construct but without PreScission protease cleavage and subsequent GSH- and second Ni-NTA purification.

2.3.3 Purification of *Saccharomyces cerevisiae* Arp8 and Arp4

Cloning, expression and purification were performed as described previously [59, 97].

2.3.4 Purification of *Saccharomyces cerevisiae* INO80 subcomplex I

S. cerevisiae Arp4, Arp8, actin and a prolonged Ino80 HSA domain (A462-F685) were cloned into the pFBDM vector. A sequence coding for a PreScission protease cleavable N-terminal octahistidine tag was added to the coding sequence of Ino80 (A462-F685). Two plasmids were merged to a single pFBDM vector carrying all four genes of interest and protein expression in High Five cells (Invitrogen, Karlsruhe) was accomplished according to a published protocol [96]. The protein subcomplex I was purified similarly to full-length human Arp8 with the exception that a linear gradient with high salt buffer (20 mM Tris-HCl pH 8.0, 1 M NaCl, 5 mM β-mercaptoethanol and 5 % (v/v) glycerol) was applied to elute the subcomplex from the Q sepharose column (GE Healthcare, Freiburg) prior to size exclusion chromatography.

2.3 Analytical size exclusion chromatography and static light scattering

Preparative size exclusion chromatography (SEC) is a final step in most protein purification procedures to yield monodispersed samples. Since the elution behavior of proteins or protein complexes depends on their size or rather hydrodynamic radius, analytical gel filtration can also be used to estimate the molecular mass of a sample and hence the state of oligomerization. A standard protein mixture with globular proteins of known molecular masses gives rise to elution peaks that elute linearly according to the logarithm of their mass. The used standard sample contains thyroglobulin (670 kDa), bovine gamma-globulin (158 kDa), chicken ovalbumin (44 kDa), equine myoglobin (17 kDa) and vitamin B_{12} (1.35 kDa) (Bio-Rad, Munich, Germany). A resulting trend line allows estimating the molecular mass of a new sample.

The elution volumes from a Superdex 200 15/150 GL column, or alternatively Superose 6 PC 3.2/30 column connected to an Ettan LC System (GE Healthcare, Freiburg, Germany) were used to estimate the molecular weight of a sample by SEC. It must be noted, that alterations to a globular fold dramatically change the hydrodynamic radius and make an accurate molecular mass determination difficult. To overcome this problem, static light scattering (SLS) can be employed after size exclusion chromatography. The protein sample scatters monochromatic light according to its molecular weight. If the laser intensity, the quantum efficiency of the detector, the full scattering volume and solid angle of the detector are known, SLS allows calculating the molecular mass of the protein sample from its light scattering intensity.

Here, molecular weight determination by SEC/SLS was performed using an ÄKTAmicro system with a Superdex 200 15/150 GL column (GE Healthcare), which is connected to a static light scattering / refractive index measurement device (Viscotek TDA270). For measurements, the supernatant after centrifugation (15 min., 16100 rpm, 4°C) was used. The system was calibrated with a sample of BSA (66.5 kDa) prior to the measurements of the samples and an independent BSA run at the end confirmed calibration and stability of the system. Data evaluation was performed using the OmniSEC software package.

2.4 X-ray crystallography

For detailed theoretical explanations of protein crystallography and X-ray diffraction based structure determination refer to several excellent text books on these topics [98-100]. A brief description of the technique is described in this chapter.

2.4.1 Protein crystallization

Proteins precipitate in supersaturated solutions driven by the thermodynamics of protein-protein interactions. In order to obtain protein crystals, this “precipitation” must occur in an ordered manner so that distinct protein interfaces regularly contact each other giving rise to crystal contacts and eventually crystal growth. This is dependent on a plethora of different parameters such as protein concentration, temperature, pH and the characteristics of one or more precipitants, which amongst others can be salt, certain polymers or organic acids. Crystal growth is the bottleneck for X-ray diffraction based structure determination and an empirical process for every protein. Hence, screening of many different conditions is usually a prerequisite to find suitable parameters that result in protein crystals, which then have to be optimized to yield crystals that give rise to sufficient diffraction for structure determination. Generally, vapor diffusion methods are used for screening and optimizing. Here, the concentrated protein solution is mixed with precipitant in solution in one drop that could hang (hanging drop technique) or sit (sitting drop) above a reservoir of the precipitant solution in a hermetic chamber. Due to the higher concentration of precipitant in the reservoir water evaporates from the protein drop, which increases the concentration of the precipitant within this drop slowly until equilibrium is reached. The correct parameters yield crystals that generally need to be optimized in order to sufficiently diffract X-rays to solve the atomic structure of the protein.

After initial hits in the Magic1 screen (AG Conti, MPI Martinsried), crystals of human Arp8 (Δ1-33) were refined to grow at 16°C in 3.9 M NaCl, 0.5 % (v/v) methanol, 50 mM Mes pH 6.1, mixed 1:1 (v/v) with

4.5 mg/ml protein solution in hanging drop vapor diffusion. Seeding with the obtained small but regular crystals yielded rod shaped crystals of up to 500 µm length after 4-5 weeks at 10°C. Crystals were cryoprotected for data collection in a buffer containing 50 mM Mes pH 6.1, 3.5 M NaCl and 25 % (v/v) glycerol.

2.4.2 X-ray diffraction

Within the wide spectrum of electromagnetic waves, X-rays have wavelengths between 0.1 and 10Å (1Å=10^{-10}m). According to the Abbé limit, two points are only recognized as individuals, if the wavelength of the electromagnetic radiation used for observation approximates their distance. For atomic bonds with a typical length of 1.497Å for a C_α-C_β bond [101], X-rays have the required wavelengths. Diffraction or rather elastic scattering occurs upon interaction of X-rays with electrons of the proteins. Due to the repetitive order of proteins within a crystal, some diffracting X-rays do not cancel each other out but interfere constructively with respect to the crystal lattice, which leads to a distinct diffraction pattern of several spots that can be recorded on a detector. The scattered waves only positively interfere, if distance d and angle θ between incident beam and imaginary lattice planes fulfill Bragg's law with n being an integer and λ the wavelength.

$$n \cdot \lambda = 2 \cdot d \cdot \sin\theta$$

The spots on the detector then can be envisaged as the result of reflections at these parallel lattice planes, whose spacing and orientation are classified by the Miller indices h, k and l.

2.4.3 Solving the phase problem for the electron density calculation

The diffracting entity of the protein crystals are the delocalized electrons and can be described by the electron density distribution ρ, which is a periodic function due to the regular repetition of proteins within the crystal. Hence for each point (x,y,z), a Fourier transformation can be applied to calculate the electron density ρ, which represents the summation of each structure factor F (h,k,l) in a normalized unit cell.

Every atom j at (x,y,z) has a distinct scattering power, which depends on the atom type giving rise to an atomic scattering factor f_j. Since all atoms contribute to the scattering, the sum over all atomic scattering factors yields the structure factor F (h,k,l).

$$F(h,k,l) = \sum_{j=1}^{N} f_j \cdot e^{[2\pi i(hx_j+ky_j+lz_j)]} \cdot e^{[-B\cdot sin^2\frac{\theta}{\lambda^2}]}$$

The last term of the equation, $e^{[-B\cdot sin^2\frac{\theta}{\lambda^2}]}$, is the B- or Debye-Waller factor and takes the thermal disorder into account. Hence, the structure factor F describes the scattering of the incident X-ray beam by the protein crystal and the intensity of a given reflection (hkl) is proportional to the square of the structure amplitude $|F_{hkl}|$, which is the measured entity in a diffraction experiment.
Since the electron density ρ of the protein must be determined to yield a molecular model and ρ is related to F (h,k,l) by a direct Fourier transformation (Fourierintegral) an inverse FT must be applied to the structure factors.

$$F(h,k,l) = V \cdot \int_{x=0}^{1}\int_{y=0}^{1}\int_{z=0}^{1} \rho(x,y,z) \cdot e^{[2\pi(hx+ky+lz)]}\, dxdydz$$

Even though the structure factor F (h,k,l) can be readily deduced from a known atomic structure, *de novo* structure determination faces the inverse problem, since F (h,k,l) is a complex number that is composed of the structure amplitude $|F_{hkl}|$ as well as phase information α (h,k,l) and the latter is lost during the experiment.

$$F(h,k,l) = |F(h,k,l)| \cdot e^{[i\cdot\alpha(h,k,l)]}$$

This is the so called “phase problem” of crystallography, which needs to be solved in order to be able to determine the electron density distribution ρ of the protein based on the diffraction data.

$$\rho(x,y,z) = \frac{1}{V}\sum_{hkl}|F(h,k,l)| \cdot e^{[-2\pi i(hx+ky+lz-\alpha(h,k,l)]}$$

Several approaches have been developed to solve X-ray structures *de novo* including isomorphous replacement and anomalous scattering techniques, or a combination thereof. Here, anomalous scatterers that diffract stronger compared to the relevant atoms within proteins are added.

Due to the availability of many high resolution structures and the modular composition of many proteins with structurally conserved domains, molecular replacement is often a suitable method.

Hereby, phases can easily be derived from known structures and used as a starting point for the interpretation of new diffraction data. In this thesis, molecular replacement was applied to solve the structure of Arp8 using the known structure of Arp4 (pdb entry: 3QB0) as search model.

The available structural model can be rotated and translated to fit into the electron density of the unknown structure, which renders the replacement to be a 6-dimensional search problem (or two 3 dimensional searches). The Patterson function is a Fourier transformation of the measured intensities at phase angle 0° and an important equation to obtain phase angles in molecular replacement as it results in the Patterson map, which depicts interatomic distance vectors.

$$P(u,v,w) = \frac{1}{V}\sum_{hkl}|F(h,k,l)|^2 \cos[2\pi(hu+kv+lw)]$$

The Patterson unit cell (u,v,w) and the real unit cell (x,y,z) have the same dimensions and therefore translation and rotation of the model structure's Patterson map can be compared with the crystal diffraction data. Newly derived coordinates of the molecules in the unit cell give rise to structure factor amplitudes $|F_{calc}|$ and the respective phase angles α_{calc}, which then iteratively are approximated onto the experimentally derived structure factor amplitudes $|F_{obs}|$.

$$F_{(h)} = (|F_{obs}| - |F_{calc}(h)|) \cdot e^{[i\alpha_{calc}(h)]}$$

One major problem in this approach is the danger of introducing substantial bias from the model structure onto the new structure. An F_o-F_c difference electron density map helps to minimize the bias and marks regions of model bias within the density, when compared to the $2F_o$-F_c map used for model building.

$$F_{(h)} = (2|F_{obs}| - |F_{calc}(h)|) \cdot e^{[i\alpha_{calc}(h)]}$$

One important measure for minimization of model bias is the R_{free}, which relates measured reflections that were not used for structure refinement, to validate how well the model fits to the data.

2.4.4 Data collection and structure determination of *Homo sapiens* Arp8 (Δ1-33)

Diffraction data to a resolution of 2.6 Å were collected on a single crystal of human Arp8 (Δ1-33) at 100K and a wavelength of 1.0 Å at beamline X06SA (Swiss Light Source, Villingen, Switzerland). Subsequently, the experimental reflection spots were processed and scaled with XDS and XSCALE [102] in space group 20 ($C222_1$). As Arp8 was predicted to have a basal actin fold as core structure, actin and Arp4 structures were plausible models for molecular replacement approaches. The structure of Arp8 has eventually been solved with a model derived from yeast Arp4 (pdb: 3QB0) with all non-identical residues cut at the β-carbon atom using CHAINSAW [103]. Molecular replacement was automatically carried out with PHASER [104] with one molecule of human Arp8 per asymmetric unit.

An initial model of high quality was obtained using cycles of automated model building with ARP/wARP [105] and BUCCANEER [106] in the CCP4 Suite [107] and completed by manual building with COOT [108]. Refinement with PHENIX [109] finally resulted in a 2.6 Å structure with good stereochemistry and reasonable R factors of R_{work}/R_{free} of 16.0/20.4 %. Coordinates have been deposited in the Protein Data Bank (accession code 4FO0).

The simulated annealing $2F_oF_c$ omit map for a bound ATP molecule was calculated using CNS [110, 111] and the images for this thesis were generated using PyMol [112] and Chimera [113].

2.5 Small angle X-ray scattering (SAXS)

Via small angle X-ray scattering, structural information can be deduced from concentrated proteins in solution, albeit with low resolution. Sample preparation is easy, when compared to protein X-ray crystallography and electron microscopy and SAXS poses no size restriction onto the measurable sample like nuclear magnetic resonance (NMR). Even though SAXS is not quite suitable as stand-alone structural technique, it can provide valuable information on the behavior of macromolecules in solution and thus, for example, help to identify crystal artifacts.

Hence, the technique complements the interpretation of high resolution structural data as the combination of SAXS and X-ray crystallography can provide interactions and assemblies of proteins within complexes or annotate crystallized domains within protein envelopes. SAXS is also suitable to monitor conformational changes upon substrate binding etc. that would otherwise disrupt crystal lattices [114].

Especially for protein complexes that are too flexible to be studied by X-ray crystallography, SAXS is a valuable complementary method, which is described in detail in reviews [114, 115] and only briefly explained here.

Just like in X-ray crystallography, a SAXS experiment measures the scattering of the incident X-rays by the electrons of the sample. But instead of an orderly arrangement along lattice points, the scattering molecules are randomly distributed in solution. It is important to note that the buffer majorly contributes to the scattering and accurate blank measurements for normalization are important.

The scattering curve is a cross-section via the radially symmetric (isotropic) pattern and describes the scattering intensity I(s) as a function of the momentum transfer $s = \frac{4\pi \sin\theta}{\lambda}$ with 2θ being the scattering angle.

At low resolution the scattering is dominated by the contribution of the radius of gyration (R_G), which describes the average distance of each single scatterer from the center of the particle that diffracts X-rays. Therefore, with help of the Guinier approximation at low resolution, where log(I(s)) is plotted against s^2 should yield a straight line, one can determine the size and hence the R_G of the scatterer.

$$I(s) \cong I_0 \cdot e^{-\frac{1}{3}R_G^2 s^2}$$

The Guinier plot also assists in extrapolating I_0, which can be used for molecular weight determination as it is unaffected by particle shape and displays merely the square number of electrons within the scattering particle. Higher s values bear information about the molecular shape of the particle.

In order to obtain spatial information of the scattering particle, it is important to extract direct information about the distances between its electrons. This is achieved using the pair-distribution function p(r), which is an autocorrelation function calculated via a Fourier transform of the scattering curve, similar to the Patterson function in crystallography.

$$p(r) = \frac{r^2}{2\pi^2} \int_0^\infty s^2 I(s) \frac{\sin sr}{sr} dr$$

The pair distribution function is a real space representation function that directly provides information about the molecule's shape, as theoretically the p(r) function is zero at r = 0 and at r ≥ D_{max}, with D_{max} corresponding to the maximum diameter of the scattering particle. Since D_{max} can only be estimated and not calculated from the experimental data, reasonable D_{max} values are chosen and then it is analyzed how well the corresponding p(r) distribution fits the scattering data.

The determination of the solution structure is then performed via a computational *ab initio* approach. According to the chosen maximal diameter of the structure the program GASBOR fills the accordant space with dummy beads that represent amino acids. The algorithm follows a trial and error approach in which for every possible state the theoretical scattering curve is computed and subsequently compared with the experimental data. These curves should align in iterative steps, leading to a dummy bead model which represents the scattering particle. For this minimization problem, additional restraints like a constant density within the molecule help to give rise to reasonable models. The quality of the resulting model can be tested upon the comparison of several GASBOR runs that yield individual models, which are subsequently aligned and averaged. All computed structures should be relatively uniform within the resolution range and the NSD (nominal spatial discrepancy) values of the averaged structures should be as close to 1 as possible.

All protein samples for SAXS measurements were purified as stated above (chapter 3). Flow-through of the concentration step was used as buffer reference for the measurements. All SAXS data were collected at beamlines X33, EMBL/DESY (Hamburg, Germany) or ID14-3, ESRF (Grenoble, France) at a cell temperature of 20°C. The molecular weight of protein samples in solution was estimated according to Porod volume analysis [116].

Human Arp8 was measured at a protein concentration of 6.15 mg/ml (full-length) or 1.5 mg/ml (truncated hArp8 Δ1-33). Data were processed with the ATSAS package [117]. Guinier analysis yielded a radius of gyration Rg= 3.1 nm and showed no obvious signs of aggregation. The Kratky plot shows a bell shaped curve indicating that hArp8 is folded in solution [116]. A set of 16 independent *ab initio* structures was calculated using GASBOR without any symmetry information given. One representative GASBOR model was chosen for representation (chapter 3.3.1) as all *ab initio* models are highly similar (nominal spatial discrepancy (NSD) values of approx. 1.0 [118]) and the bead model was transformed to an electron density using the SITUS package [119]. The theoretical scattering data of the atomic model were calculated with CRYSOL [120] and compared to the experimental scattering data.

2.6 Methods in actin biochemistry

The properties of Arp4 and truncated Arp8 in actin dynamics have been published together with the structure of Arp4 [59]. This work was performed in close collaboration with Dr. Breitsprecher (AG Faix, Hannover) who also prompted the work on the subcomplex I (Arp8-Arp4-actin-HSA), which was continued in our laboratory.

2.6.1 Pyrene actin assays

Actin for assays was purified from rabbit muscle. The batch was divided and partially labeled with pyrene according to standard protocols [121]. Prior to the actin dynamics experiments, actin and pyrene actin were mixed in appropriate ratios (5-20% pyrene-actin) and then Ca^{2+}-ATP-actin was transformed into Mg^{2+}-ATP-actin with 10x Mg exchange buffer (20 mM Tris-HCl, pH 8.0, 2 mM ATP, 1 mM $MgCl_2$, and 0.5 mM DTT). For the actin assembly assays, proteins of interest were diluted in a storage buffer (20 mM EPPS-KOH, pH 8.0, 100 mM KCl, 5 mM ß-ME, 2% (v/v) glycerol,) and 10x KMEI buffer (500 mM KCl, 10 mM $MgCl_2$, 10 mM EGTA, and 100 mM imidazole, pH 7.3) was added. 10% pyrene labeled Mg^{2+}-ATP-G-actin (in 2 mM Tris/HCl, pH 8.0, 0.2 mM ATP, 0.1 mM $CaCl_2$, and 0.5 mM DTT) in a final concentration of 4 µM were pipetted into a 96-well plate (Greiner, Frickenhausen). The assembly reaction was started by transferring the KMEI protein solution containing the Arps and the Arp subcomplex in different concentrations to the pyrene labeled actin. The polymerization of actin was monitored by measuring the fluorescence increase of pyrene actin (excitation at 364 nm and emission at 407 nm) in a Tecan Infinity-1000 plate reader (Tecan) for at least 1500 seconds. For polymerization experiments with Mg^{2+}-ADP-actin monomers, all buffers contained ADP instead of ATP. The relative polymerization rate was derived from the slopes of the fluorescence increase of, where 10–50% of the actin polymerized, while F-actin amounts at steady state was determined by measuring pyrene fluorescence 16 h after star 4°C of the reaction.

To analyze the effects of the subcomplex I on F-actin polymerization, 40 µM (20% pyrene labeled) Mg^{2+}-ATP-actin was polymerized overnight in KMEI-buffer. The assays were performed by rapidly mixing 10 µl of the subcomplex in KMEI buffer with 90 µl of a solution of 2 µM F-actin. For spontaneous depolymerization, the actin/pyrene-actin mix was diluted to 100 nM and decrease in fluorescence was measured at 407nm.

The polymerization in G-buffer (2 mM Tris/HCl, pH 8.0, 0.2 mM ATP, 0.1 mM $CaCl_2$, and 0.5 mM DTT) of actin was performed in presence of different concentrations of the subcomplex. Generally, actin cannot polymerize on its own under the low salt condition in G-buffer. Change of pyrene fluorescence was measured in a Tecan Infinity-1000 plate reader (Tecan, Männedorf/Switzerland) at 407nm in presence of subcomplex I in G-buffer.

2.6.2 Actin polymerization measured by light scattering

Light scattering as complementary assay was used to monitor actin filament growth. Here, a 1 ml quartz cuvette was filled with a final concentration of 4 µM G-actin in G-buffer. Polymerization was rapidly started by addition of KMEI buffer containing high concentrations of subcomplex I. Since scattering intensity is dependent on the size of the scattering particle, the polymerization of actin can be monitored by measuring the absorption at 232 nm in a Jasco V-630 Photometer (Jasco, Easton/USA).

2.6.3 *In vitro* TIRF microscopy

Total internal reflection fluorescence microscopy (TIRFM) is a microscopic technique that monitors fluorescence and concomitantly largely reduces background. The incident angle of the exciting laser is chosen to create an evanescent wave at the interface between a special immersion oil and the aqueous protein solution, which excites the fluorophores that are close to the interface. Fluorescently labeled actin allows for the study of nucleation and growth of single actin filaments [122]. All TIRF experiments were performed by Dr. Breitsprecher according to previous work [123].

2.6.4 Pointed end elongation assay

F-actin (20% pyrene-labeled) was used at diluted assay concentration of 20 nM capped by 3 nM CapZ, which enables seeding of pointed end elongation. Then, monomeric actin (also 20% pyrene labeled) was added to polymerize to the CapZ covered seeds at the pointed end. Fluorescence was monitored as a signal of polymerization. The Arp8-Arp4-actin HSA subcomplex was complemented in different final concentrations in independent assays and its direct impact on pointed end elongation was measured at 407 nm.

2.7 Protein cross-linking and mass spectrometry analysis

The crystallization of protein complexes is inherently difficult and only a small fraction of the many identified protein complexes have been structurally characterized [124]. Challenging multi-subunit protein complexes such as INO80 are very unlikely to crystallize as a whole and only a divide and conquer strategy with hybrid methods seems feasible to elucidate their macromolecular assembly. One

elegant approach is the lysine specific cross-linking of protein complexes with subsequent trypsin digestion and mass spectrometry analysis, which has recently been established as an integral part of hybrid structural studies of protein complexes [125, 126].

In order to elucidate the relative arrangement of the Arps and actin, an equimolar mixture of isotopically light and heavy labeled DSS (disuccinimidyl suberate; Creative Molecules, creativemolecules.com) was solved in DMF (Dimethylformamide, Sigma-Aldrich) to yield a stock solution with a final concentration of 50 mM. DSS was mixed with the aqueous protein solution containing the Arp8-Arp4-actin-HSA module to yield approximately 1 DSS molecule per lysine in the protein subcomplex. The cross-linking reaction was then incubated at 900 rpm and 30°C in a tabletop shaker (Eppendorf, Hamburg) for 30 min and quenched by addition of ammonium bicarbonate to a final concentration of 50 mM and further incubation at 37°C, 900 rpm for 10 min. The cross-linked protein complex was further purified by a Superose 6 PC 3.2/30 gel filtration column (GE Healthcare, Freiburg) on an Äkta Micro System (GE Healthcare). The cross-linked protein fraction that eluted at the same volume as the corresponding uncross-linked protein complex was pooled and flash frozen in liquid nitrogen prior to preparation for mass spectrometric analysis.

The protein digestion, tandem mass-spectrometry and evaluation of the inter-protein cross-links were performed by Dr. Franz Herzog at the ETH Zürich according to an established protocol [126].

2.8 Yeast genetics

2.8.1 Replacment of Arp4 by accordant mutants in a BY yeast strain

A heterozygous *S. cerevisiae* Arp4 (YJL081c) deletion strain was purchased from Euroscarf (Frankfurt, accession number Y21342). A pRS316 vector carrying the wild-type gene of Arp4 with the flanking genomic sequence (500 basepairs upstream and 300 bp downstream of the open reading frame) was transformed into the BY yeast cells prior to sporulation.

Table 7: Yeast strain used for *in vivo* assays

***S. cerevisiae* strain**	**genotype**	**source**
BY4743	Mat a/α; his3Δ1/his3Δ1; leu2Δ0/leu2Δ0; lys2Δ0/LYS2; MET15/met15Δ0; ura3Δ0/ura3Δ0; YJL081c::kanMX4/YJL081c	Euroscarf, Frankfurt

Sporulation was achieved according to a standard protocol with previous growth on nutrient rich GNA (glucose, nutrient broth, agar) plates and subsequent sporulation for seven days at 25°C and gentle shaking in minimal medium with 1% (w/v) potassium actetate and 0.005% (w/v) zinc acetate. Sporulation efficiency was below 10% but sufficient tetrads could be dissected. Tetrads were separated after zymolyase (G-Biosciences) lysis of the cell wall. Complete tetrads were grown on YPD and 5-FOA agar plates and selected for the Arp4 knock out cells that were complemented with the pRS316 +500 Arp4 -300 vector harboring the *URA3* gene. Expression of the *URA3* marker on pRS316 is lethal in presence of 5-fluorooretic acid and Arp4 is an essential gene. Hence, when all 4 tetrads give rise to viable colonies on YPD but only two of these colonies survive on 5-FOA, the other two colonies on YPD are Arp4 knock-out strains harboring the pRS316 +500 Arp4 -300 plasmid.

Additional transformation of pRS315 containing a mutant Arp4 gene with the genomic flanking regions (+500/-300) was required prior to plasmid shuffling. Selection occurred on -Leu plates, as pRS315 also codes for the *LEU2* marker gene.

Plasmid shuffling enables to substitute the essential Arp4 gene with Arp4 mutants, which were cloned onto a pRS315 vector. Subsequent colony growth on two subsequent 1% (w/v) FOA (5-fluorooretic acid) YPD or -LEU agar plates selected for yeast colonies harboring only the pRS315 plasmid.

A gene coding for a fusion protein of Arp4 and actin connected by a Strep II, PreScission site and FLAG linker between Arp4's C- and actin's N-terminus, with the flanking genomic sequence of Arp4 was also cloned onto the pRS315. Plasmid shuffling on 5-FOA plates with Δ*arp4* strains bearing pRS316 +500 Arp4 -300 replaced Arp4 with the accordant fusion protein.

2.8.2 DNA damage hypersensitivity of Arp4 mutants

Different Arp4 mutants as well as Arp4-actin fusion constructs with actin or Arp4 mutations were compared with the wild-type complemented yeast strain with respect to their generation time and also with respect to their resistance to genotoxic agents such as 20 mM HU (hydroxyurea), 0.005% MMS (methyl methanesulfonate), 5 µl/ml CPT (camptothecin) or 0.19 µg/ml 4-NQO (nitroquinoline-1-oxide).
HU is an inhibitor of ribonucleotide reductase and therefore leads to DNA double strand breaks due to stalled replication forks [127]. MMS induces heat-labile damage that is repaired by the base excision repair, not by homologous recombination (HR) in both *S. cerevisiae* and mammalian cells. The reason that recombination-deficient cells are sensitive to MMS is due to the role of HR in repair of MMS-induced stalled replication forks [128]. CPT binds to a topoisomerase I - DNA complex and impairs transcription and DNA replication, resulting in fork stalling and in subsequent formation of DNA double-strand breaks [129]. 4NQO has often been referred to as a UV mimetic agent. DNA damage caused by 4NQO is therefore repaired by nucleotide excision repair, but 4NQO might also lead to chromosomal breaks [130].

2.9 Electron microscopy

Electron microscopy uses highly accelerated electrons to push the Abbé limit towards nanometer resolution. In case of highly symmetric structures, such as icosahedral viruses, cryo-electron microscopy can reach near atomic resolution [131]. The major limitation of electron microscopy in structural biology is the required size of the protein specimen, which is roughly supposed to be larger than 200 kDa.
Biological samples do not provide high contrast as they are not electron-dense and interact weakly with electron radiation. Therefore, heavy atom staining with i.e. uranylacetate is a common method to produce phase contrast. Compared to cryo-EM, uranylacetate stained probes are less affected by radiation damage and sample preparation is relatively easy. The drawbacks of heavy atom staining are

limited resolution and possible artifacts due to unevenly distributed stain and the granular or microcrystalline nature of desiccated uranyl-acetate [132].

In order to assess a possible interaction of the subcomplex I (Arp8-Arp4-actin-HSA) or Arp4 and Arp8 alone with actin filaments, the proteins were incubated with 5 nm Ni-NTA nanogold, which targets His-tagged proteins [133]. This was performed by Dr. Kristina Lakomek (AG Hopfner). Arp4 and Arp8 used for this experiment contained an N-terminal hexa histidine-tag, while the HSA domain within subcomplex I was conjugated with an N-terminal octo His-tag. Prior to use, the nanogold-labeled proteins were purified by size exclusion chromatography on an S200 5/150 GL column from possible aggregates and excess of nanogold to obtain monodisperse samples.

Actin was polymerized in KMEI buffer (according to chapter 2.6.1) for 30 min to yield a stock of 5 µM actin filaments. F-actin with a final concentration of 2 µM was incubated with 0.02 µM of gold-labeled and SEC purified Arp4, Arp8 or subcomplex I for 30 minutes at 4°C. Subsequently staining was performed with 2% uranyl-acetate and the samples were subjected to carbon coated copper grids (kindly provided by Charlotte Ungewickell, AG Beckmann), air-dried and kept at room temperature until further use.

Electron microscopy images with different magnifications were taken with a Morgagni 100kV electron microscope (FEI, Eindhoven/Netherlands) and captured by a side-mounted SIS Megaview 1K CCD camera.

2.10 Protein biochemistry

2.10.1 ATPase assay

Actin-related proteins bear an ATP binding site and are therefore potential ATPases. Actin itself is a very weak ATPase as a monomer but is activated in the filaments or upon factor binding to its target binding cleft. All Arps as well as the Arp8-Arp4-actin-HSA subcomplex I showed no significant activity in a BIOMOL green assay (Enzo Life Sciences) under standard conditions and therefore we probed for ATPase activity using a more sensitive ATPase activity assay with radioactively labelled ATP.

All reactions were performed in 50mM Tris-HCl pH 7.9, 100mM NaCl, 2mM $MgCl_2$, 2mM DTT with 100 µM ATP including 5nM radioactively labeled [γ-^{32}P]ATP (Hartmann Analytic, Braunschweig). Increasing concentrations of protein (yeast Arp4, yeast Arp8, yeast subcomplex I, human Arp8) were incubated in presence or absence of nucleosomes or constituents thereof at 30°C for 30 min or 4 h. Free

phosphate, indicative of ATP hydrolysis and also nucleotide exchange, was separated by thin-layer chromatography on TLC PEI cellulose F (Merck, Darmstadt) with 1 M formic acid containing 0.5 M LiCl, then incubated on storage phosphor screens (GE Healthcare, Heidelberg) for at least 3 hours. Phosporescence was scanned on a STORM 860 scanner (Molecular Dynamics, Sunnyvale USA) and images were analysed using ImageJ.

2.10.2 Nucleosome affinity assays

The qualitative binding of Arps to chromatin and especially histones has been reported in the literature [39, 134] but the quantitative description of binding affinities has not been performed previously. It also remained unclear to what extend actin-related proteins contribute to nucleosome binding in their chromatin remodeler environment. Therefore, fluorescence based affinity assays were performed in collaboration with Duane Winkler, PhD in Prof. Karolin Luger's group.

The microplates were prepared by sequential washing with 1 M HCl, 1% Hellmanex, and Sigmacote. Each wash step was incubated for 30 min and followed by extensive rinsing with distilled water. The plates were then air-dried under an exhaust hood for 8 hours to overnight. The individual binding experiments were derived from titration of highly concentrated stocks of the recombinant Arp constructs and complexes (assay concentrations ranging from 1-5000 nM) into the fluorescently labeled histone complexes or nucleosomes. The H2A-H2B and H3-H4 complexes were labeled through Alexa 488 maleimide conjugation to H2B T112C or H4 E63C, respectively. The 30 base-pair '601' sequence linker DNA was first modified with a 5' C6 amine then conjugated with a succinimidyl ester derivative of the Atto 647N dye. The fluorescently labeled DNA was then agarose gel purified to remove excess free dye. The two-step labeling procedure has previously been described elsewhere [135].

The labeled histones, nucleosomes, etc. were kept at a constant concentration between 0.5-1 nM with a final volume of 40 µL. The reaction conditions were maintained at: 20 mM Tris-HCl pH 7.5, 150 mM KCl, 5% glycerol, 1 mM TCEP, 0.01% CHAPS, and 0.01% octylglucoside. The titrations were then allowed to equilibrate at room temperature for 20-30 minutes (in the dark) and then scanned in-plate using a Typhoon 8600 variable mode fluorimager. Specific binding events were considered as a function of the fluorescence change (whether positive or negative) across the titration series. Interactions with affinities above 5000 nM are considered to be non-specific. The fluorescence change upon binding had to be higher than 10% of the total fluorescence signal to be evaluated. The actual fluorescence signal change was quantified using the program ImageQuant TL. Data analysis and non-linear fitting of the data was

done with Graphpad Prism. All experiments were performed in replicative quadruplicates. For a more detailed explanation of the equations and reactions schemes refer to previous works from the Luger laboratory [136, 137].

3. Results

3.1 Expression and purification of Arps and their respective complexes

One prerequisite for the biochemical characterization of proteins and in particular for their crystallization is the generation of abundant and highly pure protein. Proteins that are associated within complexes often possess intrinsic unfolded domains, which aggravate their soluble expression. Actin-related proteins (Arps) directly bind to chromatin substrates and are generally members of large multi-subunit protein machineries. Therefore, expression and purification of Arps pose several challenges, some of which have been solved previously [97].

Full-length Arps have exclusively been expressed in baculovirus based insect cell expression system, while N-terminally truncated constructs of Arp8 could also be expressed in *E. coli* BL21 (chapter 2.2).

All proteins had an N-terminal histidine-tag that enabled an initial purification step via Ni-NTA resin. This was particularly important for heterologous proteins expressed in insect cells, because it was generally necessary to perform a one-step purification and SDS-PAGE analysis of the fraction after expression tests in order to know, whether the protein of interest was made. Whole cell extracts of insect cells commonly obscured heterologously overexpressed proteins on SDS-PAGE gels.

Large-scale purifications of proteins or protein complexes were subjected to anion exchange chromatography after the Ni-NTA purification step (chapter 2.3). Yeast Arp8, in particular the full-length protein, interacts very tightly with Q-sepharose and elutes roughly around 400 mM NaCl or KCl. Therefore, monomeric yeast Arp8 and protein complexes containing yeast Arp8 can be very efficiently purified via anion exchange chromatography. As Arp8 and especially subcomplex I are nucleosome binding proteins (see below), nucleic acids are co-purified on the Ni-NTA resin. DNA and putatively RNA however can also be separated from these proteins on Q-sepharose columns, since nucleic acids have an even tighter affinity and elute around 700-900 mM salt. Human Arp8 does not bind to either anion or cation exchange columns in a pH range between 6 and 8. Nonetheless, since the bulk of endogenous *T. ni* insect cell proteins and nucleic acids bind to Q-sepharose, anion exchange chromatography is a suitable second purification step also for human Arp8. For crystallization set-ups, the histidine-tag of human Arp8 was cleaved by PreScission protease and the flow-through of a subsequent second Ni-NTA purification was collected, prior to anion exchange chromatography (figure 6C). The final purification step was a size exclusion chromatography that separates the homogeneous, monodisperse protein

sample from potential aggregates (figure 6A-C). Subsequently, the purified protein or protein complex was concentrated up to 25 mg/ml without signs of aggregation.

Interestingly, after heterologous expression of Arp8 and Arp4 together with the HSA domain (INO80 A462-F685) from *T.ni* H5 insect cells, purification leads to an assembled subcomplex I with actin that was retained from the expression host. Mass spectrometric analysis of peptides derived from trypsin digestion revealed an actin isoform that is related to the actin 5C isoform of *D. melanogaster* (figure 6B).

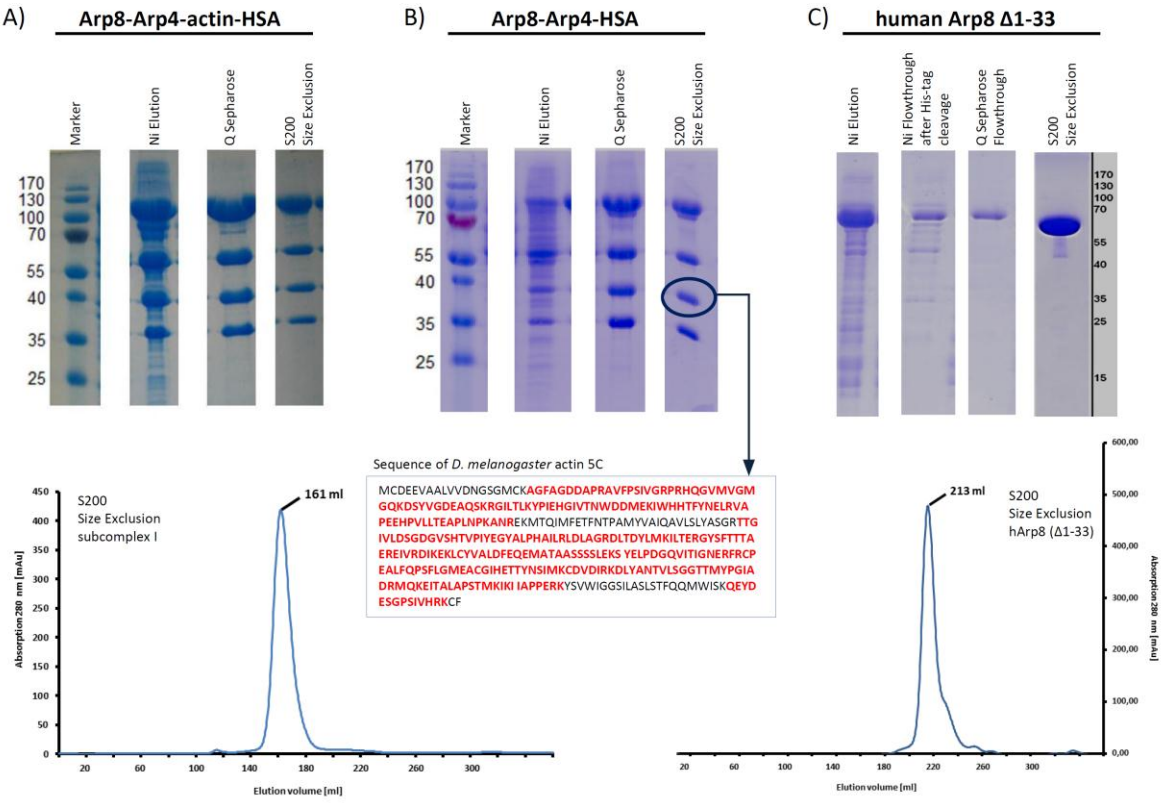

Figure 6: Purification of INO80 subcomplex I and human Arp8

A) SDS-PAGE analysis of subcomplex I (Arp8-Arp4-actin-HSA) after the individual purification steps yielding a monodisperse and very pure tetrameric complex. B) SDS-PAGE analysis of subcomplex I that retained actin (blue encircled) from the expression host. Mass spectrometry analysis after tryptic digest revealed peptide sequences (red) that largely align with the *D. melanogaster sequence* of actin 5C. C) SDS-PAGE analysis of human Arp8 after each purification step.

3.2 The crystal structure of human Arp8

In order to contribute to the explanation how Arp8 is able to fulfill the broad range of different functions (chapter 1.3.2), a truncated version of human Arp8, lacking the first N-terminal 33 amino acids (hArp8 (Δ1-33)) was crystallized in 3.9 M NaCl, 0.5 % (v/v) methanol, 50 mM Mes pH 6.1, mixed 1:1 with 4.5 mg/ml of protein solution at 16°C. This gave rise to small crystals that were used as seeds within the same condition at 10°C. Crystals grew for several weeks until they had suitable sizes for X-ray diffraction measurements (Figure 7).

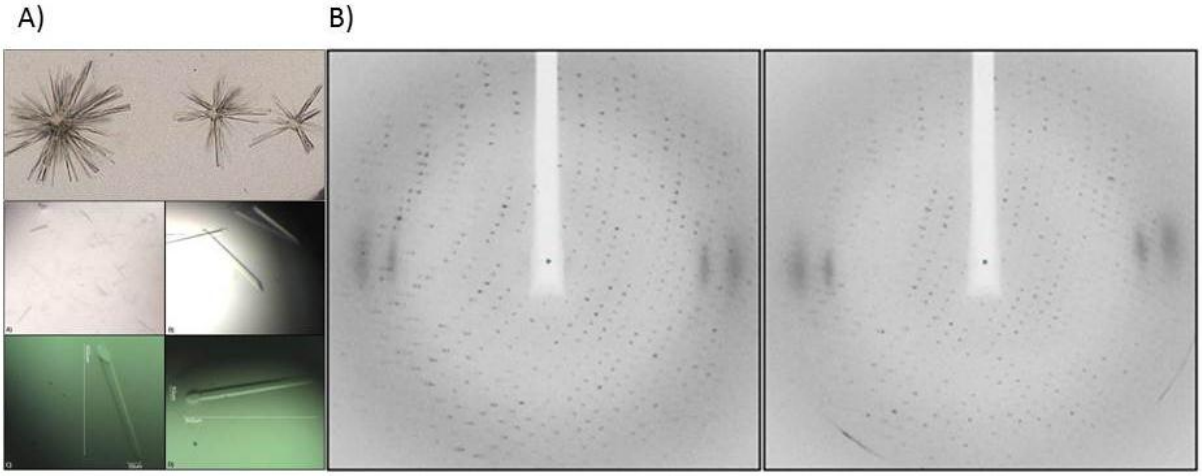

Figure 7: Crystallization of human Arp8 (Δ1-33) and the diffraction pattern of hArp8 crystals.
A) Initial hits in the high NaCl conditions of the Magic 1 screen that were further refined to yield crystals that diffracted to 2.6 Å. (B) Diffraction pattern of hArp8 (Δ1-33) crystals at beamline X06SA (PX-I) at the SLS (Swiss Light Source), Villigen / Switzerland.

Subsequently, the crystal structure of hArp8 (Δ1-33) with one molecule in the asymmetric unit was determined in space group $C222_1$ and 2.6 Å resolution (Table 8). Phases were derived from molecular replacement using PHASER with a structural model based on yeast Arp4 (3QB0) that has been crystallized previously in the laboratory [97]. Automatic model building with ARP/wARP yielded a very good initial model that was improved manually using COOT and refined with PHENIX (chapter 2.4.4).
Despite the relatively low sequence homology to actin, human Arp8 harbors the predicted actin fold [41] as its core structure.

Table 8: Data collection and refinement statistics

Data collection	
Space group	$C222_1$
Cell dimensions	
a, *b*, *c* (Å)	80.88 151.26 173.35
α, β, γ (°)	90, 90, 90
Resolution (Å)	86.68-2.59 (2.75-2.59)*
R_{obs} (%)	7.9 (67.0)
$I / \sigma(I)$	14.16 (2.17)
Completeness (%)	99.2 (98.8)
Redundancy	3.6 (3.5)
Refinement	
Resolution (Å)	44.90-2.60 (2.68-2.60)
No. of reflections	32837
R_{work} / R_{free} (%)	16.34 / 20.95
No. of atoms	
Protein	4051
Ligands/ions	93
Water molecules	146
B factors (Å^2)	
Protein	50.04
Ligands/ions	55.38
Water	44.84
R.m.s. deviations	
Bond lengths (Å)	0.008
Bond angles (°)	1.185

*Values in parentheses are for highest-resolution shells.

A structure based sequence alignment of human Arp8 with actin (figure 8) reveals that hArp8 contains five notable insertions in addition to an elongated N-terminal part at the hot spots for Arp mutations [49] as well as a few additional amino acids and also one deletion compared to canonical actin.

Monomeric and filamentous actin have been concisely reviewed recently [138] and serve as basis to discuss the structure of human Arp8.

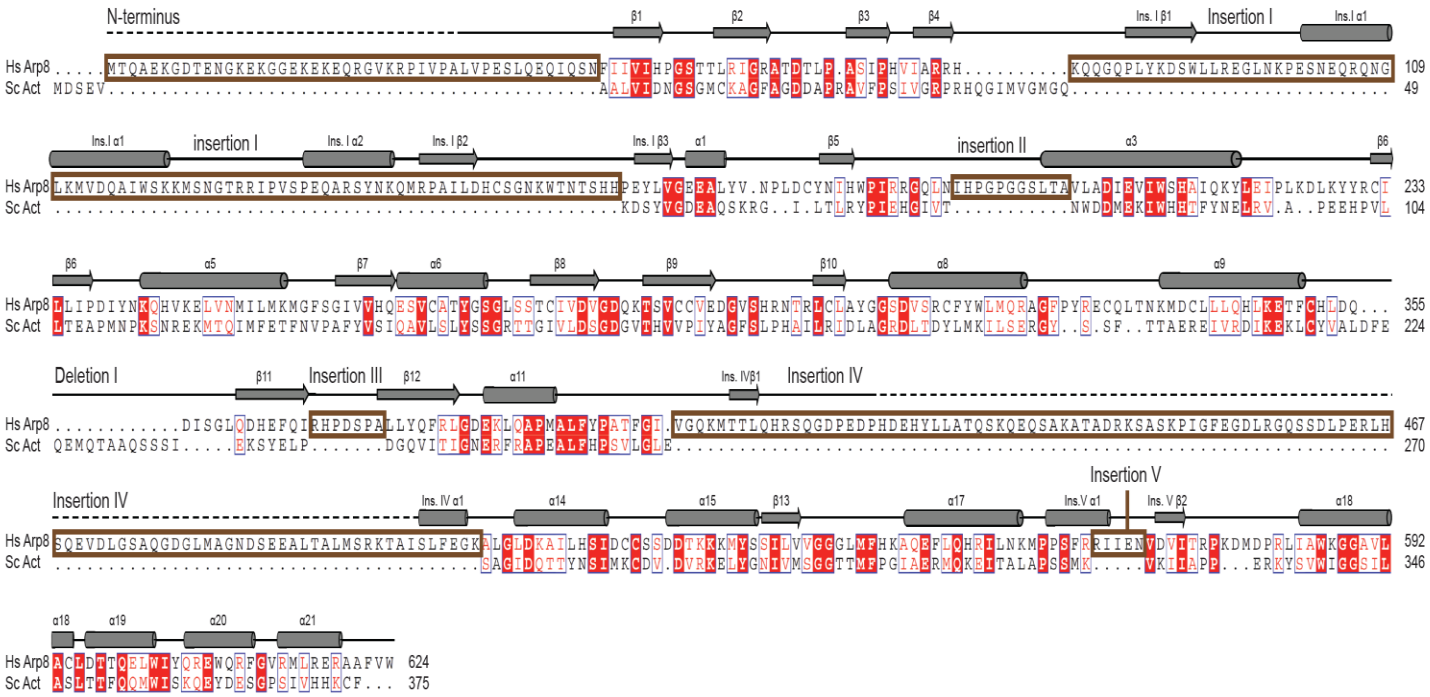

Figure 8: Structure based alignment of the amino acid sequence of human Arp8 in comparison with yeast actin. Human Arp8 possesses five distinct insertions to the actin fold next to the N-terminal tail. Moreover, a charged knob (K577-M579) and three hydrophobic amino acids (F622-W624) at the C-terminus are additional insertions to the actin fold.

Except for 91 amino acids (R411 – I501), which are part of one insertion to the actin fold, interpretable electron density for the rest of the protein construct used for crystallization was obtained.

Similar to actin, the structure of human Arp8 has a central nucleotide-binding cleft between subdomains 1 and 2 at the so called pointed end side and a target binding cleft between subdomains 3 and 4 at the barbed end (figure 9).

Engulfed by subdomains 1-4 in the center of the molecule, electron density was visible that could clearly be assigned to bound Mg^{2+} - ATP (chapter 3.4).

The N-terminal tail of human Arp8 (M1 – N46) is rather small in comparison to other Arp8 homologues, but still comprises 46 mostly charged residues and is situated towards the barbed end of the molecule. The *Saccharomyces cerevisiae* Arp8 N-terminus for example consists of 250 mostly charged residues, which might have implications in nucleosomal substrate binding (chapter 3.9).

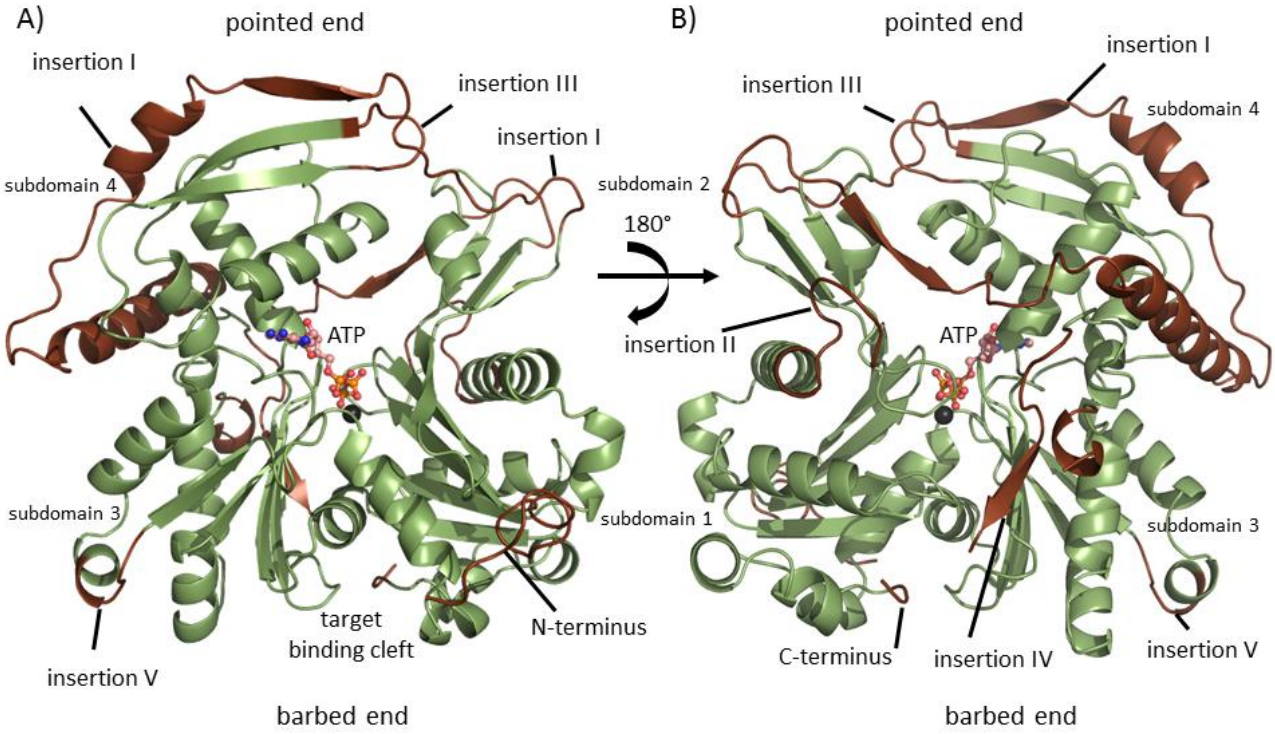

Figure 9: Crystal structure of human Arp8 (Δ1-33)
A) Classical view of the structure of Arp8 in the cartoon illustration with a bound ATP nucleotide in spheres and sticks representation. Arp8 has the core actin fold (green) comprising subdomains 1-4 engulfing the bound nucleotide. Five insertions and the elongated N-terminal region (brown) emanate from the actin fold. B) On the backside of the Arp8 molecule insertion IV originates from the hydrophobic plug region of the actin fold. However, insertion IV is largely not part of the structural model due to the lack of electron density in this region.

3.2.1 Insertions I-III rigidify the pointed end of Arp8

The first very large insertion I (K80 – H162) of human Arp8 emanates from the DNaseI binding loop (D-loop) of the actin fold and reaches over the filament facing side of the actin and forms a long helix next to subdomains 3 and 4 of the actin fold (E101 – S119), which stands out in an angle of almost 60° with respect to the center axis of the actin fold. This long helix is the most evident addition to the basal actin structure seen in the electron density and very likely to contribute to the specific functions of Arp8. Furthermore, insertion I takes a turn and progresses parallel to subdomain 4 forming a second helix (P133 – Q142) and subsequently participates in the formation of an antiparallel β-sheet (A146 – D149) with subdomain 4. Finally, it reaches back to the D-loop, covering the pointed end and hence the ATP binding cleft like a lid.

This insert is clearly a main factor that contributes to the inhibition of polymerization capability (chapter 3.3). It strongly alters the configuration of actin's D-loop, which in the actin filament reaches into the target-binding region at the barbed end of the adjacent intra-strand actin molecule [69].

The subsequent insertion II (N192 – A203) forms a loop that protrudes from the actin core between subdomains 1 and 2 resembling a second hydrophobic plug. This insert also adds an additional turn to the α-helix that is located at the transition from subdomain 2 to 1. Since the sequence of insertion II is rather hydrophobic, its physiological function is likely to involve protein-protein interactions. It is also located in proximity to the ATP binding site of Arp8, which hints towards a possible role of this insertion in the putative ATPase activity of Arp8.

The third insertion comprises only seven amino acids (R368 – A374). Nevertheless, it is a characteristic feature that aids the lid of insertion I to cover the ATP binding cleft. Insertion III expands an antiparallel β-sheet connected via a short loop by approximately 10 Å and thereby it contributes to the significantly altered surface structure of Arp8's pointed end.

Overall one can state, that insertions I-III interact with one another to wrap around both halves of the actin fold and to cover most of the pointed end of the actin fold. This rigidifies the conformation of Arp8 in contrast to actin, where subdomains 2 and 4 do not interact with one another and ATP hydrolysis and P_i release lead to a moderate swivel motion of the two principal domains. Moreover, several surface exposed hydrophobic residues as well as bound glycerol from the crystallization solution suggest, that insertion I-III also participate in protein-protein interactions.

3.2.2 Insertion IV is the second major insertion to Arp8's actin fold

The second major insertion (insertion IV) (V401 – K507) emanates from what comprises actin's hydrophobic plug and is situated on that side of actin that participates in filament formation. This insertion did not give rise to interpretable electron density after refinement except for a few residues and therefore structural information of this part remains scarce.

The fact that this insertion did not yield interpretable electron density suggests that it is highly flexible and less structured, which is in line with algorithms that propose this particular sequence to be disordered with only minor secondary structure motifs (figure 10) [139, 140]. This renders insertion IV to be a perfect candidate for various protein-protein interactions and it appears to contribute to the formation of subcomplex I (chapter 3.6).

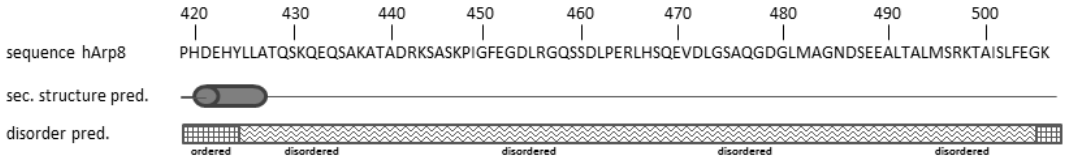

Figure 10: Secondary structure and disorder prediction of insertion IV.
The part of insertion IV that did not give rise to electron density likely possesses very little secondary structure (calculated by JNet) and is mostly disordered (calculated by DISOPRED2). Programs are available on the Gene Center Bioinformatics Toolkit page (http://toolkit.lmb.uni-muenchen.de).

3.2.3 Subtle alteration at Arp8's barbed end by insertion V

The subsequent insertion V (R565 – N569) is a relatively small insertion in human Arp8 that introduces a short α-helix into the actin structure at the outer end of the barbed end of subdomain 3 (figure 9). Despite being a rather subtle alteration, this helix is the most evident structural change at the barbed end of the actin fold followed by the slight elongation of the C-terminus by three bulky residues. Whether these differences alter the barbed end side of Arp8 significantly enough to prevent actin or other proteins from binding is not clear. This seems unlikely since most of the predominantly hydrophobic amino acids within the target-binding cleft are conserved and share great sequence identity with actin even in comparison to other aligning regions of Arp8's actin fold.

3.2.4 Structure based conservation analysis

Arp8 is conserved from yeast to man with the exception of algae, Apicomplexa and the two Metazoan phyla *Caenorhabditis elegans* and *C. intestinalis* [49]. As expected, the actin fold amino acid sequence of Arp8 in different species is highly conserved. In a sequence alignment of Arp8 from *Homo sapiens*, *Mus musculus*, *Xenopus laevis*, *Danio rerio*, *Drosophila melanogaster* and the acon worm *Saccoglossus kowalevskii*, it becomes clear that also the insertions to the actin fold show considerable sequence homology (figure 11). Insertion IV (V401-K507) shows the least conservation among the insertions, while insertion II (N192-A203) is the most highly conserved. Insertion III also depicts high sequence identity. Interestingly, insertion V (R565-569) is absent in *Drosophila melanogaster* but otherwise shares high sequence homology among species. Insertion I (K80-H160) is partially conserved. Especially, the prominent secondary structural features also possess high sequence identity, while the long stretches that wrap around the actin fold are less conserved.

The three hydrophobic C-terminal residues show almost 100% sequence identity and also the lysine of the charged knob (K577-M579) is present in all species.

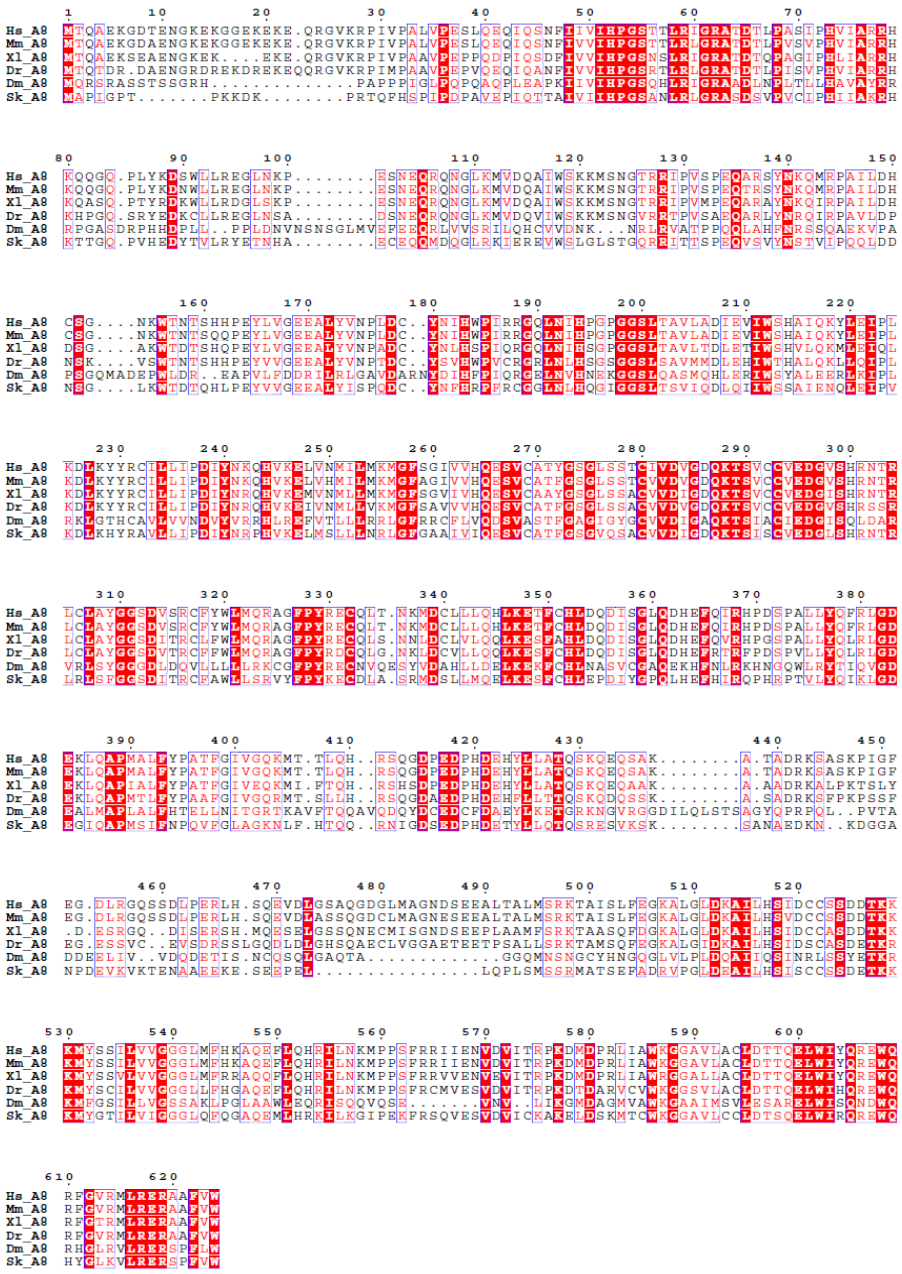

Figure 11: Multiple amino acid sequence alignment of Arp8 orthologues.
Amino acid sequences corresponding to orthologues of human Arp8 were obtained from the NCBI protein database (http://ncbi.nlm.nih.gov). Abbreviations are defined as follows: Hs, *Homo sapiens*; Mm, *Mus musculus*; Xl, *Xenopus laevis*; Dr, *Danio rerio*; Dm, *Drosophila melanogaster*; Sk, *Saccoglossus kowalevskii*. The multiple sequence alignment was generated using ClustalW (http://www.ebi.ac.uk/Tools/msa/clustalw2/) and formatted for presentation with EsPript (http://espript.ibcp.fr/ESPript/ESPript). The amino acid sequence numeration corresponds to the human protein.

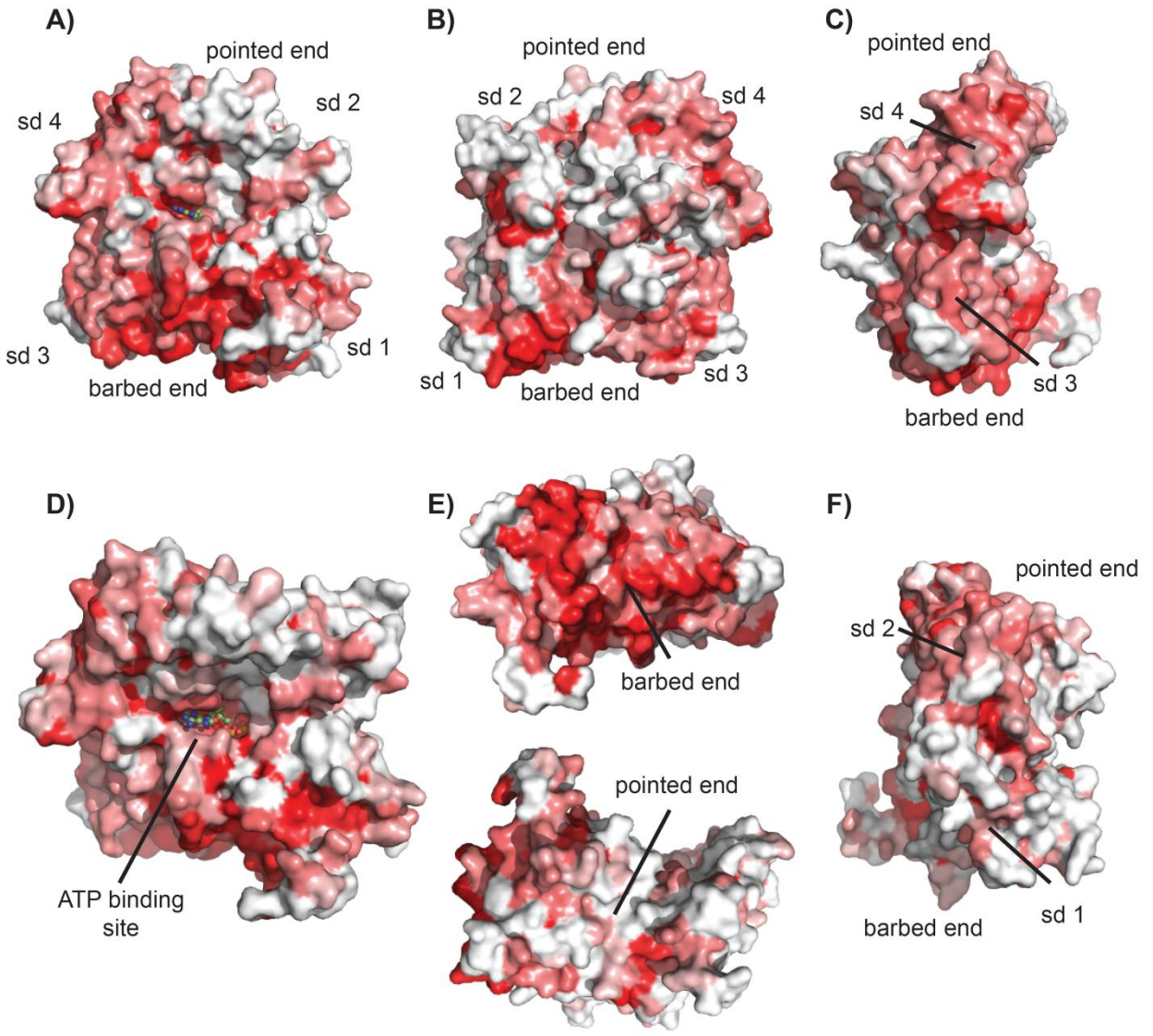

Figure 12: Sequence conservation in a surface representation of human Arp8.
Molecular surface representations of human Arp8 colored according to amino acid conservation scores calculated from multiple sequence alignments of human Arp8 by the ConSurf web server (http://consurf.tau.ac.il): from red (absolutely conserved) to white (not conserved). Human Arp8 in the classical view of the actin fold (A) and rotated by 180° (B). (C) Side view on subdomains (sd) 3 and 4 (inner domain) show that they are more conserved than the side of subdomains 1 and 2 (F). (D) The accessible ATP binding site is highly conserved. (E) The barbed end and especially the target-binding cleft of Arp8 are more conserved than the pointed end. (F) Side view on subdomains 1 and 2 (outer domain) show less conservation compared to the inner domain (C).

An according conservation surface representation of human Arp8 (figure 12) visualizes that especially the barbed end of Arp8 is highly conserved. This is particularly noteworthy as the barbed end shows little structural changes to the barbed end of actin except for the subtle alterations of insertion V (R565-N569) and the three C-terminal hydrophobic residues F622-V623-W624.

3.2.5 Insertions to the actin fold explain Arp8's lack of polymerization capability

All in all, major changes to the pointed end and the filament facing side of the actin fold (figure 13) serve as explanation why Arp8 itself cannot form filaments. However, as only two out of three interfaces involved in polymerizing comprise large structural differences, the structure also gives leeway for possible interactions of Arp8 with canonical actin's pointed end or actin-binding proteins (ABPs) that bind to Arp8's accessible target-binding cleft. Also, it must be noted that Arp8 is still capable to form a complex with Arp4 and actin at the HSA domain of the INO80 complex [12, 39].

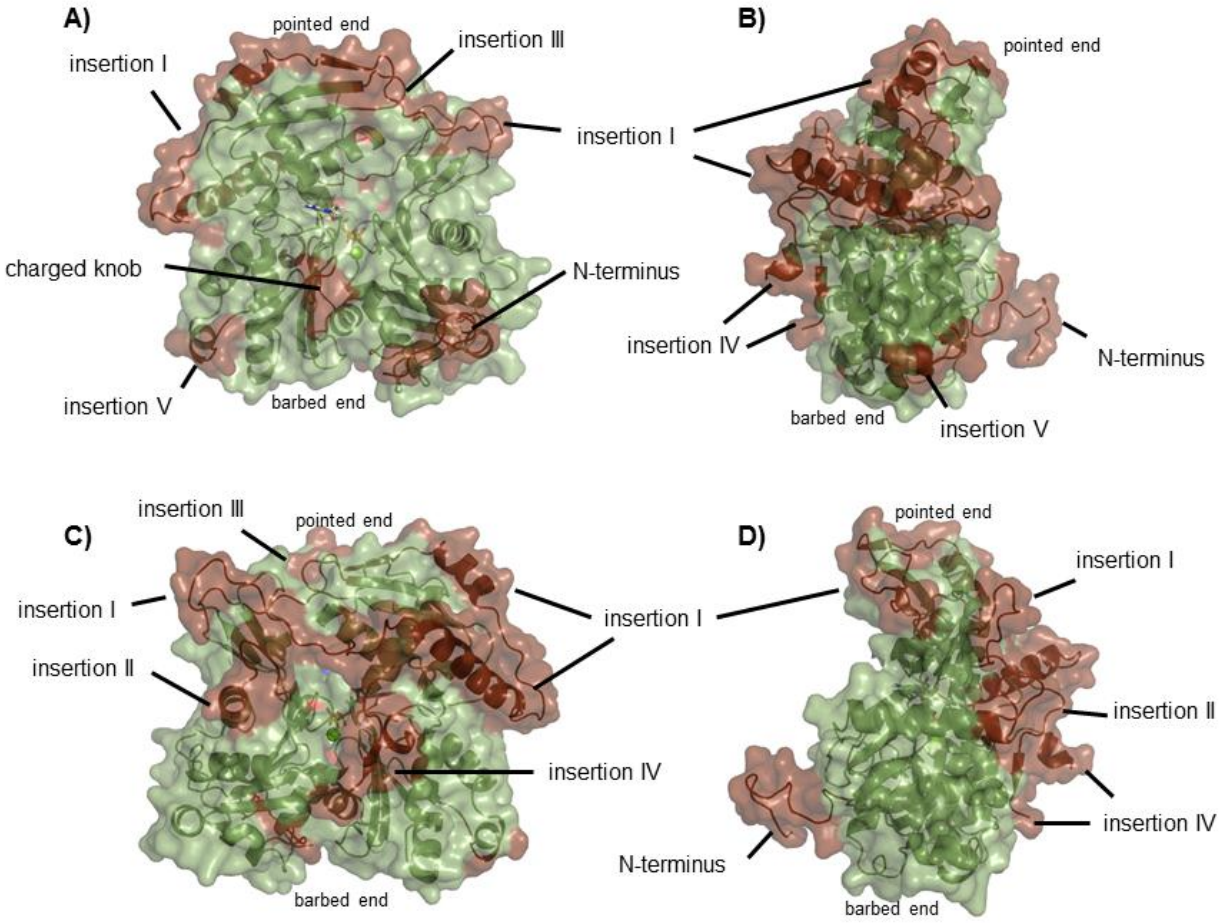

Figure 13: Surface representations of human Arp8.
The Surface presentations highlight the insertions of Arp8 (brown) compared to the basal actin fold (green). (A) The classical view on the actin fold depicts the closure of the pointed end of human Arp8, but otherwise only minor changes to the surface of the actin fold. (B) View onto the inner domain of the actin fold. Here, insertion I markedly alters the surface at the pointed end side of the inner domain. (C) Rear view of the actin fold. Insertion I reaches over this "filament-facing" side of actin and insertion IV, which mostly lacks in the density, emanates from the hydrophobic plug of the basal actin fold, (D) The view onto the outer domain of the actin fold shows only minor changes compared to the actin core.

3.2.6 Arp8 crystal contacts

Symmetric crystal contacts between N-terminal and C-terminal residues of two adjacent Arp8 (Δ1-33) molecules formed in the crystal lattice might shed light on a possible interaction between two human Arp8 proteins that could also have physiological relevance.

The crystal structure of hArp8 was submitted to the PDBe server PISA (Protein Interfaces, Surfaces and Assemblies) [141] and the complex formation significance score (CSS) was calculated to be 0.186 for one dimer generated by symmetry operation, which indicates that the interface could play an auxiliary role in complex formation. The interface area comprises an area of 1126 $Å^2$ and involves 38 amino acids of each truncated monomer. Six hydrogen bonds (distances < 3.25 Å) are involved and contribute to a calculated interface Δ^iG of -15.6 kcal/mol. The missing N-terminal amino acids (M1-A33) in the crystallized construct comprise a characteristic sequence motif of alternating lysine and glutamate residues, which might add several more contacts for a possible human Arp8 dimerization.

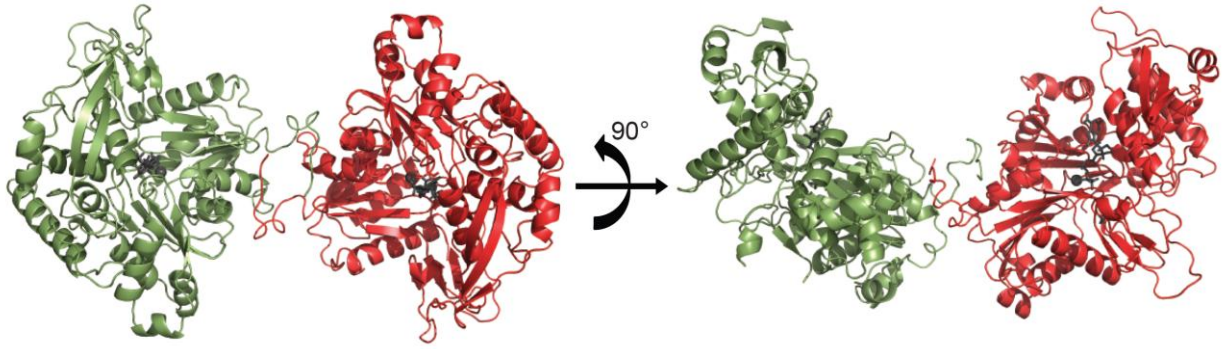

Figure 14: Dimer of human Arp8 formed in the crystal.
Two human Arp8 (Δ1-33) molecules (green and red) contact each other at the truncated N-terminus and C-terminal residues. The mostly hydrophobic surface area comprises 1126 $Å^2$ and could serve as an auxiliary interaction surface in dimer formation.

3.3 Arp8 is monomeric in solution

3.3.1 SAXS envelope structure of Arp8

The solution structure of human Arp8 was determined by SAXS (small angle X-ray scattering) and the oligomerization state was examined by SLS (static light scattering) measurements to endorse possible Arp8 polymerization or dimerization. The SAXS analysis of *S. cerevisiae* Arp8 already determined Arp8 to be monomeric in solution [59] and this was also confirmed for full-length and truncated (Δ1-33) human Arp8 (figure 15). The Kratky plot (figure 15B) indicates that the protein sample was properly folded and the P(r) distribution already suggests that human Arp8 consists of a large globular domain with a smaller protrusion (figure 15C).

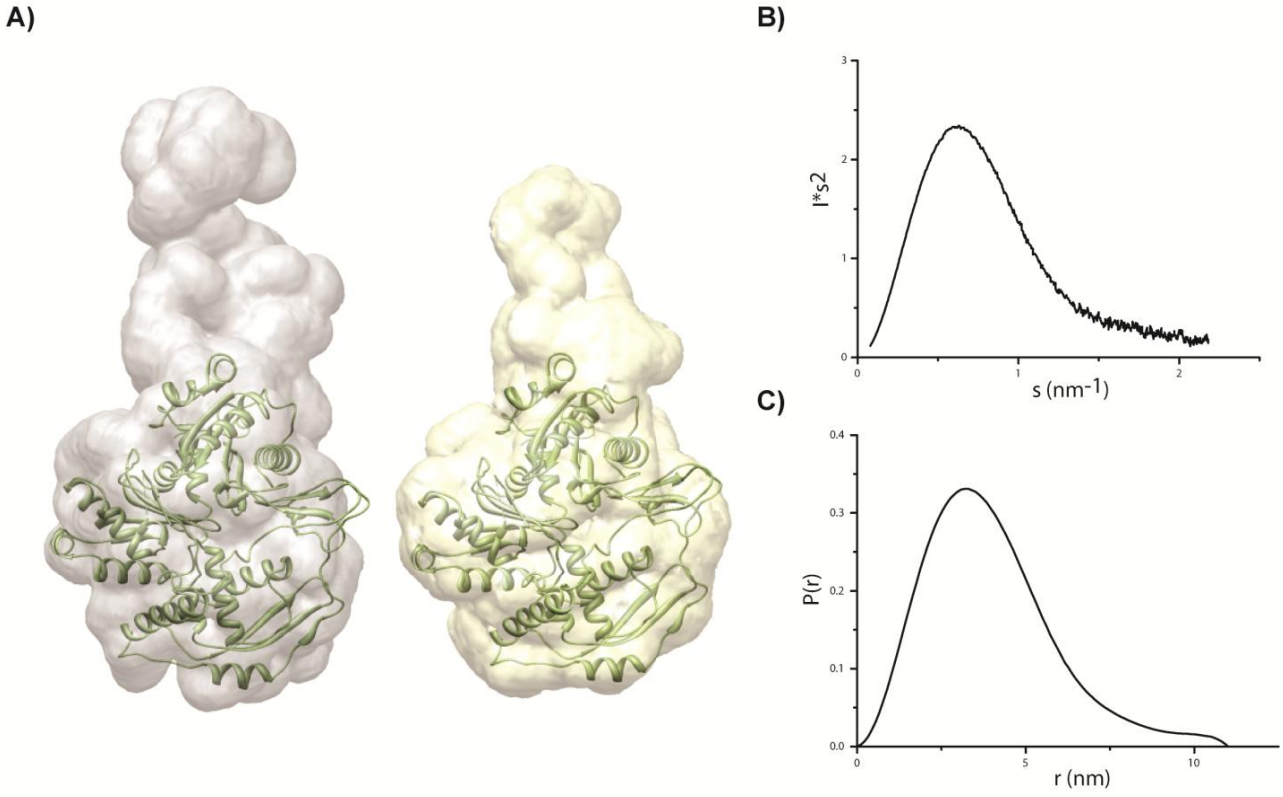

Figure 15 : Small angle X-ray scattering (SAXS) structure of human Arp8.
(A) Comparison of SAXS *ab initio* structure envelopes for full-length (grey) and the N-terminally truncated human Arp8 (yellow) with the crystal structure of human Arp8 Δ1-33 (green) docked into the SAXS density. The protrusion at the top is slightly elongated in the full-length protein, but otherwise the SAXS structures are virtually identical.
(B) The Kratky plot ($I*s^2$ *vs.* s) of the truncated hArp8 shows a bell-shaped curve typical of a folded protein.
(C) The P_r distribution function shows a slight tailing to higher radii indicating a potential elongated protrusion as also seen in the *ab initio* models (A).

The final *ab initio* bead model agreeably provides space for the X-ray structure of Arp8 to fit in. Two major differences when compared to the actin envelope arise even at this low resolution: Full length hArp8 obviously possesses a protrusion that corresponds to the elongated N-terminus of Arp8, which is not present in actin. Furthermore, the solution structure of Arp8 does not show the typical flatness of actin but appears bulgy. This can be explained by parts of insertion I and the large Insertion IV covering the back side of Arp8. According to the SAXS envelope, the unresolved 92 amino acids of insertion IV (H410 – I501) are most likely packed onto the side of Arp8, from which insertion IV emanates (figure 16B). Since this side of the actin fold gives rise to important contacts for actin filament formation, insertion IV also seems to stabilize the monomeric state of Arp8 in solution.

Overall, the X-ray structure can be convincingly docked into the SAXS envelope and insertion IV that is mostly missing in the electron density can be allocated to the part of the bulge that spans over subdomains 1 and 3 on the back side. The molecular weight in solution calculated from Porod volume [116] were 78 kDa for full length Arp8 and 70 kDa for the crystallized construct (hArp8 Δ1-33)), which both indicate that human Arp8 like its yeast homologue is a monomer in solution (human Arp8 chain mass = 70.5 kDa, truncated construct = 66.9 kDa). This is also supported by the fact, that the theoretical scattering curve of monomeric hArp8 calculcated with CRYSOL from the crystal structure is clearly supporting the measured data, whereas the theoretical scattering curve of the potential hArp8 dimer (chapter 3.2.6) is deviating from the measured curves (figure 16A).

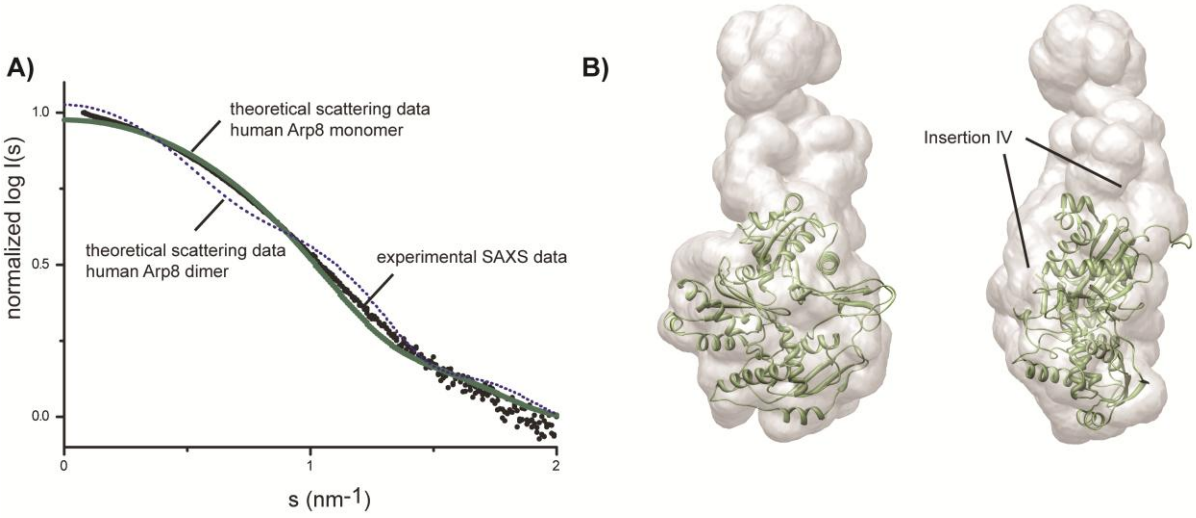

Figure 16. Solution structure of human Arp8.
(A) Theoretical SAXS scattering curves calculated with CRYSOL for monomeric and dimeric human Arp8 show that Arp8 is a monomer in solution. (B) X-ray structure of human Arp8 Δ1-33 docked into the *ab initio* SAXS model of full-length hArp8. The solution structure of human Arp8 provides extra density for insertion IV.

3.3.2 Static light scattering experiments with Arps

Additionally, size exclusion chromatography (SEC) was performed with subsequent static light scattering (SLS) measurements for a more accurate determination of the molecular weight compared to SEC alone. The molecular weights obtained by static light-scattering confirm the monomeric state of yeast and human Arp8 as well as of yeast Arp4 and the INO80 subcomplex I, consisting of Arp8, Arp4, actin and the HSA domain (table 9).

The results for every protein illustrate that all samples are monodispersely monomeric in solution and do not contain oligomerized species. Moreover, SLS with the purified subcomplex I clearly indicates, that it comprises only one of each Arps and monomeric actin.

Hence, there was no observation of any dimerization in solution for purified full-length yeast or human Arp8 nor for Arp4 or the subcomplex I. Therefore, the contacts made in the crystal lattice of truncated human Arp8 do at least not suffice for Arp8 dimerization in solution but might play a role in a putative Arp8 dimerization triggered by auxiliary factors, for instance upon binding to the nucleosome (chapter 3.9). It cannot be ruled out that the pseudo-symmetric nucleosomal substrate binds to more than one Arp8 molecule simultaneously triggering dimerization.

Table 9: Molecular weights of Arps and INO80 subcomplex I derived from SLS and SAXS data

Sample	Calculated monomeric molecular weight [kDa]	Molecular weight determined by SEC/SLS [kDa]	Polydispersity [M_W/M_N]	Molecular weight derived from Porod-volume (SAXS) [kDa]
human Arp8 (full-length)	70.5	70	1.001	78
human Arp8 (Δ1-33)	66.9	69	1.006	70
yeast Arp8	100.2	101	1.001	105
yeast Arp4	54.8	56	1.004	51
yeast subcomplex I (Arp8-Arp4-actin-HSA)	223.2	220	1.003	n.d.
BSA (calibration control)	66.5	68	1.003	n.d.

3.4 ATP is tightly bound to human Arp8

Electron density in the nucleotide-binding cleft of Arp8 (figure 17) clearly indicated the presence of a bound ATP molecule and a metal ion that coordinates the β and γ phosphates of the nucleotide in distances that would argue for a Mg^{2+} ion(approx. 2 Å). As neither ATP nor magnesium were added into purification buffers or crystallization setups, this observation strongly suggests the absence of significant ATPase activity for the human Arp8 monomer aloof from its remodeler host INO80 or other binding partners.

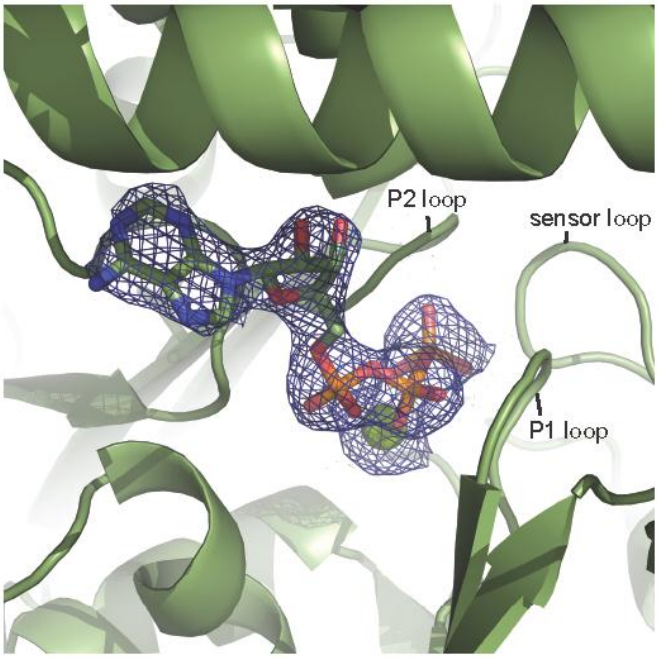

Figure 17: Electron density for ATP bound to human Arp8.
The blue mesh corresponds to the electron density of a simulated annealing $2F_oF_c$ omit map contoured at 5.0 σ. The bound ATP molecule is shown in stick representation and Mg^{2+} as sphere (light green). Surrounding regions of Arp8 harboring the nucleotide coordinating residues are represented in cartoon mode.

Arp4 crystals showed the same phenomenon, which indicates that Arp4 also strongly binds to ATP but lacks noteworthy ATPase activity. Actin itself is a very weak ATPase in its monomeric state and becomes stimulated > 40.000 fold in the filament [74]. Therefore it would be conceivable that Arps also show inducible ATPase activity, if the ATP binding site is similar to actin's. The nucleotide-binding site in Arp4, however, is significantly altered compared to actin. This argues for an exclusively structural role of ATP in Arp4 [59]. On the contrary, structural differences between actin and Arp8 are less pronounced, which is surprising since Arp4 is more closely related to actin than Arp8.

The most obvious structural difference between the ATP binding sites of Arp4 and actin is the shielding of ATP from the solvent within the nucleotide binding cleft. In Arp4, the α-helix covering the nucleotide (α9) of subdomain 4 is elongated by one and a half turns compared to actin, which causes a strong positional shift of this helix and protects the bound nucleotide [59]. The very same helix (α9) in Arp8 ($K337^{Arp8}$ – $F350^{Arp8}$) is not prolonged compared to actin ($T203^{act}$ – $L216^{act}$) [142] and shows only a very slight positional shift towards the nucleotide (figure 18).

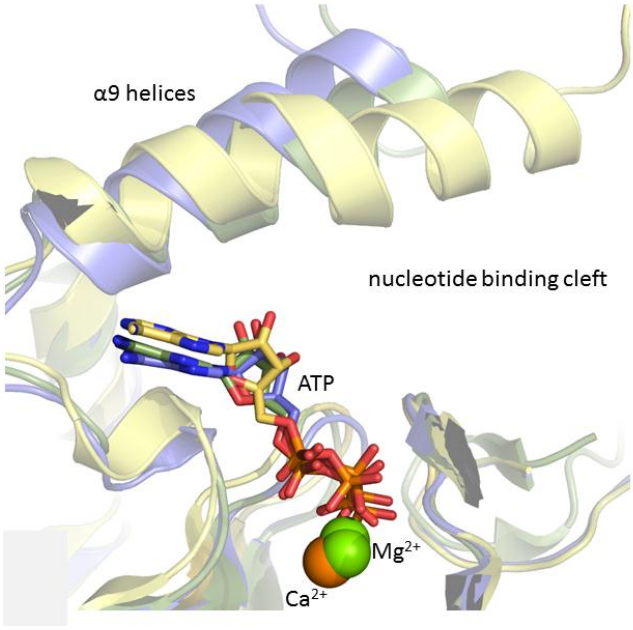

Figure 18: Comparison of the nucleotide binding cleft.
The alpha helix (α9) that covers the nucleotide binding cleft in Arp4 (yellow) is prolonged compared to actin (blue) and Arp8 (green). This results in a stronger shielding of the bound nucleotide. Additionally, electron density corresponding to the bound metal cation has a larger distance to the nucleotide in Arp4. Bond lengths argue for a Ca^{2+} in Arp4 instead of Mg^{2+}, which appears to be present in the structures of actin and Arp8. Overall, the nucleotide binding cleft of Arp8 resembles actin more compared to Arp4.

It must be noted that α9 of Arp8 has bulkier residues at the exit site of the nucleotide-binding cleft ($K337^{Arp8}$, $M338^{Arp8}$) compared to actin ($T203^{act}$, $A204^{act}$) and the lid of insertion I and the elongated β-strands of insertion III of Arp8 also cover the pointed end closing the cleft more tightly compared to actin. Therefore, it seems possible that these slight differences contribute to a putative stronger retainment of ATP in Arp8 compared to actin.

The catalytic cycle of ATP hydrolysis in actin has recently been reviewed [138]. In short, Mg^{2+}- ATP is engulfed by the P1 and P2 loops in actin at the bottom of the nucleotide binding cleft. The γ phosphate is coordinated by $S14^{act}$ *inter alia*. Activation of ATPase activity in the filament or via certain actin binding

factors occurs upon a slight conformational change that pushes Q137^{act} towards the γ-phosphate. Upon ATP hydrolysis and phosphate release, S14^{act} rotates to contact the β phosphate of the remaining ADP, allowing a methylated histidine meH73^{act}, located in the sensor loop, to penetrate into the space that was previously occupied by the γ phosphate (figure 19 C,F) [143]. This movement propagates along subdomain 2 to the D-loop influencing the width of the nucleotide-binding cleft as well as the conformation of the D-loop [144]. The rearrangements weaken the interaction with the adjacent intra-strand actin molecule, reducing the stability of the filament.

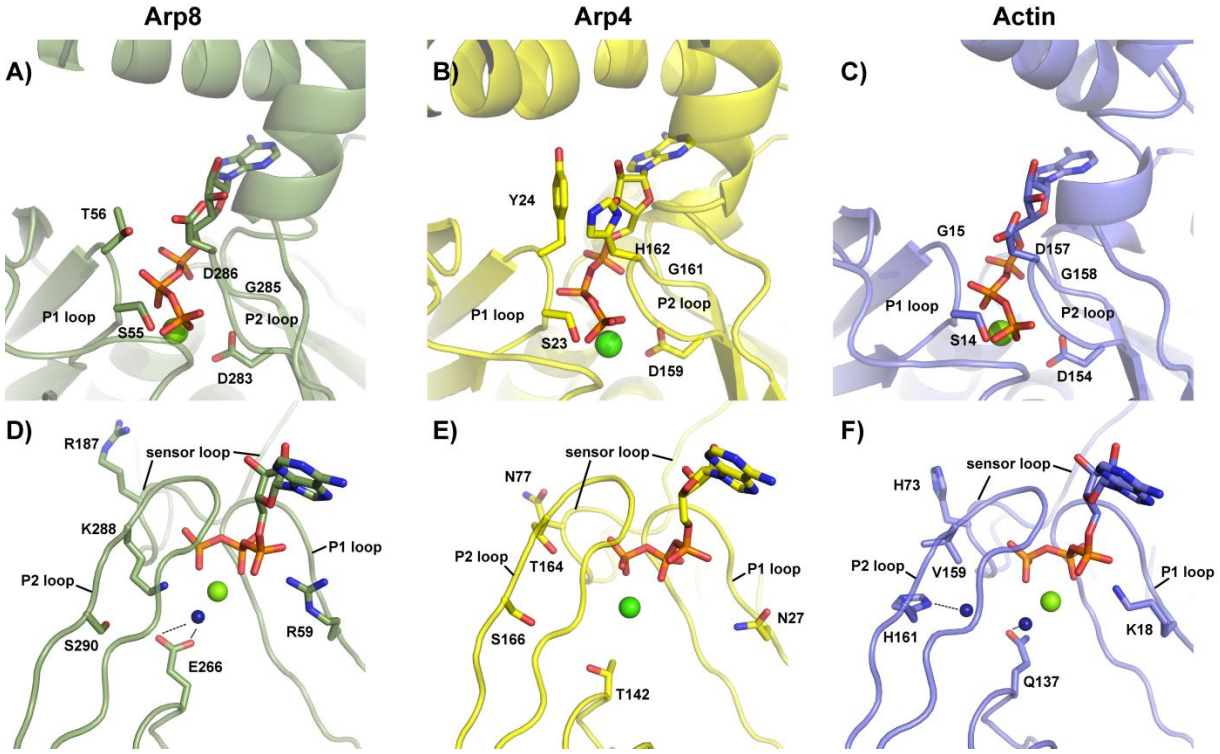

Figure 19. Close up of human Arp8's active site in comparison to Arp4 and actin.
(A,D) Human Arp8 coordinates ATP similar to actin. (B,E) ATP in yeast Arp4 (pdb: 3BQ0) is more shielded compared to actin or Arp8. (C,F) ATP in actin (pdb: 1YAG) is bound by residues in the P1 and P2 loops.

The "active" center of Arp4 appears to be an ATP binding site with degenerated ATPase activity. Alteration of active site residues in the P1 and P2 loops of Arp4, namely G15^{act} to Y24^{Arp4} and D157^{act} to H162^{Arp4}, further stack the ribose of the nucleotide and the substitution of catalytically active H161^{act} and especially Q137^{act} by S166^{Arp4} and T142^{Arp4} suggests, that the ATP in Arp4 does not hydrolyze enzymatically (figure 19 B,E) [59].

On the contrary, Arp8's nucleotide-binding site depicts only minor changes to the residues involved in the catalytic cycle of actin's ATPase. $G15^{act}$ of the P1 loop is replaced by $T56^{Arp8}$, which could in principle aid $S55^{Arp8}$ in complexing the β phospate, once hydrolysis and phosphate release is completed. The main residues involved in metal ion coordination and nucleotide-binding of the P2 loop remain the same in Arp8 compared to actin as $D154^{act}$, $G156^{act}$ and $D157^{act}$ structurally align with $D283^{Arp8}$, $G285^{Arp8}$ and $D286^{Arp8}$.

Filament-activated $Q137^{act}$ seems to play a critical role in ATP hydrolysis [145], as $Q137^{act}$ is in closer proximity to the γ-phosphate in polymerized actin [69, 146] and stimulates the ATPase more than 40,000 fold [74]. In Arp8 this residue is altered to $E266^{Arp8}$, which could basically fulfill similar tasks, if an interdomain rotation similar to the one happening in the filament can occur.

The histidine $H73^{act}$ of the sensor loop is substituted by $R187^{Arp8}$ in Arp8. Basically, it is conceivable that this arginine takes over the sensor part in Arp8 and mediates a similar conformational change along subdomain 2. However, the acceptor of this movement would be insertion I instead of the D-loop and the putative repositioning of residues would then spread along the lid that covers Arp8's pointed end. An alternative acceptor of this putative conformational movement could also be insertion II, which is in close proximity to the sensor loop (compare figure 9B, chapter 3.2).

In summary, the nucleotide-binding site suggests, that Arp8, like actin, is an extremely weak ATPase in its monomeric state. However, a binding partner could induce the subtle changes necessary to stimulate the ATPase and hence trigger conformational changes at Arp8's pointed end via insertion I, which then might contribute to Arp8 manifold roles (further discussed in chapter 4.2.1).

3.5 ATPase activity of Arp4, Arp8 and the INO80 subcomplex I

The structure based hypothesis that Arp8 but not Arp4 might have inducible ATPase activity was tested first with a standard BIOMOL Green assay (Enzo life sciences, Lörrach) that did not detect to any measurable ATPase activity above background for Arp4, Arp8 and also the Arp8-Arp4-actin-HSA containing subcomplex I. The more sensitive ^{32}P ATP (Hartmann Analytics, Braunschweig) hydrolysis assay, however, indicated that Arp8 as well as subcomplex I have very low basal ATPase activity, while Arp4 did not hydrolyze ATP above background. A quantitative analysis of the results is rather difficult as either the hydrolysis or nucleotide exchange rate or both are rather low and the error of the measurement is relatively high. The overall turnover of ATP per Arp8 or subcomplex I is clearly below one nucleoside triphosphate per protein molecule and minute, as 1 µM of protein or protein complex

hydrolyze less than 30 µM of ATP in 30 minutes (figure 20). The hydrolysis rate of the yeast subcomplex I is slightly elevated compared to monomeric Arp8, the turnover rate is roughly twofold compared to yeast Arp8, which can most likely be explained by the presence of actin in the subcomplex, as it putatively also contributes to the low basal ATPase activity. Human Arp8 on the other hand appears to be slightly more active than yeast Arp8 but less active than the yeast subcomplex I.

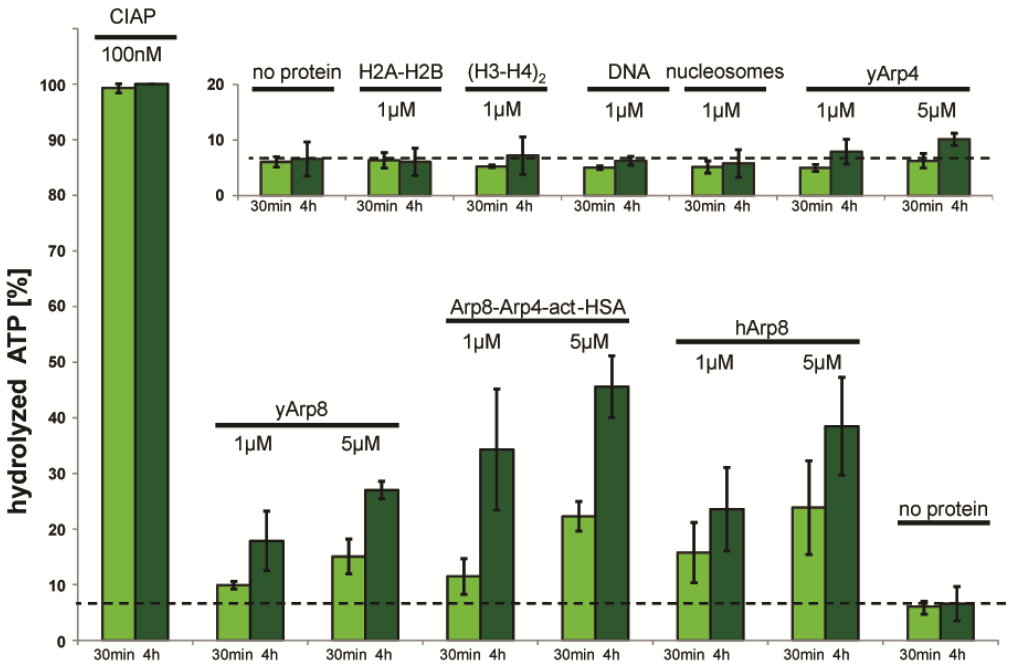

Figure 20: ATPase activity of actin-related proteins Arp4 and Arp8 and the subcomplex I.
Low basal ATPase activity was found for yeast and human Arp8 but not for yeast Arp4. The Arp8-Arp4-actin-HSA subcomplex I of INO80 has a slightly higher activity than Arp8 but does not show any sign of efficient stimulation of the ATPase of either Arp8 or actin within this subcomplex. Arp4, H2A-H2B dimers, $(H3\text{-}H4)_2$ tetramers, DNA and nucleosomes have no measurable ATPase activity in comparison with the control reaction without proteins. No significant stimulation of the ATPase activity of Arp8 or subcomplex I was triggered by canonical nucleosomes and its constituents (compare figure 21).

The very low but measurable ATPase activity of Arp8 as opposed to the lack of detectable ATP hydrolysis in presence of Arp4 also indicates that Arp8, but not Arp4, might indeed be an inducible ATPase. Therefore, potential binding partners for Arp8 have been tested with respect to stimulation of Arp ATPase activity (figure 21), but neither canonical H2A-H2B dimers, $(H3\text{-}H4)_2$ tetramers nor nucleosomes or naked DNA have been found to significantly stimulate the ATPase activity of either yeast or human Arp8 or subcomplex I. Arp4's lack of ATPase activity does not change in presence of nucleosomes, DNA or histone complexes.

Since the subcomplex I does not show any significant increase in activity compared to Arp8, this suggests that neither the ATPase of actin nor Arp8 are activated in this tetrameric module of INO80 giving rise to the question how the subunits arrange in this module.

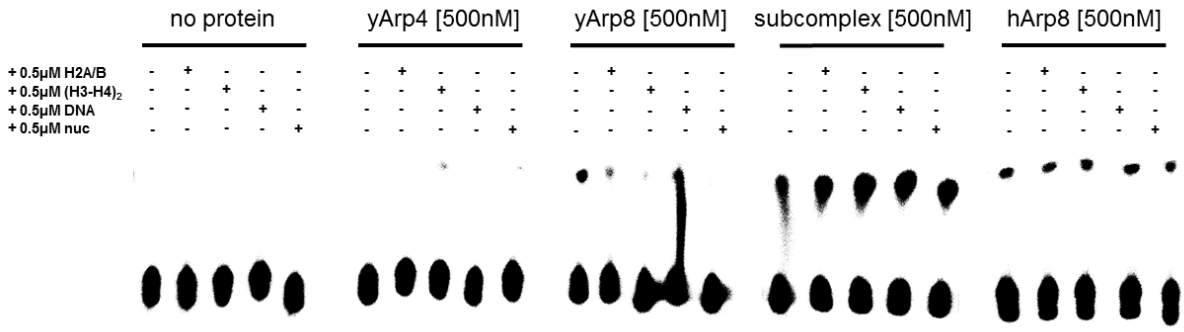

Figure 21: Basal [γ-^{32}P] ATP hydrolysis by Arps and lack of ATPase stimulation by nucleosomes.
Chromatography of the ATPase reaction sample (incubated for 4 hours at 30°C) separates [γ-^{32}P] ATP from hydrolyzed [γ-^{32}P] phosphate. No significant stimulation of the ATPase activity could be observed in presence of H2A-H2B, $(H3-H4)_2$, 146 bp "601" sequence DNA or 207 bp nucleosomes.

3.6 Cross-link based structural constraints in the INO80 subcomplex I

Since crystallization experiments of the subcomplex I did not give rise to reasonably diffracting crystals yet, cross-linking experiments with the *S. cerevisiae* INO80 submodule consisting of Arp8, Arp4, actin and the HSA domain were performed in order to gain insights into the overall architecture of the subcomplex. Given that the smallest repetitive unit of the actin filament is an actin trimer and the subcomplex I contains two Arps and actin and hence three actin fold proteins, it would be conceivable that the arrangement of the Arps and actin are filament like (chapter 1.4, figure 4).

In F-actin, the DNase binding loop of one actin molecule binds to the target binding cleft of a neighboring one. The hydrophobic plug of the third actin also interacts with the interface of the two adjacent actin molecules [69]. Hence, F-actin appears to be made of two chains that gradually turn around each other to form a slowly turning right-handed helix, because the twist per molecule (–166.6°) is close to 180°. But the actual symmetry is a single left-handed helix with approximately 2.2 molecules per turn.

In assumption that the subcomplex resembles the filament structure, two actins of an actin trimer would have to be replaced by Arp8 and Arp4, respectively. This however seems unlikely, since the region

of the hydrophobic plug, which is essential for filament formation, is covered by a major insertion in both Arp8 and Arp4. The large insertion IV of Arp8 and insertion II of Arp4 likely impair F-actin like contacts within subcomplex I.

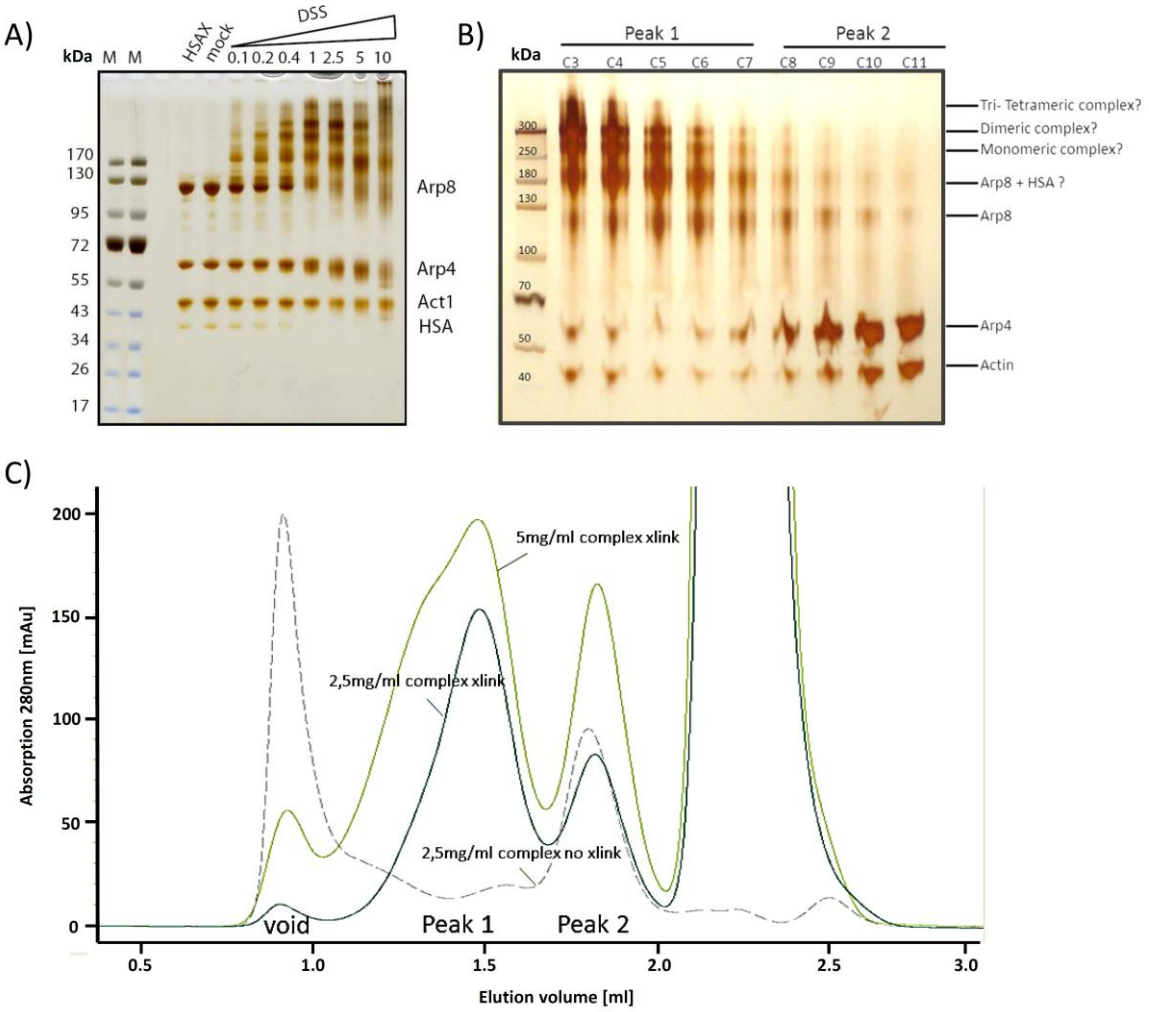

Figure 22: Cross-linking experiments of the subcomplex I
A) Silver-stain SDS-PAGE gel of an initial titration assay with increasing concentration of the cross-linker disuccinimidyl suberate (DSS). A molar ratio of DSS/lysine of approximately 0.5 appears to be optimal. B) Silver-stain SDS-PAGE gel of cross-linked subcomplex I (2.5 mg/ml) further purified by size exclusion chromatography. C) Two distinct peaks are visible in the chromatogram and higher molecular weight fractions of peak 2 have been analysed by mass spectrometry.

The amount of validated cross-links between Arp8, Arp4 and actin is relatively low (table 10), so that a reliable molecular model of how the three proteins interact with one another could not be generated so far. Additionally, cross-link data is derived from the yeast proteins and only the crystal structures of yeast actin and Arp4 are known within the subcomplex. The structure of human Arp8 serves as a basis to

allocate the accordant sequence aligned lysine residues of yeast Arp8 (chapter 8.3). The exact relative localization of the proteins within the subcomplex is further aggravated by the fact that the cross-linking lysines of yeast Arp8 are located within the elongated N-terminus and insertion IV and therefore possess additional structural flexibility (figure 23).

Nonetheless, the information provided by cross-linking suffices to rule out a filament-like arrangement and to deduce some basic concepts on the architecture of subcomplex I.

Table 10: Arp4, Arp8 and actin inter-protein cross-links

Arp8 N-terminus ARP8 K132	Arp4 subdomain 4 ARP4 K267
Arp8 N-terminus ARP8 K165	Arp4 subdomain 3 ARP4 K436
Arp8 insertion IV ARP8 K688	actin subdomain 3 Actin K328
Arp4 insertion I ARP4 K218	actin subdomain 3 Actin K326

Actin's filament opposing side of subdomain 3 ($K328^{act}$ and $K326^{act}$) cross-links to insertion IV of Arp8 ($K688^{Arp8}$) and insertion I of Arp4 ($K218^{Arp4}$). Additionally, Arp4 cross-links with its subdomains 3 and 4 to the N-terminus of Arp8 (figure 23, table 10).

Hence, the barbed end and the concave side of actin are coordinated by Arp4 and 8, which corroborates the results of the actin critical concentration assays that suggested Arp4 to bind to the barbed end of actin and Arp8 to bind actin distinct from either barbed or pointed end [59]. The combination of the biochemical and the cross-link data suggests that actin in the subcomplex I is exposed at its pointed end and also at its hydrophobic plug. The HSA domain crosslinks to insertion II of Arp4 and extensively to the N-terminus of Arp8 (for a list of cross-links refer to chapter 8.2), but no cross-link between actin and the HSA domain met the threshold requirements. This further indicates that actin is relatively accessible in the subcomplex.

One has to note, that the exact arrangement of Arp4 and Arp8 to one another cannot be deduced, since the N-terminal tail of yeast Arp8 is putatively very flexible and cross-linking data involving this tail does not give rise to any positional information of the actin fold core of Arp8.

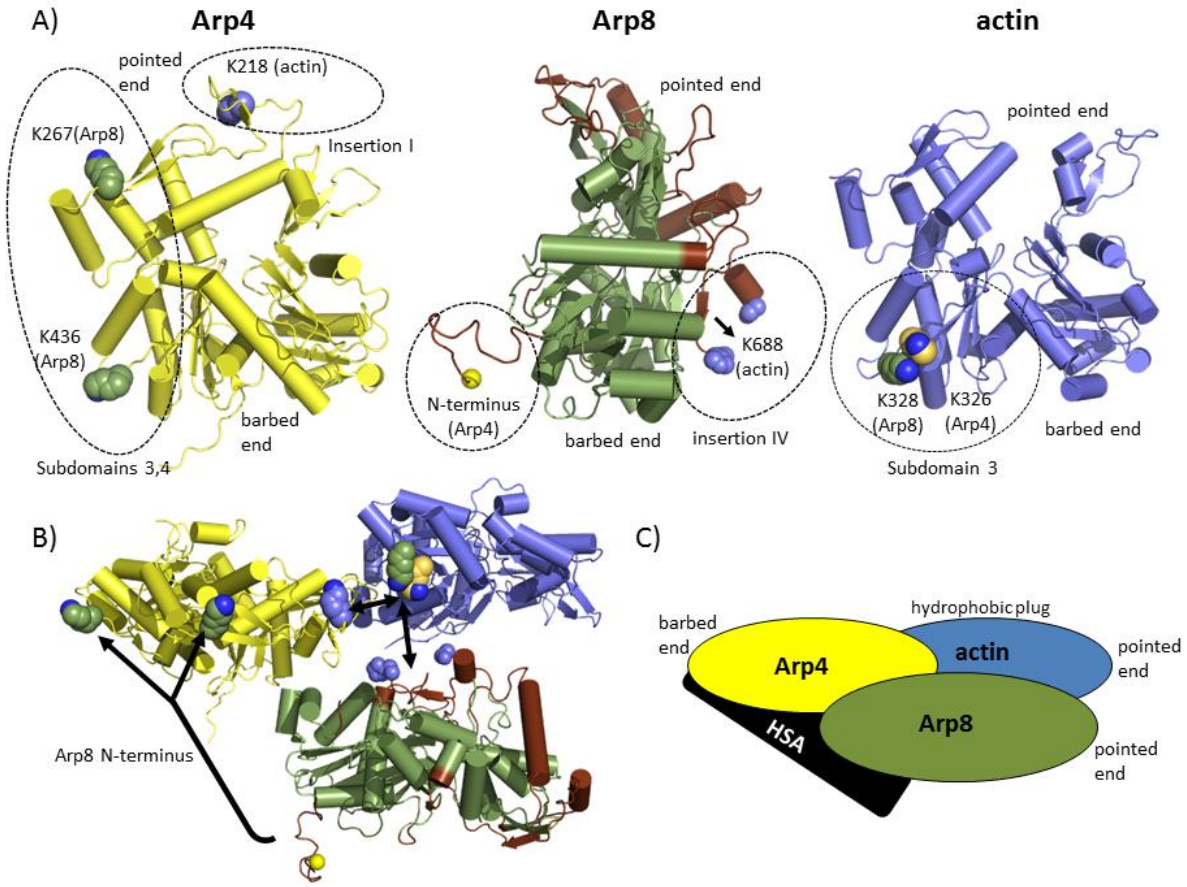

Figure 23: inter-protein cross-links between Arps and actin in subcomplex I

A) Location of the inter-protein cross-linked lysines in Arp4, Arp8 and actin. Cross-link partner in parentheses. The locations of cross-linking lysines in yeast Arp8 are derived from the crystal structure of human Arp8 and subsequent sequence alignment to yeast Arp8. B) One possible arrangement of Arps and actin of subcomplex I that would agree with the cross-link constraints as well as the actin critical concentration assays with Arp4 and Arp8 [59]. C) The resulting working model of the subcomplex I arrangement harbors an actin with exposed pointed end and hydrophobic plug.

3.7 Actin dynamics of subcomplex I

Arp8 and Arp4 reinforce their individual effects to sequester actin from filaments. Biochemical assays suggest that Arp8 is capable of binding to filaments and subsequently depolymerizes these with slow kinetics, while Arp4 appears to bind to free ADP-actin [59]. Together, they maintain actin in a monomeric state and putatively incorporate it into the INO80 remodeler.

An Arp8-Arp4-actin complex could not be stably purified and it remains to be shown whether this heterotrimer is a transient intermediate before remodeler incorporation or whether the order of protein assembly onto INO80 is different.

Once the HSA domain is present, the subcomplex is stable and actin and Arps are tightly bound. In case only Arp8, Arp4 and the HSA domain are expressed in *T. ni* cells, actin is retained from the expression host suggesting a very tight binding of actin to the complex (chapter 3.1). This is further corroborated by the observation that exchange of complexed actin with pyrene-actin in G-buffer does not occur.

Notably, when assembled into the subcomplex, the properties of Arp8 and Arp4 in actin dynamics change dramatically, as described as follows.

3.7.1 TIRF microscopy reveals enhanced filament nucleation

Using TIRF microscopy on oregon-green (OG) labeled actin filaments, the inhibitory effect of Arp4 on filament growth and also on nucleation could be visualized [59].

The same TIRF assay (performed by Dr. Dennis Breitsprecher, AG Faix, Medizinische Hochschule Hannover) using the subcomplex I instead of Arp4 yielded a very different result. In presence of Arp8-Arp4-actin-HSA OG labled actin nucleated more easily giving rise to an elevated number of filaments albeit slower filament growth. 6 µM of subcomplex increased the number of filaments approximately 2.5 fold in this *in vitro* assay and concomitantly slowed down the growth of each filament significantly. While roughly 11 actin subunits per second assemble in this assay with only actin present, 6 µM of subcomplex I diminished the filament growth rate to about 6 subunits per second (figure 24).

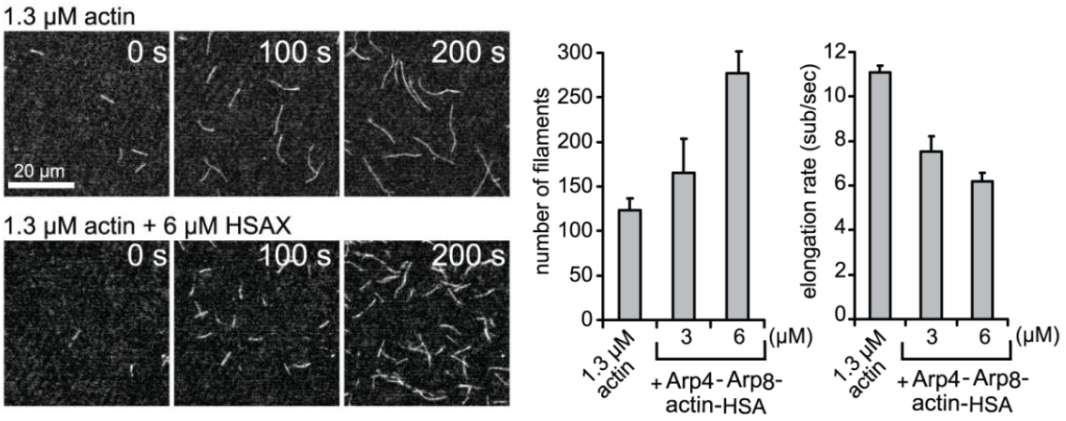

Figure 24: Actin polymerization in presence of subcomplex I.
TIRF microscopy studies of actin polymerization reveal more but shorter filaments in presence of subcomplex I. Within the first 100 seconds of the actin *in vitro* polymerization, more nucleation events occur with subcomplex I compared to the actin only control. Lengths of filaments are significantly decreased, indicating slower growth when subcomplex I is added to the assay.

3.7.2 Pyrene-actin polymerization assay in presence of the subcomplex I

A standard method to monitor actin (de-) polymerization is the pyrene based assay [147]. Here, fluorescence of pyrene that is linked to $C374^{act}$ is monitored as a result of actin dynamics. The fluorescence of pyrene is approximately 20-fold stronger in the filament at appropriate excitation and emission wavelengths compared to monomeric actin. The increase in quantum yield is due to a more dense packing of pyrene within F-actin.

Interestingly, results of the pyrene assay in presence of the subcomplex I suggested a negative effect of the subcomplex on actin polymerization. Increasing amounts of subcomplex I did not alter the initial burst of actin polymerization compared to the actin only control but lead to lower overall fluorescence in a subcomplex I concentration dependent manner (figure 25A). This is in stark contrast to the results of TIRF microscopy studies with actin and subcomplex I.

3.7.3 Actin polymerization monitored by light scattering

Due to the results in the pyrene based actin polymerization assay (chapter 3.7.2), we probed for the change in light scattering at 232nm, a more direct method to monitor actin polymerization. However, it is rarely used due to its insensitivity [148].

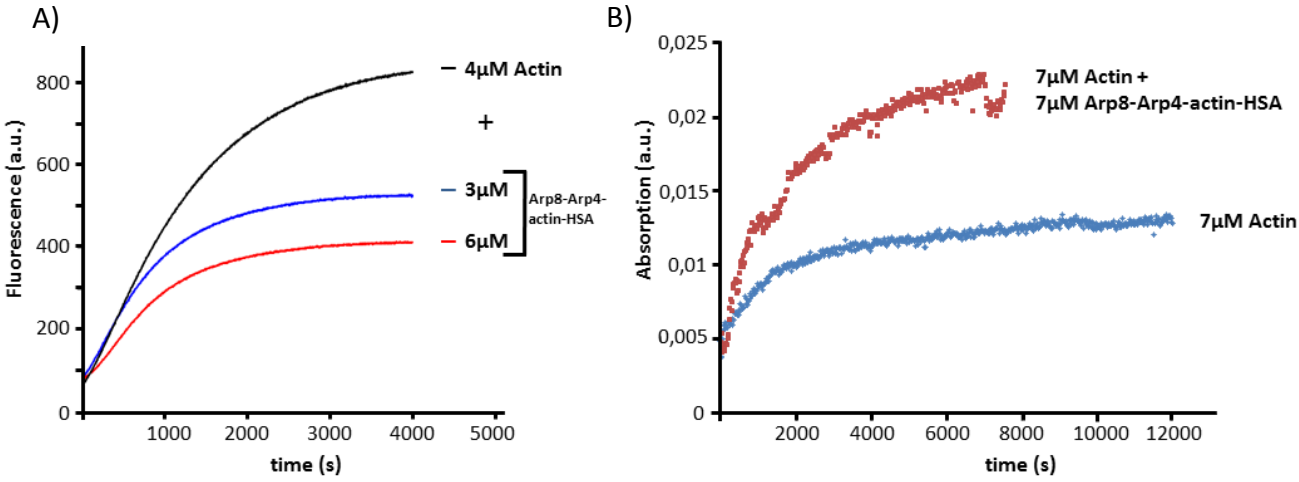

Figure 25: Comparison between pyrene based and light scattering based polymerization assays.
The results of the standard pyrene based polymerization assay oppose the observation by TIRF microscopy. A) Addition of subcomplex I appears to decrease the polymerization rate and to lower actin filaments at steady state. B) The polymerization assay in presence of subcomplex I measured by light scattering suggests that subcomplex I increases the polymerization rate and eventually leads to more filaments.

Actin polymerization visualized by light scattering showed a clear dosage dependent increase upon addition of the subcomplex. At concentrations of 7 µM actin and 7 µM subcomplex, the increase in scattering signal after 8 minutes was approximately 2,5-fold more in presence of the subcomplex than without (figure 25B), corroborating previous TIRF microscopy results.

3.7.3 Subcomplex I triggers pointed end growth

Even though the pyrene assay shows a smaller signal than anticipated for polymerization assays, it can be used to monitor significant positive changes in polymerization. Although the results cannot be evaluated in a quantitative manner, increase in fluorescence can be interpreted as increased polymerization also in the presence of subcomplex I. Indeed, the actual effect is likely to be more significant than the signal suggests, as polymerization signals with subcomplex need to overcome the enigmatic quenching effect of Arp8-Arp4-actin-HSA.

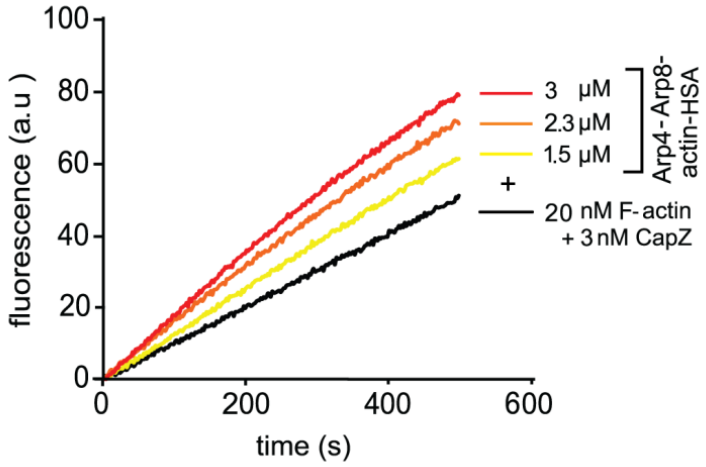

Figure 26: Pointed end elongation assay in presence of subcomplex I.
Diluted F-actin in presence of CapZ can be used as pointed end polymerization seed. Subcomplex I promotes pointed end growth of actin filaments in this pyrene based assay.

Interestingly, the subcomplex I enhances the pyrene fluorescence in a pointed end elongation assay (figure 26). Here, barbed ends of actin filaments are capped by the capping enzyme CapZ allowing only for pointed end filament growth. Arp4 alone interacts with the barbed end of free actin and therefore inhibits pointed end filament polymerization. The subcomplex on the other hand, seems to significantly increase pointed end elongation in a concentration dependent manner. This could be explained by providing additional nucleation points and is in concert with the observation in TIRF microscopy, where more but slower growing filaments appear, which is indicative of pointed end growth.

3.7.4 Subcomplex I stabilizes actin filaments

F-actin spontaneously depolymerizes when diluted below the critical concentration of 100 nM. At this concentration, actin filaments depolymerize from the pointed as well as from the barbed end and monomers are released. The subcomplex I decreases the transition from F-actin to G-actin significantly (figure 27A). Hence, subcomplex I appears to stabilize actin filaments by either providing anchor points for filaments or by decorating F-actin.

Interestingly, the Arp8-Arp4-actin-HSA module does not reverse the spontaneous depolymerization assay even at concentration as high as 15 µM of subcomplex, which also means that 15 µM of actin is added to the reaction. This is in line with the finding that the subcomplex is inherently stable and does not lose its actin component. However, it cannot be ruled out completely that the subcomplex partially

disassembles and effects of additional monomeric actin as well as effects of free Arp4 and Arp8 add up to yield the present results in an unknown mechanism.

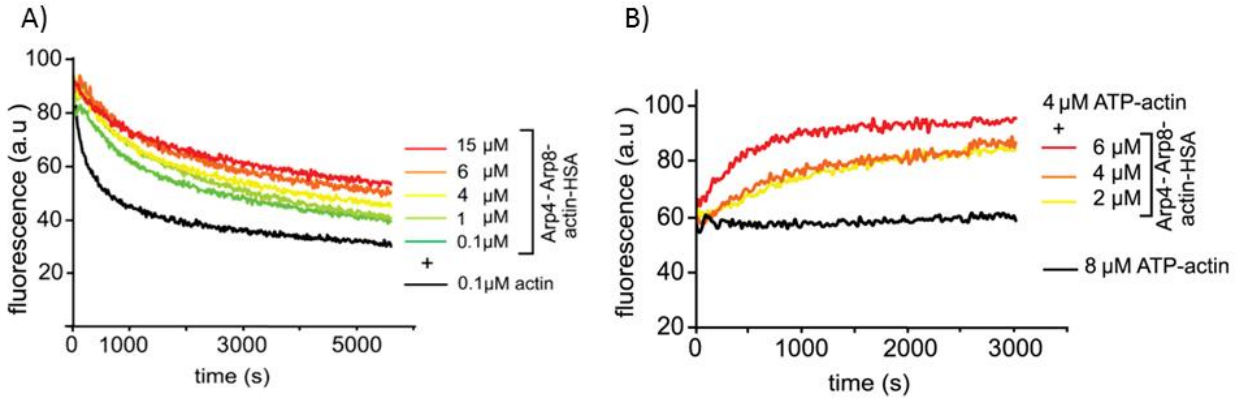

Figure 27: Stabilization of actin filaments by subcomplexI
A) Spontaneous depolymerisation assay in presence of subcomplex I. F-actin dilution to 100 nM concentration leads to spontaneous depolymerisation. Subcomplex I appears to stabilize existing filaments and to oppose the depolymerisation process. B) Spontaneous polymerization in G-buffer. In presence of subcomplex I, actin filaments seem to assemble in G-buffer, which does not occur in the actin control due to low salt conditions.

Moreover, subcomplex I triggers pyrene fluorescence, indicative of actin filaments, in G-buffer. Under these low salt conditions, concentrations of actin as high as 8 µM do not polymerize, but addition of subcomplex I appears to nucleate and to stabilize polymeric actin in G-buffer (figure 27B).

Due to the quenching phenomenon of the subcomplex I on pyrene fluorescence in actin polymerization assays (compare 3.7.2 with 3.7.3), one can state that the observed effect of F-actin stabilization is putatively even more apparent.

All in all, it is apparent that the subcomplex I does influence actin dynamics dramatically, but the nature of this interaction remains enigmatic, especially since pyrene based fluorescence is weakened by Arp8-Arp4-actin-HSA in a standard polymerization assay (chapter 3.2.7).

3.7.5 Electron microscopy of Arps and actin filaments

Given that cross-link experiments suggest a partially exposed actin within subcomplex I (chapter 3.6) and actin dynamics experiments corroborate a participation of complexed actin via its pointed end (chapter 3.7), it is apparent to probe for the association of the subcomplex to actin filaments.

In order to visualize binding of the Arp8 module to existing filaments, 5nm Ni-NTA nanogold (Nanoprobes, Yaphank/USA) was fused to the respective histidine tags to visualize Arp4, Arp8 and subcomplex I by negative stain electron microscopy. Prior to incubation with F-actin on the grid, the nanogold bound proteins were further purified by size exclusion chromatography omitting unlabeled subcomplex I, aggregates and excess of nanogold label. Interestingly, subcomplex I seems to preferentially associate with actin filaments (figure 28D) compared to nanogold Arp4 (figure 28B) and appears to be slightly enriched at filament branchpoints. These experiments have been performed by Dr. Kristina Lakomek (AG Hopfner).

Incubation of actin filaments in presence of Arp8 (figure 28C) seems to disrupt of F-actin, which is in line with prior biochemical experiments [59]. This effect has only been observed with Arp8 but needs to be reproduced for further validation.

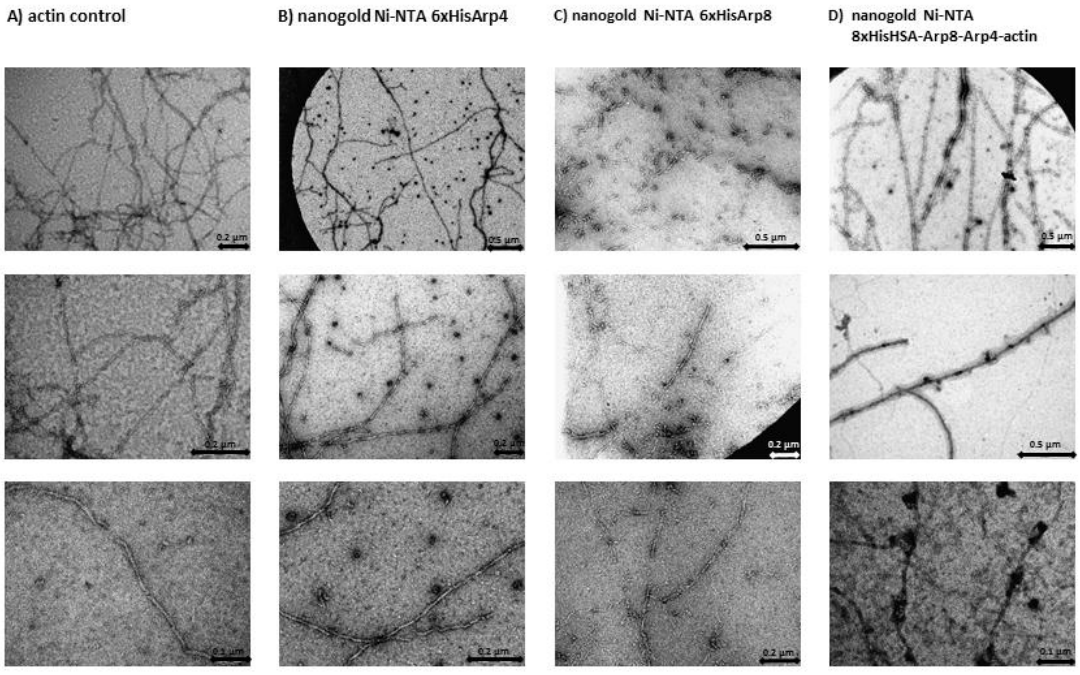

Figure 28: Nanogold labeled Arps and subcomplex I and their interaction with F-actin
A) Uranylacetate stained actin filaments in different magnifications. B) Nanogold labeled Arp4 does not seem to interact with actin filaments. C) Nanogold labelled Arp8 appears to sever actin filaments. D) Actin filaments seem to interact with subcomplex I as the majority of nanogold labels are observed in the vicinity of actin filaments.

3.8 Effect of actin within chromatin remodelers

It is inherently difficult to study the effect of actin in the context of chromatin remodeling *in vivo*, since mutations of actin show strong phenotypes that are usually due to altered functions within the cytoskeleton. The *in vitro* results for subcomplex I (chapter 3.7) indicate that actin also in the context of chromatin remodeling indeed plays a role in actin dynamics. Therefore, the question arises to what extend mutations within members of the subcomplex affect actin dynamics and which phenotypes can be observed for the accordant mutants *in vivo*.

3.8.1 Arp4 mutations

The packing of Arp4 crystals comprised two Arp4 "dimers" per asymmetric unit that interacted via their barbed end with one another [97]. One hydrophobic helix of yeast Arp4 (L462-L468), reminiscent of the WH2 domain of the protein ciboulot, intimately interacts with the very same helix of the adjacent Arp4 molecules in the crystal dimer. Superpositioning of actin onto one of the Arp4 molecules suggested a potential barbed to barbed interaction, which could be envisaged to also occur for actin and Arp4 [97]. Heterologously expressed yeast Arp4 harboring mutations within this hydrophobic helix strongly impairs the negative effect of wild-type Arp4 on actin polymerization *in vitro* (figure 29B).

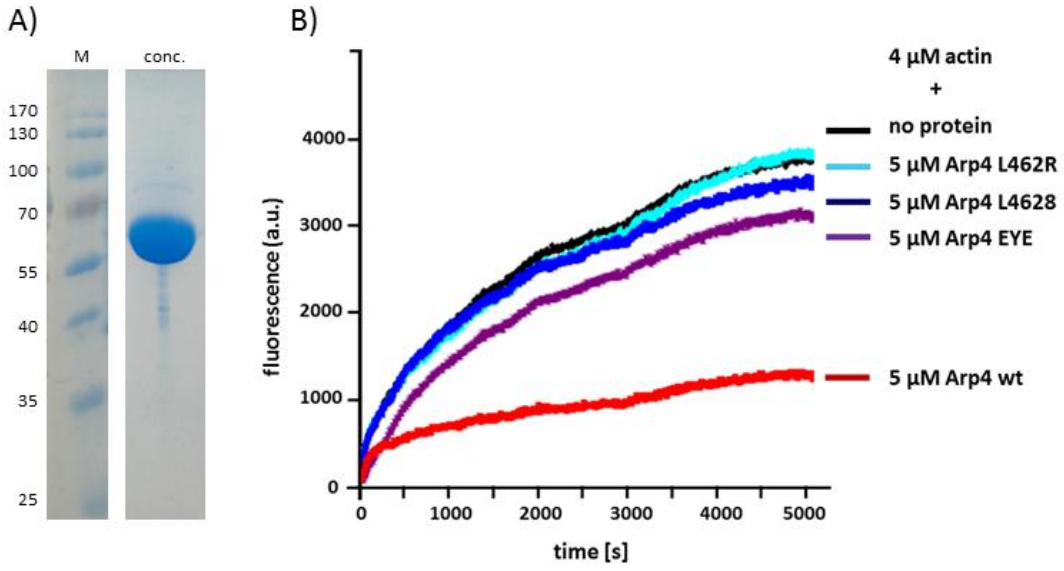

Figure 29: Impact of Arp4 mutations on actin dynamics
A) Purification of yeast Arp4 EYE (L462E/F465Y/L468E) as example for purity of Arp4 mutants. M: marker, conc.: concentrated sample after size exclusion chromatography. B) Polymerization assay in presence of wild-type yeast Arp4 and yeast Arp4 mutants. Mutations in the hydrophobic helix L462-L468 strongly impair the capability of Arp4 to hamper actin polymerization.

However, no difference between the mutations could be observed. Arp4 L462R, Arp4 L468R and Arp4 EYE all lose the capability of wild-type Arp4 to efficiently impair actin polymerization (figure 29).

For the accordant *in vivo* experiments mutated Arp4 was cloned into pRS315 vectors, which have been transformed into *S. cerevisiae* BY *arp4*Δ (pRS316 +500 Arp4 -300) cells. Subsequent plasmid shuffling on FOA plates yielded yeast strains in which Arp4 is replaced by the accordant mutant protein (chapter 2.8). Mutations within the barbed end helix (L463-L468) show strong phenotypic effects. The more hydrophilic the originally hydrophobic WH2-like helix, the stronger the growth phenotype becomes, which is in contrast to the *in vitro* polymerization assays, where all mutations approximately have the same effect in the concentration range tested. In dot spot assays on YPD and YPD with genotoxic agents (chapter 2.8), Arp4 EEE (L462E/P465E/L468E) shows a stronger growth deficiency compared to Arp4 EYE (L462E/P465Y/L468E), which in turn displays a stronger phenotype than either L462R or L468R mutated Arp4.

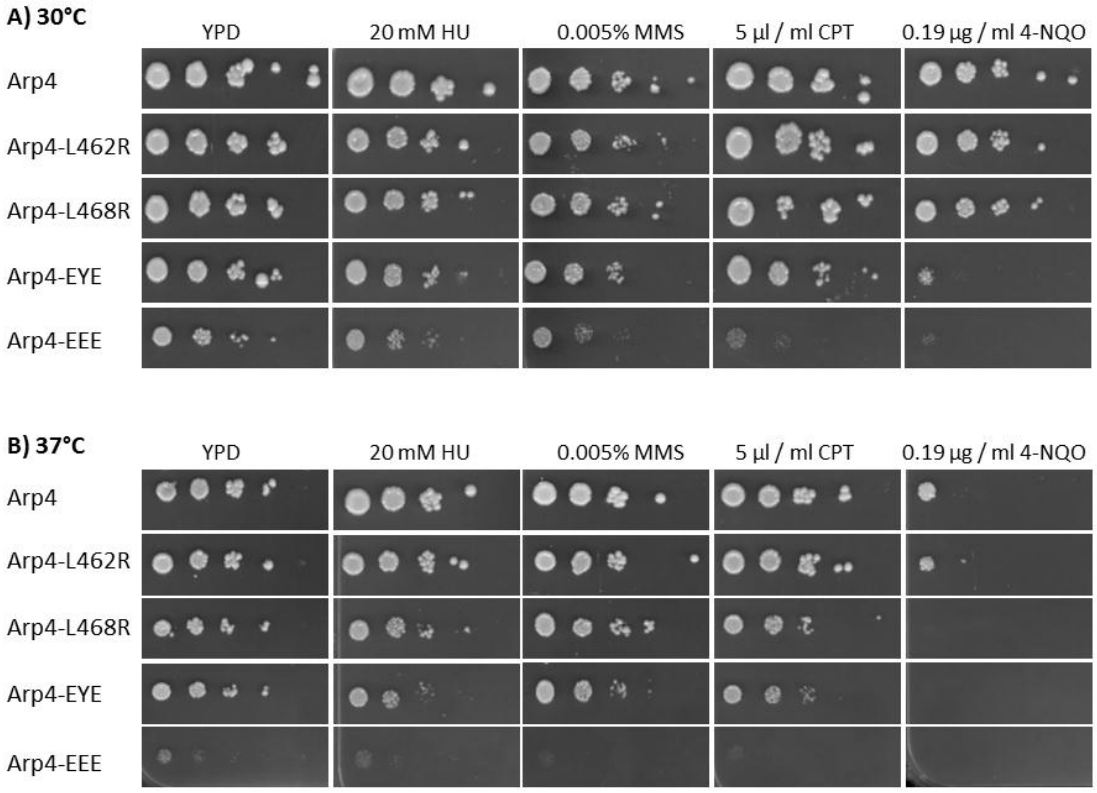

Figure 30: *In vivo* effects of Arp4 mutations.
48h growth of wild-type Arp4 and different mutants on YPD and YPD containing genotoxic agents at 30°C (A) or 37°C (B).
Arp4-EYE: L462E, F465Y, L468E; Arp4-EEE: L462E, F465E, L468E mutations.
The growth phenotype correlates with the hydrophobicity of the helix L462-L468 of Arp4. The more hydrophilic Arp4's helix L462-L468 is, the stronger the growth impairment. DNA damage hypersensitivity can clearly be assigned to both triple mutants and to a much weaker extent to both single mutants.

Growth on agents such as hydroxyurea (HU), methyl methanesulphonate (MMS), 4-nitro-quinoline (4-NQO) or camptothecin (CPT) induces genotoxic stress onto the yeast colonies. Wild-type yeast can overcome low doses of these agents due to efficient DNA repair mechanisms and hence, mutations impairing DNA repair can be revealed (chapter 2.8.2).

For the interpretation of the actual impact of the Arp4 mutations within the helix L462-L468 it has to be taken into account that growth phenotypes already occur under optimal conditions on YPD at 30°C. Nonetheless, a quite dramatic phenotype for the triple mutant Arp4 variants (EYE and EEE) can be observed on all genotoxic agents especially during growth on 4-NQO (figure 30A), suggesting that this mutation has an impact on proficient DNA damage repair.

Growth at 37°C, which already poses stress on yeast cells, strongly increases the growth phenotypes of the yeast Arp4 mutant strains. Here, cells harboring the Arp4 EEE mutant are barely viable even on YPD medium and the deficiency in DNA repair becomes more evident for the Arp4 EYE mutants at 37°C. Also the strains with the single point mutants show mild DNA damage hypersensitivity and L468R appears to be the slightly more harmful mutation compared to L462R (figure 30B).

3.8.2 Mutating actin in the context of chromatin remodeling

Within chromatin modifying complexes actin is always accompanied by Arp4 and both proteins form a transient heterodimer [77]. Therefore, fusion proteins of Arp4 and actin have been cloned into pRS315 vectors and the genes encoding for these fusion proteins with or without mutations have been shuffled into yeast strains in order to replace wild-type Arp4 by the accordant fusion protein. This should in principle enable the introduction of actin mutants solely in the context of chromatin remodeling without affecting the cytoskeleton.

The N-terminus of actin fused to the C-terminus of Arp4 via a Strep II–PreScission site-FLAG linker yields a fusion protein (chapter 2.8), which shows no apparent phenotype compared to the wild-type BY strain under normal growth conditions or also under genotoxic stress (figure 31). Different actin mutants such as polymerization incompetent actin G13R [149] were introduced to probe for the effect of mutant actin. Generally, one can state that cells expressing mutant actin within the fusion protein grow slower than strains harboring the unmutated fusion protein on YPD and also have weak additional growth defects on agar plates with genotoxic agents. The most significant phenotype however was caused by the Arp4 EYE mutation within the fusion protein. Here, a dominant negative effect was clearly visible already under optimal growth conditions since the EYE mutation (L462E/P465Y/L468E) within the fusion

protein had a much more severe growth defect than the EYE mutation on Arp4 alone (compare figures 30 and 31). Under low doses of HU, MMS, CPT or 4-NQO cells containing the fusion protein harboring the EYE mutation in the Arp4 component are barely viable.

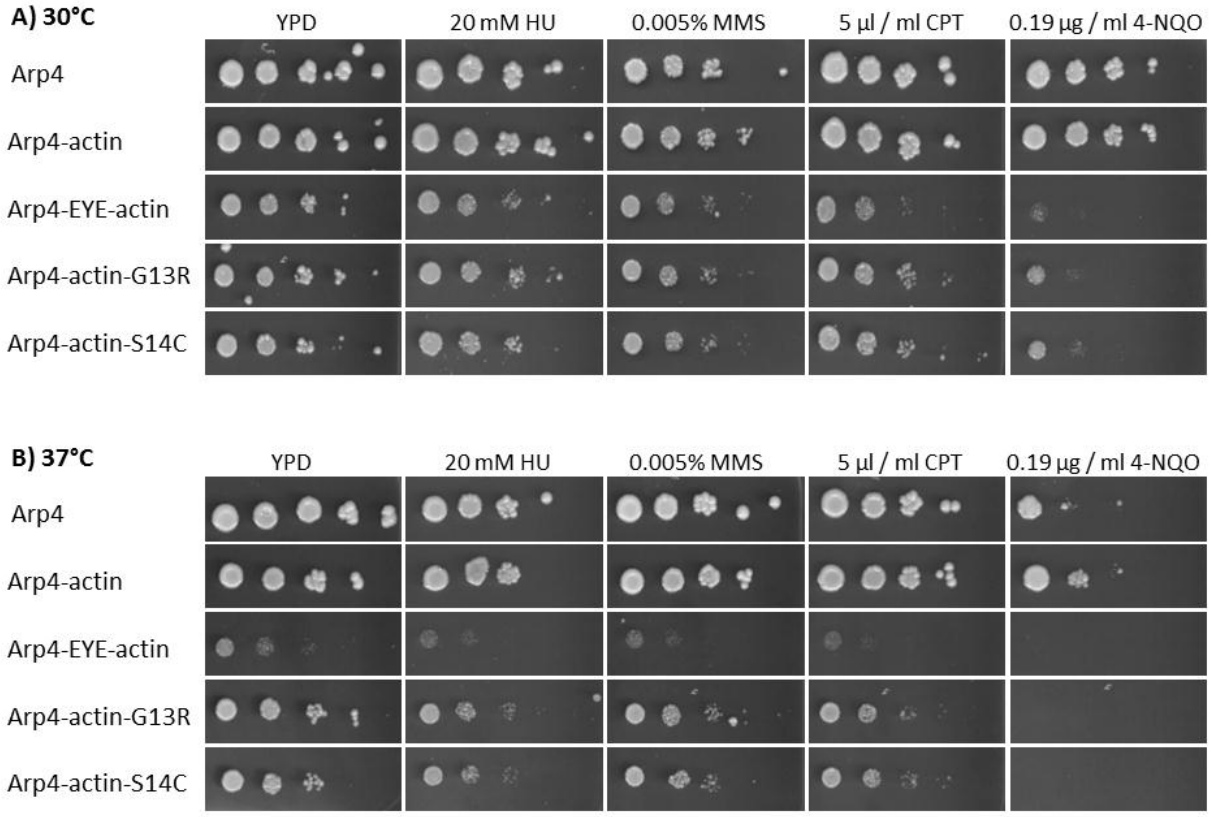

Figure 31: *In vivo* effects of actin mutations in chromatin modifiers.
48h growth of wild-type Arp4, the Arp4-actin fusion protein and different fusion protein mutants on YPD and YPD containing genotoxic agents at 30°C (A) and 37°C (B).
The fusion protein shows no obvious growth defects compared to wild-type Arp4.
Arp4-EYE-actin: fusion protein with L462E, F465Y, L468E mutations in the Arp4 part; Arp4-actin-G13R/S14C: G13R or S14C mutation in the actin part of the fusion protein. The EYE mutation in the Arp4 part of the fusion protein shows strong growth defects and additionally also DNA damage hypersensitivity. Actin mutations in the fusion protein have milder growth defects but also confer hypersensitivity to genotoxic agents.

The *in vivo* experiments indicate that the hydrophobicity of the L462-L468 helix at the barbed end of Arp4 is important for Arp4 function and impaired growth might in part be caused by altered properties of Arp4 in *in vitro* actin dynamics experiments (chapter 3.8.1). Interestingly, the Arp4 EYE mutation shows a more severe growth phenotype, when actin is fused to the Arp4 mutant. Possible implications are discussed in detail (chapter 4.4.1). Moreover, actin mutations within the fusion protein show growth

phenotypes, indicating that actin within the fusion protein is functional and actin dynamics mediated by actin within chromatin modifying complexes is important for cell growth and DNA damage repair. However, control experiments showing that the actin within the fusion protein fully replaces monomeric actin in the chromatin modifiers INO80, SWR1 and NuA4 still have to be performed.

3.9 Dissecting the role of Arps in nucleosome binding

The chromatin binding properties of Arps have been discovered roughly a decade ago [39, 134] and based upon these findings, Arps have been discovered to play important roles in the recognition of certain chromatin states. However, the initial binding experiments were limited to incubation of GST-fused Arps with membrane spotted histones and subsequent salt washes or yeast two hybrid screens, which provide qualitative but no quantitative results.

In collaboration with Prof. Karolin Luger's laboratory, Duane Winkler, PhD, performed fluorescence titration based affinity assays of Arp8, Arp4 and the subcomplex I with histone complexes and 207 bp DNA nucleosomes and 30 bp DNA. Alexa 488 maleimide conjugated H2B (T112C) within H2A-H2B dimers and H4 (E63C) in $(H3\text{-}H4)_2$ tetramers or nucleosomes as well as Atto 647N labeled DNA gave rise to change in fluorescence upon binding to actin-related proteins and the subcomplex I. This enables to determine quantitative dissociation constants to dissect the contributions of Arp8 and Arp4 in binding of subcomplex I to DNA, histone complexes and nucleosomes (chapter 2.10.2).

Table 11: Dissociation constants and Hill coefficients for human Arp8

***Hs* Arp8 (Δ1-33)**	**K_d^{app} ($x10^{-9}$M)**	**Hill Coefficient**	**Overall Fit (R^2)**
30 bp DNA	6329 ± 2727	2.4 ± 1.1	0.97
H2A-H2B	367 ± 131	0.76 ± 0.3	0.85
$(H3\text{-}H4)_2$	65.1 ± 6.4	1.37 ± 0.2	0.97
207bp nucleosome	62.6 ± 16	2.11 ± 0.4	0.91
***Hs* Arp8**	**K_d^{app} ($x10^{-9}$M)**	**Hill Coefficient**	**Overall Fit (R^2)**
30 bp DNA	6938 ± 3448	2.6 ± 0.6	0.95
H2A-H2B	555 ± 158	0.91 ± 0.2	0.92
$(H3\text{-}H4)_2$	110 ± 40.4	1.11 ± 0.3	0.96
207bp nucleosome	51.0 ± 9.6	1.31 ± 0.4	0.96

3.9.1 Arp8 binding to histone complexes, DNA and nucleosomes

All Arp8 variants tested bind $(H3\text{-}H4)_2$ tetramers and nucleosomes with roughly comparable affinity, while the interaction with H2A–H2B dimers is about 4- to 6-fold weaker. The values obtained for the truncated human Arp8 (Δ1-33) are similar to those for full-length human Arp8 (table 11). Both polypeptides bind weakly to DNA (K_d approximately 6-7 μM) and with medium affinity to H2A-H2B dimers (367 ± 131 nM for the truncated construct and 555 ± 158 nM for full-length human Arp8).

Tetramers and also nucleosomes are bound with 4-6 fold higher affinity by human Arp8 compared to H2A-H2B dimer binding (table 11). However, Hill coefficients slightly but significantly diverge between full-length human Arp8 and the construct lacking most of the N-terminal protrusion. The Hill coefficient is a measure for cooperative binding. A Hill coefficient > 1 indicates that first binding events increase the affinity for subsequent ones. The hArp8 (Δ1-33) construct displayed a higher cooperativity in nucleosome binding (Hill-coefficient 2.11 ± 0.4), compared to wild-type hArp8 (Hill-coefficient 1.31 ±0.4) (table 11).

Yeast Arp8 follows a similar binding trend compared to the human orthologue and displays weak binding to DNA (1919 ± 182 nM) and H2A-H2B (1951 ± 796 nM) and approximately 4-6 fold higher affinity to tetramers (485 ± 196 nM) and nucleosomes (314 ± 35 nM). The overall affinity is lower for the yeast protein, which may be caused by differences in chromatin targeting [53-55] or due to the inter-species protein set-up as the *Xenopus laevis* histones used in these experiments could be more compatible with human Arp8 (table 11) compared to yeast Arp8 (table 12). The Hill coefficient of full-length yeast Arp8, which has a very long N-terminus (approx. 250 amino acids) was determined to be 2.13 ± 0.3, again indicative of cooperative binding to nucleosomes. Interestingly, binding to $(H3\text{-}H4)_2$ tetramers gave rise to Hill coefficients of roughly 1 for all Arp8 variants tested and therefore suggest no cooperativity in Arp8 to tetramer binding (table 12).

Table 12: dissociation constants and Hill coefficients of yeast Arp4, Arp8 and subcomplex I

***Sc* Arp4**	**K_d^{app} ($x10^{-9}$M)**	**Hill Coefficient**	**Overall Fit (R^2)**
30 bp DNA	NB	-	-
H2A-H2B	NB	-	-
$(H3\text{-}H4)_2$	74.3 ± 10	2.41 ± 0.6	0.89
207bp nucleosome	204 ± 67	2.06 ± 0.7	0.85
***Sc* Arp8**	**K_d^{app} ($x10^{-9}$M)**	**Hill Coefficient**	**Overall Fit (R^2)**
30 bp DNA	1919 ± 182	1.7 ± 0.2	0.99
H2A-H2B	1951 ± 796	0.85 ± 0.2	0.95
$(H3\text{-}H4)_2$	485 ± 196	0.87 ± 0.2	0.92
207bp nucleosome	314 ± 35	2.13 ± 0.3	0.98
***Sc* Arp8-Arp4-actin-HSA**	**K_d^{app} ($x10^{-9}$M)**	**Hill Coefficient**	**Overall Fit (R^2)**
30 bp DNA	366 ± 23	2.1 ± 0.3	0.99
H2A-H2B	853 ± 358	1.91 ± 0.8	0.81
$(H3\text{-}H4)_2$	182 ± 66.4	1.01 ± 0.2	0.95
207bp nucleosome	63.6 ± 6.2	3.13 ± 0.7	0.94

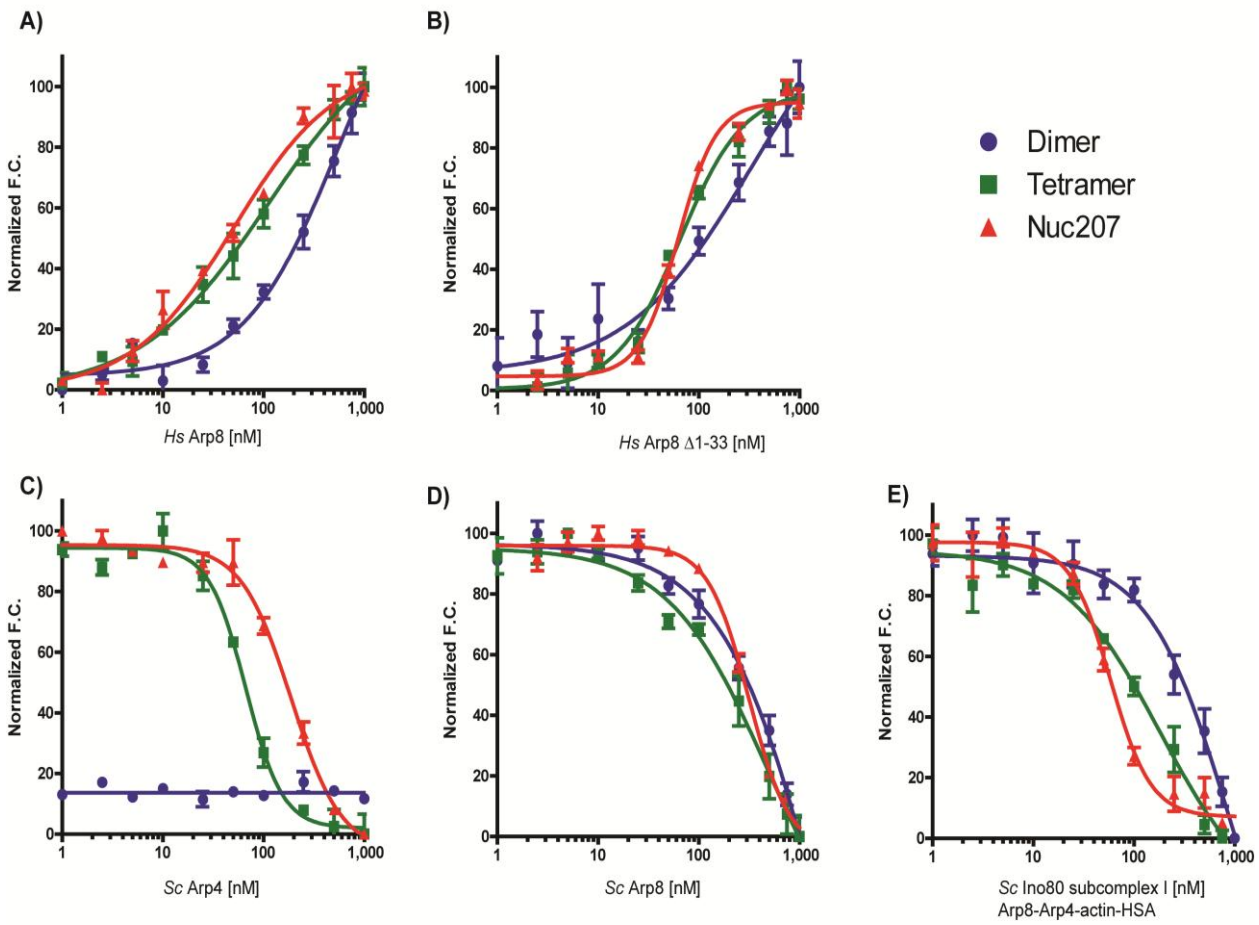

Figure 32: Contribution of Arps to histone and nucleosome binding.
Fluorescence based affinity measurements of *H. sapiens* full-length Arp8 (A), human Arp8 Δ1-33 (B), *S. cerevisiae* Arp8 (C), yeast Arp4 (D), *S. cerevisiae* INO80 subcomplex I (Arp8-Arp4-actin-HSA) (E) to H2A-H2B dimers (blue data points), $(H3\text{-}H4)_2$ (green) and nucleosomes (red). Binding affinities and Hill coefficients are determined by titration of Arps or complex to fluorescently labeled histones or nucleosomes, and monitoring of fluorescence change over the titration series. Change of fluorescence (increase or decrease) upon substrate binding depends on alterations to the microenvironment of the attached fluorophore upon specific binding events.

3.9.2 Arp4 binding to histone complexes, DNA and nucleosomes

In this assay yeast Arp4 did not bind to either DNA or H2A-H2B dimers, even though interaction with H2B and especially H2A was determined for Arp4 insertion II in yeast two hybrid experiments [134]. At this point, it must be noted, that the fluorescence titration assay only monitors binding, if the binding event alters the microenvironment of the Alexa 488 dye. As the chromophore is attached to the histone fold, binding to e.g. the histone tails could remain unnoticed in these experiments.

Nonetheless, Arp4 binds to tetramers and nucleosomes and interestingly prefers $(H3\text{-}H4)_2$ tetramers (74.3 ± 10 nM) over nucleosomes (204 ± 67 nM). Thereby, Arp4 binds both substrates with a Hill coefficient above 2 (table 12) pointing towards cooperativity.

Together, these data show that Arp4 and Arp8 have unique properties in histone and nucleosome binding and concomitantly suggest that Arp4 interacts with tetramer surfaces that are at least partially masked in the nucleosome.

3.9.3 Subcomplex I binding to histone complexes, DNA and nucleosomes

Assessing the histone and nucleosome binding properties of the yeast INO80 subcomplex Arp8–Arp4–actin-HSA showed that the complex exhibits a roughly 3-fold higher nucleosome affinity (63.6 ± 6.2 nM) compared to tetramers (182 ± 66.4 nM). H2A-H2B dimers are more tightly bound by the subcomplex (853 ± 358 nM) than by yeast Arp8 alone but still with about 4-5 fold less affinity as compared to subcomplex I tetramer binding (table 12). Intriguingly, the subcomplex binds nucleosomes with a very high Hill coefficient of 3.13 ± 0.7, while its interaction with $(H3–H4)_2$ displays no signs of cooperativity. For example, oxygen binding of hemoglobin, which is one of the standard examples of cooperativity, exhibits a Hill coefficient of 2.8.

The data give rise to the conclusion that the contribution of Arp8 to the nucleosome binding ability of INO80 is significant but enhanced by further subunits. Notably, Arp4 binds to the histone $(H3–H4)_2$ complex with a K_d of 74.3 ± 10 nM, which is more tightly than the affinity of the subcomplex I for this substrate (182 ± 66.4 nM). Therefore, Arp4 most likely also contributes to the tetramer affinity of the Arp8 module, however potent $(H3–H4)_2$ binding by Arp4 appears to be compromised in the sub-complex. This finding is corroborated by the fact that monomeric Arp4 shows strong cooperativity in binding to the tetramer (Hill coefficient = 2.41 ± 0.6), while the subcomplex does not (Hill coefficient = 1.01 ± 0.2).

In contrast to monomeric Arp8 or Arp4, the subcomplex exhibits significant DNA binding to 30 bp linker DNA (366 ± 23 nM), which is most likely mediated by the HSA domain of INO80, which was identified to be a DNA binding domain [150].

Taken together, Arp8 and Arp4 as well as the HSA domain contribute to nucleosome binding, while a possible involvement of actin still has not been assessed in more detail. As wild-type actin polymerizes under physiological conditions, it seems unsuitable for usage in this assay.

Despite a clear involvement in subcomplex to nucleosome binding, Arp4 seems to be mostly hampered in exhibiting its preferred binding mode to histones within the Arp8 module.

These results shed light on the interplay of INO80 complexed actin-related proteins Arp4 and Arp8 in nucleosome binding and will be discussed in this thesis (chapter 4.5).

4. Discussion

Despite a growing body of evidence that nuclear actin-related proteins (Arps) have important roles in the recognition of certain chromatin states, the functional and mechanisistical understanding of nuclear Arps is still limited. As nuclear Arp4 always associates with monomeric actin in chromatin modifying complexes, research on nuclear Arps should take the presence of nuclear actin into account.

The roles of nuclear actin as well as its polymerization state are still under controversial debate, as phalloidin stainable actin filaments have not been observed in the nucleus. Nevertheless, FRAP experiments with GFP-fused actin point towards a rapid equilibrium between monomeric and polymeric actin in the nucleus [60]. Also more and more evidence accumulates that actin and the regulation of actin dynamics is important for several nuclear processes. For example, the Arp2/3 complex is a seven subunit protein complex, which enables actin filament branching and nucleation [151, 152], when activated by WASP [153]. Despite identified as a key regulator of actin dynamics in the cytoplasm, the Arp2/3 complex is also localized in the nucleus. Here, the complex associates with RNA Polymerase II and is important for transcriptional regulation [44].

It has also been shown that nuclear polymeric actin appears to be required for proper transcriptional activity of all three RNA polymerases [78, 154, 155]. More specifically, the actin depolymerizing agent latrunculin inhibits transcription and RNA polymerase I can be repressed by an antibody versus actin and rescued by providing polymerization competent actin [79]. The capability of nuclear Arps 4 and 8 to participate in actin dynamics is another significant finding that contributes to the hypothesis that actin is a very important factor in several nuclear processes [59].

Furthermore, long-range chromatin movement, triggered by gene activation, is also dependent on actin [83, 156]. In a different line of evidence, INO80 has been shown to facilitate subnuclear chromatin motion, which depends on its Arp8 module [157]. Now, it would be interesting to probe for a possible connection of INO80 dependent local chromatin mobility with larger chromatin movements and whether the Arp and actin subunits of INO80 are involved in both processes. As a prerequisite for the putative participation of the INO80 complex in actin dependent chromatin movement the chromatin remodeler should directly or indirectly interact with actin. A direct interaction mediated by its own actin subunit appears to be the most obvious possibility. Even though it appears obvious to examine nuclear Arps complexed to their host remodelers with respect to their impact on actin dynamics, this has not been done before, probably due to the limited knowledge and controversial debate on nuclear actin.

4.1 Subcomplex I of INO80 interacts with actin

The question that specifically needs to be answered is whether the remodeler associated Arps actively participate in nuclear actin homeostasis and if that is the case, how they achieve this. The *in vitro* experiments revealing effects of INO80 subcomplex I (Arp8-Arp4-actin-HSA) on actin dynamics in this PhD thesis strongly suggest that also the chromatin remodeler INO80 as a whole is capable of interacting with actin.

The HSA domain of Ino80 plays a vital part first in recruiting actin and second in orchestrating the properties in actin dynamics. Heterologously co-expressed Arp8, Arp4 and actin in *T. ni* H5 insect cells could not be purified as a complex, but additional expression of the HSA domain yields the very stable tetrameric subcomplex I that can be purified to homogeneity. Interestingly, if only Arp8, Arp4 together with the HSA domain are expressed in *T. ni* cells, an actin isoform close to *D. melanogaster* actin 5C is retained from the expression host to form the stable tetrameric Arp8 module (subcomplex I). This also gives rise to the problem that it cannot be ruled out that the subcomplex contains a mixture of interspecies actin, if yeast actin is expressed. This needs to be validated by tagging actin in a way that formation of the tetrameric complex remains uncompromised but discrimination between *S. cerevisiae* actin and *T. ni* actin can be easily visualized.

As opposed to monomeric Arp4 and Arp8, which together impair actin polymerization and promote depolymerization, the tetrameric subcomplex appears to nucleate actin filaments *in vitro* albeit it also slows down filament growth. An obvious explanation for slower F-actin formation would be preferred pointed end over barbed end growth and indeed in a pointed end growth assay, subcomplex I stimulates the assembly of filaments via the pointed end. Therefore, it apparently does not meet the requirements to be a *bona fide* actin nucleator, which promotes barbed end filament growth [158]. On the other hand, when compared to the F-actin nucleation factor Spire, a few common properties come into focus. Spire possesses four WASp-homology 2 (WH2) domains that each bind to actin and are separated by short linkers. Hence, Spire is able to form a prenucleation complex that resembles a single-stranded segment of a nascent filament consisting of four actin monomers. Spire remains associated with the filament after nucleation, but it is not clear, whether it allows free barbed end elongation [159] or if Spire associates with the barbed end and blocks further barbed end elongation [160]. In fact, fluorescence microscopy shows that actin filament growth after addition of low concentrations of Spire resembles F-actin formation in presence of subcomplex I (compare figure 33 with 24).

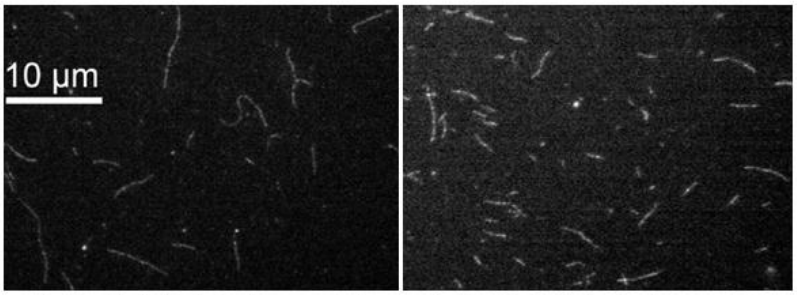

Figure 33: Comparison of fluorescence microscopic images of 1µM rhodamin-actin filaments with and without addition of 0.25 µM Spire after 30 seconds. Adapted from Bosch *et al.* [160]

Especially the actin polymerization assay in G-buffer could be interpreted in a way that subcomplex I is capable of arranging a few actin monomers poised for elongation, which corresponds to the increase in pyrene fluorescence, but the actual filament cannot form due to salt conditions of the G-buffer. Further comparisons between Spire and the Arp8 module of INO80 with respect to their actin dynamics properties might help to understand how INO80 interacts with actin.

The fact that pyrene based actin assays are suboptimal for analyzing the effects of subcomplex I on actin dynamics significantly aggravates these experiments and more direct methods such as light scattering consume very large amounts of protein. As $C374^{act}$ conjugated pyrene has an enhanced quantum yield in the filament, probably due to constricted degrees of freedom in F-actin compared to G-actin, it is interesting to note that this effect is greatly reduced in filaments, when subcomplex I is present. This is not only another indirect hint, that this Arp8 module indeed interacts with actin but could also contribute to the solution of the riddle why nuclear actin can be of polymeric nature [60] yet still unstainable by phalloidin [161]. Immunoblots with actin antibody 2G2 suggest distinct conformations between cytoskeletal and nuclear actin (figure 34) [162]. Whether these differences are due to a different decoration of actin filaments within the different compartments or to an intrinsic structural difference of actin filaments remains to be analyzed. The pyrene assay based results in presence of subcomplex I indicate the latter, which opens up the intriguing possibility that nuclear Arps within chromatin modifying complexes might contribute to a nuclear polymeric actin conformation that appears to be distinct from cytoplasmatic actin filaments.

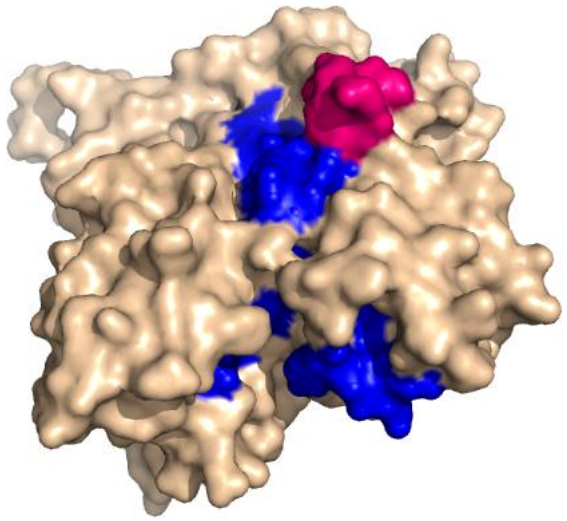

Figure 34: Surface structure of actin. Nonsequential epitopes (aa131-139, aa155-169, and aa176-187, colored in blue) are recognized by actin antibody 2G2, which was raised against the lower dimer. These epitopes are either located at the barbed end or right in the vicinity of the hydrophobic plug region of actin, which is colored pink. Both epitopes are masked in cytoplasmatic F-actin according to the Oda actin filament model.

4.2 Structure of Arp8

In order to comprehend how INO80 could interact with actin, it is necessary to elucidate the structure of the Arp8 module, in particular how the actin subunit is incorporated into the chromatin remodeler together with Arp4 and Arp8. While high resolution structures of the actin polypeptide [68, 142] are available for more than a decade, structural information on monomeric Arp4 and Arp8 have recently been published [59, 163].

Arp8 like all other structurally characterized Arps contains the basal actin fold extended by several insertions that very likely account for loss and gain of functions. The 2.6 Å high resolution structure now provides the framework to study Arp8 function on a mechanistic level.

4.2.1 Is Arp8 a physiological ATPase?

Despite a more distant relationship to actin compared to Arp4, the ATP binding site of Arp8 is much more akin to actin's active site, suggesting that Arp8 could also function as an inducible ATPase *in vivo*.

In line with this assumption, very low basal ATPase activity could be monitored for yeast and human Arp8, while Arp4 was found to be inactive in these assays (chapter 3.5).

It has been reported that binding of ATP to Arp4 causes Arp4 to dissociate from complexes whereas a lack of ATP increases the amount of Arp4 that is incorporated in high molecular species [164]. As ATP seems to be essential for the structural integrity of Arp4, these results could also be interpreted in a way that Arp4 deprived of ATP is prone to aggregation.

Whether the low ATPase activity detected in Arp8 could be stimulated by other factors remains to be shown. Actin itself is an inducible ATPase that needs to be activated from the barbed end side and the barbed end of Arp8 appears to be accessible for binding partners and not obscured by large insertions to the actin fold. Moreover, the barbed end is highly conserved within Arp8 orthologues and also in comparison with actin (chapter 3.2.4).

In case that ATPase activity is important for Arp8's function, it would be interesting to assess possible conformational changes that are triggered by ATP hydrolysis and phosphate release. In actin, the sensor loop translates the conformational movement towards the DNase binding loop, where the free energy barrier for folding is reduced in the ATP bound state, which leads to a filament with lower persistence [144]. The DNase binding loop does not exist in Arp8. Insertion I that covers Arp8 like a lid would be a possible acceptor of the conformational change that goes along with phosphate release. As insertion I has some exposed hydrophobic residues and also bound several glycerol molecules in the crystallization condition, it is conceivable that this particular insertion does not only play a major role in impairing Arp8 polymerization but also in mediating protein-protein interactions. The nucleotide state could therefore be important for regulating the affinity to potential binding partners. This could alternatively or additionally occur at the shorter insertion II, which is in very close proximity to the sensor loop and comprises mostly hydrophobic residues that are highly conserved (chapter 3.2.4).

As the ATPase of actin is stimulated > 40,000 fold in the filament [74], it would be conceivable that the arrangement of the three actin-fold proteins in subcomplex I trigger activity. However, the ATPase within subcomplex I is not significantly enhanced, which indicates that neither the ATPase of actin nor Arp8 are efficiently activated within the subcomplex. This argues for a different conformation of Arp8, Arp4 and actin compared to the trimeric actin building block in F-actin [69].

Optionally, the nucleotide exchange could be impaired and it would be interesting to probe for the nucleotide state of Arp8 and actin within the subcomplex. UV crosslinking of the Arp8 module and subsequent mass spectroscopy analysis did not give rise to results to answer this question yet.

Putative activating factors for the Arp8 ATPase remain to be found, since known binding partners like nucleosomes, $(H3\text{-}H4)_2$ histone tetramers, H2A-H2B dimers or DNA did not trigger ATPase activity of Arp8 alone or of the subcomplex I significantly. Post-translationally modified histones or histone variants like H2A.Z are potential candidates to have an impact on the activity. Also other possibly modified subunits of INO80, such as the INO80 specific subunit 4 [165], could play a role in enzymatic activation.
Since the subcomplex is involved in actin dynamics, actin filament association is also a potential scenario, in which ATPase activity of subcomplex I could have physiological relevance.

4.2.2 Putative grappling hook and crow lever of Arp8

Arp8 has no impact on actin polymerization on its own but it slowly depolymerizes actin filaments with a preference for ADP-bound actin [59]. On the contrary, Arp4 is able to inhibit actin polymerization and rapidly depolymerizes actin filaments. One possible explanation is that Arp4 binds to monomeric G-actin, changing the equilibrium of the polymerization reaction and that Arp8 can bind to actin filaments and sever these once they reach the less stable ADP state. Preliminary data from electron micrographs support this hypothesis, showing shredded actin filaments after incubation with Arp8 (chapter 3.7.5). The observed activities are consistent with a possible function of Arp4 and Arp8 to integrate actin as a stochiometric component into the INO80 complex.
In case Arp8 is indeed capable of severing actin filaments to sequester monomeric actin, one could envision that Arp8 utilizes parts of its actin fold core to compete for actin filament contacts. Given that insertion I of Arp8 possesses conformational flexibility that may be nucleotide dependent, insertion III at Arp8's pointed end could get exposed. This is noteworthy, because insertion III elongates a loop of the actin fold that is implicated in regular filament contacts by approximately 10 Å and the amino acids at the tip of the loop are highly conserved and match those of actin that are responsible for the binding to the adjacent actin's barbed end. This gives rise to the speculation that insertion III could function as a grappling hook, which can intrude into ADP-actin filaments to displace adjacent molecules.

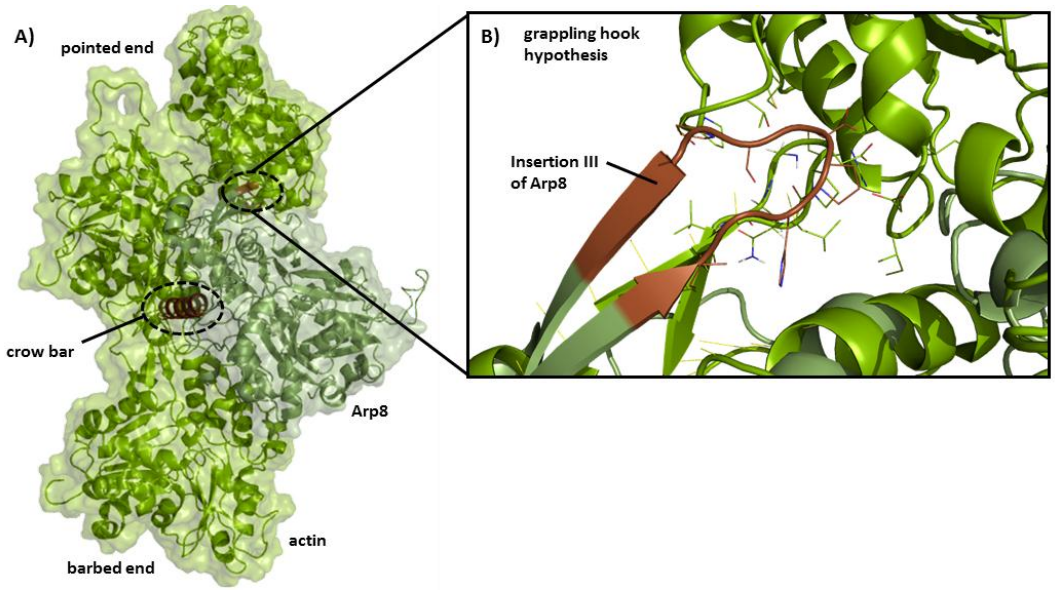

Figure 35: Structure based hypothesis of F-actin severing by Arp8. (A) Arp8 (dark green) attaches to the actin filament (light green) and competes with actin filament contacts using the tip of insertion III as a grappling hook and disrupts ADP F-actin by utilizing helix E101-S119 as a crow bar to disrupt further filament contacts. (B) Close up of insertion III in an overlay of Arp8 onto an actin building block of the filament. The conserved proline-aspartate motif at the tip of the loop might compete for actin filament contacts.

In order to disrupt the filament, a second striking feature of Arp8 might come into play. A very large helix within insertion I is situated at the interface of the inner domain of Arp8's actin fold (subdomains 3 and 4). Compared to the relatively flat actin structure, this is the most prominent orthogonal secondary structure element and would be suitable to function as a crowbar that pushes towards the interface of the two neighboring actin molecules of the filament. This opens up the possibility that Arp8 indeed is capable to bind to F-actin and compete with actin for intra-strand interaction. Subsequently, Arp8 might disrupt F-actin and thereby slowly sequester actin from filaments.

The fact that Arp8 alone does not impair pyrene monitored actin polymerization [59] is not controversial with this grappling hook and crowbar hypothesis, because the F-actin severing activity might depend on ADP filaments, which need to be formed in the time course of the assay. Also, fragments of actin filaments will not necessarily alter the pyrene based fluorescence signal significantly, if the majority of actin building blocks remain filament associated.

Mutating the tip of insertion III (H369 – P373) or the crowbar helix of insertion I (E101 – S119) could put this hypothesis to the test.

4.3 Architecture of subcomplex I

With the structures of yeast actin (1YAG), yeast Arp4 (3QB0) and human Arp8 (4FO0) and inter-protein cross-links of the yeast subcomplex I (Arp8-Arp4-actin-HSA) available, models of the overall architecture of the tetrameric subcomplex can be deduced.

However, only very few cross-links between actin, Arp4 and Arp8 could be evaluated (chapter 3.6), which might be indicative of tight interaction interfaces that cannot be accessed by the cross-linker DSS or lack of lysines that are in the vicinity of protein-protein contacts. Additionally, many of the few available inter-protein cross-links are located within insertions that are not resolved in the electron density of Arp4 and Arp8 crystalstructures. Moreover, it is conceivable that these regions undergo major conformational changes during complex assembly.

This, together with the relatively wide distance constraint of up to 30 Å for C_αs of cross-linked lysine residues and possible differences between the human and yeast Arp8 structures, make it impossible to deduce a solid and detailed molecular arrangement from the cross-link data and rigid-body fitting of the X-ray structures. Nevertheless, some important findings can be extracted from the cross-link data.

4.3.1. Arp4 and Arp8 with actin assemble in a non-filament structure

Comprising three proteins with a central actin fold, subcomplex I could easily be envisioned to have an actin filament-like set up [69], in which two molecules interact barbed to pointed end and the third molecule is located adjacent to their interface. Thereby, the regions of the hydrophobic plugs are facing inwards.

The hydrophobic plug is a hot spot for Arp insertions to the actin fold and in both Arp4 and Arp8 the largest insertion emanates from this point, which makes a filament-like structure between actin and these two Arps improbable if not impossible. Indeed, the validated cross-link $K688^{Arp8}$ – $K328^{actin}$ clearly shows that Arp8 interacts with the outer side of actin's subdomain 3 with respect to the filament (chapter 3.6). This also corroborates the hypothesis that Arp8 is able to attach to and subsequently sever existing filaments.

$K328^{actin}$ also interacts with insertion I of Arp4, which emanates from the pointed side of Arp4. Since $K328^{act}$ is located towards actin's barbed end, this cross-link is in line with the biochemical data that argued for a binding of Arp4 to actin's barbed end [59, 123]. However, this cross-link opposes the hypothesis that actin and Arp4 interact in a barbed to barbed orientation [166] reminiscent of the lower

dimer [70]. Further cross-links between Arp4 and insertion V of Arp8 ($K332^{Arp4}$ – $K775^{Arp8}$) as well as Arp4 and the N-terminus of Arp8 ($K122^{Arp4}$ – $K176^{Arp8}$) suggest that Arp4 could sit at the barbed end of actin, while Arp8 might be located on top of the actin-Arp4 heterodimer and all three proteins are aligned with respect to their barbed to pointed end configuration. Arp8's actin fold however would have to be turned around by 180° compared to the filament arrangement.

As stated before, this hetreotrimeric assembly of Arp8, Arp4 and actin appears to be rather transient and the HSA domain, which is essential to trap the Arp8-Arp4-actin complex in a stable conformation, cross-links to various lysines of Arp8's large N-terminus ($K158^{Arp8}$, $K163^{Arp8}$, $K211^{Arp8}$, etc.) and also to insertion V ($K775^{Arp8}$ – $K526^{INO80}$) as well as to K326 of Arp4 but not with actin.

4.3.2 Accessibility of actin within subcomplex I

The exact arrangement of the subcomplex remains enigmatic and should be subjected to further crystallization trials, in order to determine the atomic model.

Nonetheless, the available structures and cross-link data strongly suggest, that the pointed end as well as the filament facing side of actin are at least partially exposed in the subcomplex. This is very intriguing since it renders actin within INO80 and possibly other chromatin remodelers poised to interact with other actin molecules. As its barbed end appears to be blocked by Arp4, actin is unlikely to function as nucleation seed, but *in vitro* pointed end elongation clearly indicates the capability of actin within the INO80 environment to participate in actin dynamics (chapter 3.7).

The complex could thus stimulate the formation of new actin filaments from the pointed end, or bind to existing filaments and stabilize them. In support of this, the BAF complex, a chromatin remodeler that also contains Arp4 and actin can interact with cofilin and profilin as well as with DNase I, which strongly indicates that this complex participates in actin dynamics [167]. However, it must be noted, that cofilin and profilin bind to the barbed end of actin, while DNase I binds the DNase binding loop at the pointed end. This points towards both an accessible barbed and pointed end of actin in the BAF complex. It would have to be tested, however, if cofilin and profilin could also alternatively interact with Arp4 despite its partially obstructed barbed end due to insertion II. Moreover, the BAF complex also binds to pointed ends of actin filaments and stabilizes them in the presence of phosphatidylinositol-4,5-bisphosphate [168].

We propose that also INO80 comprises an at least partially accessible actin molecule within the remodeler as INO80 appears to exclusively expose the pointed end of its actin component. Accessible

actin seems to widen the task portfolio of chromatin remodelers as a possible joint connector between chromatin and nuclear polymeric actin.

4.3.3 Comparison with the Arp2/3 complex

The Arp 2/3 complex was first identified in 1994 [169] and is the best studied complex in which actin-related proteins are present up to date. The complex consists of seven proteins that are capable to adhere to existing actin filaments and nucleate new actin filaments to form Y-shaped branches, which are implicated in regulating the actin cytoskeleton [170]. The Arp2/3 complex on its own is a very inefficient actin nucleator and requires activation by nucleation promoting factors and a mother actin-filament [171, 172]. A wealth of factors that influence the Arp2/3 complex highly regulate its function in various processes such as cell migration, adhesion [173, 174] but also transcription [44].

The structure of the seven membered Arp2/3 complex (1K8K) has been solved by X-ray crystallography [152]. Actin-related proteins 2 and 3 are engulfed by the other subunits ARPC1-5 (Arp2/3 complex subunits 1-5). Interestingly, electron density is weak for Arp2, suggesting conformational flexibility of Arp2 in the inactivated complex. Subdomains 1 and 2 are missing in the atomic model of Arp2, while electron density sufficed to locate subdomains 3 and 4.

An overlay of the actin structure (1YAG) on subdomains 3 and 4 of Arp2 clarifies why the Arp2/3 complex is a weak nucleator on its own. The orientation of the two Arps does neither resemble a short pitch actin nucleation seed (Figure 36 A), where two adjacent actin molecules face each other, nor a long pitch nucleation seed, where two actins are oriented barbed to pointed and expose their hydrophobic plug towards the same side (Figure 36 B). Instead, the hydrophobic plugs of the Arp2 and Arp3 molecules are in opposite directions. In order to efficiently nucleate actin filaments, Arp2 must either rotate by approximately 180° to yield a long pitch nucleation seed or it must shift towards the pointed end by the length of half an actin molecule to form a short pitch nucleation seed with Arp3. The latter has been discovered to be the physiological relevant seed and the conformational change towards the short pitch elongation template serves as structural basis for filament formation and explains how the Arp2/3 complex can be regulated. In comparison, the subcomplex I of INO80 exhibits an orientation of Arp8 and Arp4 together with actin that seems to be distinct at least from a short pitch arrangement, since both Arp4 and Arp8 cross-link to actin's subdomain 3 at the filament opposing side. As Arp8 cross-links there with its insertion IV, which emanates fromArp8's hydrophobic plug, it seems to locate in a

position towards actin that is completely distinct from the filament architecture and also from the Arp2/3 complex.

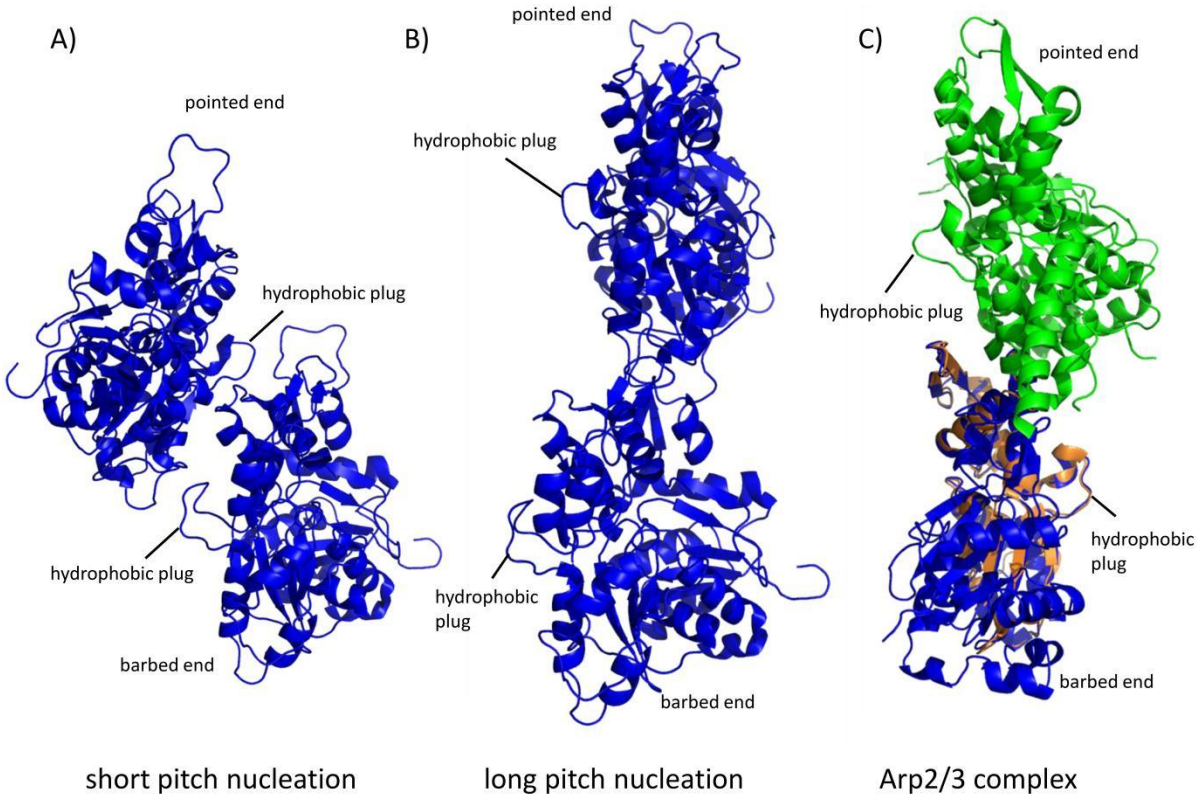

Figure 36: Conformation of potential short-pitch (A) or long-pitch (B) nucleation seeds of actin molecules (blue) that could facilitate actin filament formation. (C) Arp2/3 location within the complex, without illustration of the accompanying subunits ARPC1-5. The actin fold (blue) superposed onto Arp2 (light orange) highlights Arp2's location within the complex. Arp3 (green) and Arp2 are oriented in a barbed to pointed end orientation but distinct from a long pitched arrangement as their hydrophobic plugs are facing towards opposite sites. Hence, a conformational shift must occur for Arp2/3 to be an efficient F-actin nucleator.

Insertion I of Arp4, which is situated at the pointed end, links, like Arp8, to subdomain 3 of actin at the outer barbed end and together with the notion that Arp4 binds to the barbed end of actin one could envision that Arp4 together with actin could possibly take on a long-pitch orientation that is stabilized by Arp8 and the HSA domain. Since the barbed end and the hydrophobic plug of Arp4 are altered by its histone binding insertion II [134], this putative long-pitch orientation of Arp4 and actin would only facilitate pointed end elongation *in vitro*, which is consistent with the observation in TIRF microscopy (chapter 3.7.1).

One has to note that due to the limited amount of inter-protein cross-links and the wide distance constraint for each cross-link, the exact arrangement of the subcomplex I of INO80 remains mostly enigmatic and speculative. Nonetheless, it appears that the Arp8-Arp4-actin-HSA module represents a new conformational arrangement of actin fold proteins that is distinct from the actin filament or the Arp2/3 complex. This is further corroborated by the observation of different biochemical properties of subcomplex I compared to either F-actin or the Arp2/3 complex in actin dynamics.

4.4 Actin mutations in the context of chromatin remodeling

Actin mutants incorporated only in chromatin modifiers would be a very elegant way to probe whether the loss of polymerization capability has an impact on the overall function of actin containing complexes like INO80, SWR1 and NuA4 in yeast. Hence, in living yeast the essential Arp4 was replaced by an Arp4-actin fusion protein, which showed no evident phenotypes other than the wild-type in the performed experiments (chapter 3.8). This could either mean that fused actin was functionally incorporated into the complexes or that monomeric actin is assembled into the complexes nonetheless, while the actin part of the fusion protein is attached as non-functional entity.

A suitable control would be the heterologous expression of subcomplex I with an accordant Arp4-actin fusion protein. Since the subcomplex lacking actin sequesters an actin isoform from the expression host, an SDS-PAGE analysis after purification would shed light on the integration of the fusion protein into the remodeling complex. Another possibility is the purification of these complexes directly from the accordant yeast strain. After purification, Western blots against actin should reveal a single band shifted by 55 kDa due to the fused Arp4, if correct fusion protein incorporation does occur. Both controls have not been successfully achieved so far and therefore, all results derived from the fusion protein complementation have to be considered preliminary at this point.

Based on our initial hypothesis of a barbed to barbed end interaction between Arp4 and actin, actin's N-terminus was fused to the C-terminus of Arp4, which should in principle allow the formation of a barbed to barbed interface. The relatively long linker (Strep tag II / PreScission Protease Cleavage Site / FLAG tag) grants conformational freedom for the positioning of actin with respect to Arp4, but is probably still too short for an Arp4 pointed end to actin barbed end interaction, which now seems more plausible according to available cross-links (chapter 3.6).

Nonetheless, actin mutants seem to show an effect. Mutated actin in the fusion protein displays mild growth phenotypes and DNA damage hypersensitivity (chapter 3.8.2). This is not expected, if actin of the

fusion protein was deprived of a physiological relevance. It cannot be ruled out however that these actin mutants alter the solubility or half-life of the fusion protein or have additional effects on Arp4, as for example the actin mutant G150P binds irreversibly to the actin chaperone CCT [149]. Therefore, it would be beneficial, if mutation studies of a fusion protein were be accompanied by i.e. fluorescence microscopic studies.

4.4.1 Mutating Arp4

The helix L462 - L468 of Arp4 was proposed to play a role in actin binding due to its similarity to a WH2 like helix and the barbed to barbed interaction of Arp4 molecules in the crystal lattice [97]. Therefore, different mutations changing the hydrophobicity of the helix were generated. *In vivo* experiments showed a growth phenotype dependent on the severity of mutations. Arp4 L462R or Arp4 L468R mutations displayed moderate growth phenotypes while triple mutants L462E / F465Y / L468E (EYE) and in particular L462E / F465E / L468E (EEE) were extremely hampered in their growth. Additional DNA hypersensitivity could also be assessed for these mutants. The accordant heterologously expressed and purified Arp4 mutants all lost the capability of efficiently inhibiting actin polymerization in pyrene-actin assays, but no evident correlation between type of mutation and strength of the effect was observed. Effects due to aggregation can be largely excluded, because all mutant Arp4 proteins eluted similarly to wild-type Arp4 from a size exclusion chromatography column.

It seems that helix L462-L468 plays a role in establishing the properties of Arp4 with respect to actin dynamics. Whether the behavior of mutant Arp4 in actin polymerization assays implicates a direct binding of actin to this helix, which is in contrast the Arp4-actin cross-link in the subcomplex, or is the result of a different effect remains to be shown.

In yeast *in vivo* experiments, the Arp4-actin fusion protein with the Arp4 EYE mutation has a much stronger phenotypic effect compared to the EYE mutation in monomeric Arp4. This finding gives rise to speculations on the role of helix L462-L468 of Arp4 in actin dynamics, especially in the context of subcomplex I or INO80, as fusion of actin does not rescue but aggravates the Arp4 EYE mutation.

Based on the cross-link between Arp4 and actin (chapter 3.6) as well as the *in vitro* polymerization assays of the mutants (chapter 3.8.1), one could speculate that Arp4 could use both pointed and also the barbed end to interact with actin. It would be conceivable that Arp4 is capable of binding actin with its pointed end to form subcomplex I, but the exposed barbed end might still be able to interact barbed end to barbed end with other actin molecules reminiscent of the lower dimer as suggested based on the

Arp4 interactions in the crystal lattice [97]. Since, actin barbed end binding proteins cofilin and profilin as well as pointed end binding DNase I can interact with the Arp4 and actin containing BAF complex [167] (chapter 4.3.2), it would be conceivable that the pointed end of actin actin and the barbed end of Arp4 in remodeling complexes are capable of binding actin binding proteins. This could be tested by pull down experiments of Arp4 with actin-binding proteins, such as the mentioned cofilin and profilin or also DNaseI. The binding properties, however, could also depend on other Arp4 interaction partners (e.g. INO80 subunits or histones), as the localization of the flexible insertion II might be crucial for the accessibility of Arp4's barbed end.

4.5 Interactions of Arps with chromatin

Nuclear Arps 4 and 8 have been found to interact with core histones [39, 134] and both Arps contribute to the recognition of chromatin marks in DNA repair [175].

In collaboration with Duane Winkler, PhD of Prof. Luger's laboratory, we assessed the interaction of Arps 4 and 8 individually and within subcomplex I with nucleosomes and core histone complexes as well as DNA in a quantitative manner.

The previously published qualitative results for Arp4 and Arp8 could be validated, as both proteins prefer $(H3\text{-}H4)_2$ tetramers over H2A-H2B dimers and further quantified. Consistent with previous results, no DNA binding could be detected for Arp4 [176]. Interestingly, weak DNA binding of Arp8 could be measured but is in the micromolar range and should only provide minor contributions to INO80's chromatin affinity. Nonetheless, INO80 lacking Arp8, Arp4 and actin appears to be significantly hampered in DNA binding [39]. This finding is difficult to explain, as the DNA-binding region of INO80 (DBINO) indeed coincides with the Arp binding HSA domain [12], but also confers DNA binding as isolated GST fusion domain without Arps present [150].

It would be possible, that in the INO80 context, the DBINO/HSA region can be obscured by other subunits of the complex and the Arps and actin are necessary to expose this particular region to contact DNA. Alternatively, an INO80 complex deprived of Arp8, Arp4 and actin could lose its structural integrity and therefore its deficiency in DNA binding and ATPase activity could possibly be explained by aggregation.

At first view, it was surprising that in the fluorescence titration assay no interaction with H2A-H2B was measured for Arp4 (chapter 3.9.2) as Arp4 was reported to be essential for the recognition of phosphorylated serine 129 H2A in yeast [53]. However, fluorescence change occurs only, if the binding

partner interacts with the fluorophore. Hence, it is possible that Arp4 binds to H2A-H2B without influencing the fluorescence of the Alexa 488 dye conjugated to H2B at the T112C mutation.

In general, the lack of significant affinity to H2A-H2B dimers for Arp4, Arp8 and subcomplex I in this assay, opens up the possibility to discriminate between canonical histones and histone modifications or variants, if they are recognized with higher affinity. Therefore, measuring binding affinities of Arps 4 and 8 and the subcomplex I to various physiological H2A-H2B dimers containing variants and/or post-translational modifications would greatly enhance our understanding on how INO80 is able to discriminate between distinct epigenetic forms of nucleosomes.

4.5.1 Arp4 binds tighter to histone tetramers than to nucleosomes

Nucleosomes are not the rigid structures as assumed previously. Single-molecule approaches led to new insights into the highly dynamic nature of nucleosomes that were not apparent from crystal structures [177]. Various crystal structures represent just one snapshot of the nucleosome and PTMs and histone variant incorporation can shift the equilibrium between different structural states. This affects the interaction of nucleosomes with non-histone proteins and hence the level of chromatin fiber compaction [178].

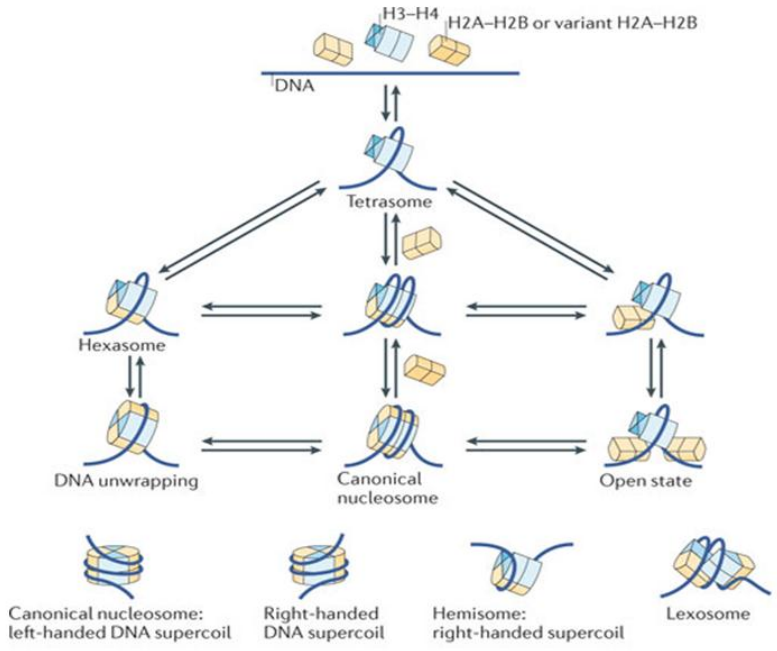

Figure 37: Nucleosome dynamics between different states.
Nucleosome assembly has several intermediate states that eventually lead to a fully assembled nucleosome. The first step appears to be always the formation of a tetrasome. Adapted from Luger et al. 2012 [178]

The important finding that Arp4 prefers $(H3\text{-}H4)_2$ tetramers over nucleosomes points towards a role of Arp4 in binding to assembly or disassembly intermediates of nucleosomes (chapter 3.9.2). As Arp4 plays a vital role in the cycle of H2A.Z incorporation and eviction [179], sustaining $(H3\text{-}H4)_2$ tetrasomes in an open state for remodeling activities during nucleosome dynamics (figure 37) could be one important function for Arp4. Due to the very stable interaction with tetramers, co-crystallization of Arp4 with $(H3\text{-}H4)_2$ might yield crystal structures that clarify how Arp4 and in particular insertion II interact with tetramers or tetrasomes and will help to understand how Arp4 functions mechanistically in chromatin modifying enzymes.

4.5.2 Nucleosome binding of subcomplex I

The subcomplex I binds weakly to H2A-H2B dimers, with reasonable physiological affinity to $(H3\text{-}H4)_2$ tetramers and relative tight affinity to nucleosomes (chapter 3.9.3). Arp8 contributes to all affinities but is supported by other subunits of the subcomplex, as all K_d values to the accordant substrate are lower for the subcomplex compared to Arp8. Within the Arp8 module, the HSA domain must be largely responsible for DNA binding, since neither Arp4 nor Arp8 have significant affinity to DNA and no DNA binding is reported for actin.

The subcomplex binds weaker to tetramers than Arp4 alone. This gives rise to the assumption that the binding interface between Arp4 and the tetramer is partially blocked in the context of INO80. Arp4 is supposed to bind to its histone substrate via insertion II [134], which also cross-links to regions of Arp8. Therefore, it seems likely that Arp8 compromises the tetramer binding capability of Arp4. In contrast, the H2A.Z incorporation machinery SWR1 or chromatin modifier NuA4 that lack Arp8 could make use of Arp4's putative high affinity to tetrasomes.

Another intriguing finding is that subcomplex binding to nucleosomes displays a very high Hill coefficient of 3.13 ± 0.7, which is a measure for high cooperativity. In case, two subcomplexes bind to one nucleosome this would argue for additional contacts between two Arp8-Arp4-actin-HSA modules. Since the nucleosome has a pseudosymmetric structure with two copies of each of the core histones, it would be quite conceivable that it provides a second binding site for the subcomplex. However, since H3 and H4 seem to contribute strongly to Arp binding to nucleosomes and the tetramer should in principle also provide a second binding interface, it is also important to compare the Hill coefficients of the Arps to tetramer interactions. Here, Arp4 shows signs of cooperativity, while Arp8 or the subcomplex do not. Therefore the high affinity of Arp4 might at least partially be due to cooperative binding of two Arp4

proteins to the tetramer. Whether the subsequent binding event is hampered in SWR1 or NuA4 remains to be shown, but it appears to be impaired in INO80, where Arp8 is present.

Therefore, it seems more plausible that the high Hill coefficient of the subcomplex-nucleosome binding is due to binding of two nucleosomes to one subcomplex I. This could be explained for example by opposite arrangement of Arp8 and Arp4 histone interaction sites within subcomplex I. This hypothesis can be tested by using single labeled dinucleosomes as substrates, which should confer high affinity binding to the subcomplex by simultaneous decrease of the Hill-coefficient. Alternatively, nucleosome and histone binding stoichiometry assays could shed light on the number of binding interfaces that are provided by histone complexes or nucleosomes for the subcomplex and *vice versa* [180]. In line with this hypothesis, INO80 was shown to act as a precise nucleosome spacing factor that positions nucleosomes leaving a 30bp linker DNA [181], which argues for two distinct nucleosome binding sites at the vicinity of INO80's DBINO/HSA domain.

4.5.3 Arp8 crystal dimer as physiological relevant nucleosome binder?

The crystal contacts of Arp8 indicated that Arp8 might form a dimer, involving symmetric interactions of the truncated N- and C-termini. In solution, however, Arp8 was always found to be a monomer by SAXS and SLS experiments (chapter 3.3). Therefore, the question arises, whether Arp8 could dimerize upon nucleosomal substrate binding. Indeed, for *S. cerevisiae* Arp8 nucleosome binding, a Hill coefficient of roughly 2 was measured, while truncated *H. sapiens* Arp8 (Δ1-33) also showed cooperativity in the same range. Interestingly, wild-type *H. sapiens* Arp8 lost most of this cooperativity, indicating that the N-terminus could hamper binding of a second Arp8 molecule, even though the K_d values are comparable. This would mean that human and yeast Arp8 could indeed bind to nucleosomes with different stoichiometries, which would be in line with findings that Arp8 does have species specific properties [55, 58]. Also, it must be noted, that yeast Arp8 possesses a very long N-terminal domain of approximately 250 amino acids opposed to human Arp8 with an N-terminus of only 45 amino acids prior to the actin fold. As a next step in clarifying the binding mode of Arps on histones and nucleosomes, specific stoichiometry binding assays with nucleosomes [180] should be performed.

4.6 Interdependence of chromatin remodeling and actin dynamics?

As Arps are clearly involved in nucleosome recognition and binding as well as in actin dynamics even within the context of the chromatin remodeler, it would be interesting to probe for interdependence between these two tasks. For this purpose, the research areas of actin dynamics and chromatin remodeling have to be combined to yield suitable experimental setups.

As stated before, subcomplex I appears to alter the structure of F-actin and herewith the quantum yield of pyrene in the filament (chapter 3.7.2), so for unambiguous results more direct methods than pyrene based actin assays, such as TIRF microscopy, must be used.

Nuclear actin filaments and nucleosomes can be visualized in nuclei that are placed into germinal vesicles (GV) *of Xenopus laevis* expressing GFP-UtrCH (green fluorescent protein – Utrophin Calponin Homology), which binds to actin and cherry labeled H2B. Interestingly, in this set up actin filaments play an important role in reprogramming these differentiated nuclei back to the pluripotent state [82]. Incubation of nuclei with nuclear Arp proteins and complexes fused to other fluorescent proteins prior to implanting into GVs could visualize whether a co-localization occurs. Subsequently, mutations in nucleosome binding sites or putative actin interaction surfaces of the fluorescent fusion constructs could be introduced to monitor alterations. Another possible readout would be the expression profile of pluripotency genes such as *Oct4* (octamer-binding transcription factor 4) assessed via real time PCR in presence of wild-type or mutated Arps. Despite the difficult setups for accordant experiments, it would be an exciting finding if the INO80 complex connects chromatin remodeling on the one hand with the regulation of nuclear actin dynamics on the other hand via its Arp8-Arp4-actin-HSA subcomplex.

4.7 A possible role of Arps in regulation and maintenance of nuclear structure

A possible connection between actin dynamics and chromatin remodeling via Arps could link external stimuli to altered transcription profiles in the nucleus. There is mounting evidence that nuclear envelope lamina spanning complexes (NELSCs), such as the LINC complex are potential transmitters of tensional force from the actin cytoskeleton to the nucleoplasm [89, 161]. NELSCs can stabilize nesprin 1α dimers, which have tight affinity to emerin and lamin A [87]. Lamins, in particular lamin A, are integral parts of the inner nuclear membrane that have actin binding domains and could regulate the concentration of nuclear actin. Thereby lamins potentially influence pathways important for transcription, nuclear export,

chromatin remodeling and movement as well as nuclear assembly that require nuclear myosin 1c and polymerizable actin [86].

Emerin directly binds to the pointed end of F-actin and strongly stimulates filament elongation *in vitro* [90] and it also interacts with barrier-to-autointegration factor (BAF), via its LEM domain (LAP2, emerin, MAN1). BAF is a conserved chromatin binding protein that is vital for cell division, which recruits emerin to chromatin and regulates higher-order chromatin structure during nuclear assembly [182]. As NELSCs interact with actin on both sides of the nuclear envelope, they would be suitable candidates to link the actin cytoskeleton with nuclear actin associated structures [161].

The results of this thesis suggest an exposed pointed end of actin within INO80 and possibly in other actin containing chromatin remodelers. Therefore, it seems most interesting to perform binding studies with subcomplex I and emerin, which could provide first insights into a possible connection of chromatin remodeling and nuclear architecture.

The compartimentalization of the nucleus plays roles in the regulation of transcription [183] and active genes are non-randomly positioned near the surface of chromosome territories [184]. Alteration of the transcription profile often involves relocalization of the specific gene, as shown for HXK1 encoding hexokinase 1 [84]. Also, unrepairable double strand breaks (due to the lack of homologous sequences) are directed to the nuclear periphery [85]. Therefore, long-range chromatin movement occurs upon distinct events that alter chromatin structure and depends on nuclear actin [83]. The anchor point on chromatin necessary for directed movement remains enigmatic to this date.

Interestingly, Arp6 plays a role in the spatial arrangement of chromatin and this function is partially independent of its host remodeler complex SWR1. In particular, Arp6 seems to be involved in long-range interactions between nuclear pores and different families of growth-regulated genes [185] as well as in the overall spatial organization of chromatin [186]. Arp5 also seems to contribute to the maintenance of nuclear architecture [187], giving rise to the speculation that Arps, whether complex-associated or not, have important functions in nuclear compartmentalization.

In light of a possible direct interaction of chromatin remodelers with polymeric actin [168], which in turn associates with the nuclear lamina, Arps would be suitable candidates to couple the chemomechanic force of chromatin associated machineries to scaffolds that maintain nuclear architecture.

5. Summary

The INO80 complex is involved in multiple important cellular tasks, such as transcriptional regulation, replication fork progression, checkpoint regulation and DNA double strand break repair, but knowledge on how INO80 acts within these processes is very limited. Generally, mechanistic insight into chromatin remodeling is scarce due to the lack of structural knowledge on whole chromatin modifiers as well as on many of their subunits. Indeed, several subunits for example of the INO80 remodeling complex have no annotated function up to date.

Actin-related proteins (Arps) as well as monomeric actin are conserved subunits of the chromatin remodeler and interestingly, Arps have been found to recognize and bind nucleosomes and appear to distinguish between epigenetic marks.

Arps within their remodeler environment played a central part in this study and different structural techniques such as X-ray crystallography or small angle X-ray scattering (SAXS) were combined with functional assays to study their biochemical properties and interaction with actin and chromatin.

One major part of this thesis was the structural elucidation of ATP-bound human Arp8 by X-ray crystallography with a resolution of 2.6 Å. Several insertions to the core actin fold give rise to gain and loss of functions compared to actin. The pointed end half of Arp8 is remarkably altered by insertions I-III, which play crucial roles in hampering Arp8 polymerization. The Arp8 structure also points towards inducible Arp8 ATPase activity, akin to actin.

In order to structurally analyze Arp8 in the complex-bound form, lysine-specific cross-linking and subsequent mass spectrometry analysis have been performed. The accordant distance constraints between Arp8, Arp4 actin and the HSA domain suggest strong interaction of Arp4 and in particular Arp8 to the HSA domain. Moreover, the arrangement points towards an exposed pointed end of actin within INO80 that could participate in actin dynamics. Indeed, the whole subcomplex stabilizes filaments and promotes pointed end elongation *in vitro*, corroborating the cross-link results.

Next, actin mutations in the context of chromatin remodeling were introduced into *S. cerevisiae* Δ*arp4* strains making use of a mutated fusion protein consisting of Arp4 and actin to reveal specific effects of non-polymerizable actin in chromatin remodelers. Slight growth defects and mild DNA damage hypersensitivity could be observed for mutated actin and strong effects were monitored for mutated Arp4 in the fusion protein.

Probing the Arps' interaction with nucleosomes and histone complexes in a quantitative manner by fluorescence titration assays dissected the contribution of single subunits of Arp8-Arp4-actin-HSA to

nucleosome binding. H2A-H2B dimers were only weakly bound and the main interface of Arps 4 and 8 to nucleosome binding appears to be at the $(H3\text{-}H4)_2$ tetramer, while the HSA domain obviously contributes to nucleosome binding via its DNA affinity. Strong binding of Arp4 to histone tetramers is obscured in the INO80 context, suggesting a different mode of action for Arp4 in other chromatin modifiers.

The structure of human Arp8 together with these biochemical and cell biological data provides a great advance in “Arp research” and will help to understand the various tasks, Arps are involved in.

Most excitingly, these results point towards a possible dual role of Arps connecting chromatin remodeling complexes with nuclear actin dynamics and indicate a putative involvement of Arps in the actin-mediated large scale movement of chromatin.

6. References

1. Holliday, R., *Mechanisms for the control of gene activity during development.* Biol Rev Camb Philos Soc, 1990. **65**(4): p. 431-71.
2. Arrowsmith, C.H., et al., *Epigenetic protein families: a new frontier for drug discovery.* Nat Rev Drug Discov, 2012. **11**(5): p. 384-400.
3. Xu, W. and M. Xu, *A special issue on 'epigenetics'.* Acta Biochimica et Biophysica Sinica, 2012. **44**(1): p. 1-2.
4. Bassett, A., et al., *The folding and unfolding of eukaryotic chromatin.* Current Opinion in Genetics & Development, 2009. **19**(2): p. 159-165.
5. Tollervey, J. and V.V. Lunyak, *Epigenetics: Judge, jury and executioner of stem cell fate.* Epigenetics, 2012. **7**(8): p. 823-840.
6. Hopfner, K.-P., et al., *Swi2/Snf2 remodelers: hybrid views on hybrid molecular machines.* Current Opinion in Structural Biology, 2012. **22**(2): p. 225-233.
7. Dürr, H., et al., *X-Ray Structures of the Sulfolobus solfataricus SWI2/SNF2 ATPase Core and Its Complex with DNA.* Cell, 2005. **121**(3): p. 363-373.
8. Thoma, N.H., et al., *Structure of the SWI2/SNF2 chromatin-remodeling domain of eukaryotic Rad54.* Nat Struct Mol Biol, 2005. **12**(4): p. 350-356.
9. Clapier, C.R. and B.R. Cairns, *The biology of chromatin remodeling complexes.* Annu. Rev. Biochem., 2009. **78**: p. 273-304.
10. Eberharter, A. and P.B. Becker, *ATP-dependent nucleosome remodelling: factors and functions.* J Cell Sci, 2004. **117**(Pt 17): p. 3707-11.
11. Flaus, A., et al., *Identification of multiple distinct Snf2 subfamilies with conserved structural motifs.* Nucleic Acids Res, 2006. **34**: p. 2887-2905.
12. Szerlong, H., et al., *The HSA domain binds nuclear actin-related proteins to regulate chromatin-remodeling ATPases.* Nat Struct Mol Biol, 2008. **15**(5): p. 469-476.
13. Mohrmann, L. and C.P. Verrijzer, *Composition and functional specificity of SWI2/SNF2 class chromatin remodeling complexes.* Biochim Biophys Acta, 2005. **1681**(2-3): p. 59-73.
14. Flanagan, J.F. and C.L. Peterson, *A role for the yeast SWI/SNF complex in DNA replication.* Nucleic Acids Research, 1999. **27**(9): p. 2022-2028.
15. Carey, M., B. Li, and J.L. Workman, *RSC Exploits Histone Acetylation to Abrogate the Nucleosomal Block to RNA Polymerase II Elongation.* Molecular Cell, 2006. **24**(3): p. 481-487.
16. Corona, D.F., et al., *ISWI is an ATP-dependent nucleosome remodeling factor.* Mol Cell, 1999. **3**: p. 239-245.
17. Corona, D.F.V. and J.W. Tamkun, *Multiple roles for ISWI in transcription, chromosome organization and DNA replication.* Biochimica et Biophysica Acta (BBA) - Gene Structure and Expression, 2004. **1677**(1–3): p. 113-119.
18. Ryan, D.P., et al., *The DNA-binding domain of the Chd1 chromatin-remodelling enzyme contains SANT and SLIDE domains.* EMBO J, 2011. **30**(13): p. 2596-2609.
19. Marfella, C.G.A. and A.N. Imbalzano, *The Chd family of chromatin remodelers.* Mutation Research/Fundamental and Molecular Mechanisms of Mutagenesis, 2007. **618**(1–2): p. 30-40.
20. Hauk, G., et al., *The chromodomains of the Chd1 chromatin remodeler regulate DNA access to the ATPase motor.* Mol Cell, 2010. **39**: p. 711-723.
21. Murawska, M. and A. Brehm, *CHD chromatin remodelers and the transcription cycle.* Transcription, 2011. **2**(6): p. 244-253.
22. Murawska, M., et al., *dCHD3, a Novel ATP-Dependent Chromatin Remodeler Associated with Sites of Active Transcription.* Molecular and Cellular Biology, 2008. **28**(8): p. 2745-2757.

23. Sugiyama, T., et al., *SHREC, an Effector Complex for Heterochromatic Transcriptional Silencing.* Cell, 2007. **128**(3): p. 491-504.
24. Ruthenburg, Alexander J., et al., *Recognition of a Mononucleosomal Histone Modification Pattern by BPTF via Multivalent Interactions.* Cell, 2011. **145**(5): p. 692-706.
25. Sen, P., et al., *A new, highly conserved domain in Swi2/Snf2 is required for SWI/SNF remodeling.* Nucleic Acids Research, 2011. **39**(21): p. 9155-9166.
26. Krogan, N.J., et al., *A Snf2 Family ATPase Complex Required for Recruitment of the Histone H2A Variant Htz1.* Molecular Cell, 2003. **12**(6): p. 1565-1576.
27. Kobor, M.S., et al., *A Protein Complex Containing the Conserved Swi2/Snf2-Related ATPase Swr1p Deposits Histone Variant H2A.Z into Euchromatin.* PLoS Biol, 2004. **2**(5): p. e131.
28. Mizuguchi, G., et al., *ATP-Driven Exchange of Histone H2AZ Variant Catalyzed by SWR1 Chromatin Remodeling Complex.* Science, 2004. **303**(5656): p. 343-348.
29. Papamichos-Chronakis, M., et al., *Global Regulation of H2A.Z Localization by the INO80 Chromatin-Remodeling Enzyme Is Essential for Genome Integrity.* Cell, 2011. **144**(2): p. 200-213.
30. Shen, X., et al., *A chromatin remodelling complex involved in transcription and DNA processing.* Nature, 2000. **406**(6795): p. 541-544.
31. Conaway, R.C. and J.W. Conaway, *The INO80 chromatin remodeling complex in transcription, replication and repair.* Trends in Biochemical Sciences, 2009. **34**(2): p. 71-77.
32. Klymenko, T., et al., *A Polycomb group protein complex with sequence-specific DNA-binding and selective methyl-lysine-binding activities.* Genes & Development, 2006. **20**(9): p. 1110-1122.
33. Jin, J., et al., *A Mammalian Chromatin Remodeling Complex with Similarities to the Yeast INO80 Complex.* Journal of Biological Chemistry, 2005. **280**(50): p. 41207-41212.
34. Bao, Y. and X. Shen, *INO80 subfamily of chromatin remodeling complexes.* Mutation Research/Fundamental and Molecular Mechanisms of Mutagenesis, 2007. **618**(1–2): p. 18-29.
35. Wu, W.-H., et al., *Swc2 is a widely conserved H2AZ-binding module essential for ATP-dependent histone exchange.* Nat Struct Mol Biol, 2005. **12**(12): p. 1064-1071.
36. Jónsson, Z.a.O., et al., *Rvb1p/Rvb2p Recruit Arp5p and Assemble a Functional Ino80 Chromatin Remodeling Complex.* Molecular Cell, 2004. **16**(3): p. 465-477.
37. Chen, L., et al., *Subunit Organization of the Human INO80 Chromatin Remodeling Complex.* Journal of Biological Chemistry, 2011. **286**(13): p. 11283-11289.
38. Wu, W.H., et al., *N terminus of Swr1 binds to histone H2AZ and provides a platform for subunit assembly in the chromatin remodeling complex.* J Biol Chem, 2009. **284**(10): p. 6200-7.
39. Shen, X., et al., *Involvement of Actin-Related Proteins in ATP-Dependent Chromatin Remodeling.* Molecular Cell, 2003. **12**(1): p. 147-155.
40. Bao, Y. and X. Shen, *SnapShot: Chromatin remodeling: INO80 and SWR1.* Cell, 2011. **144**(1): p. 158-158 e2.
41. Poch, O. and B. Winsor, *Who's Who among the Saccharomyces cerevisiae Actin-Related Proteins? A Classification and Nomenclature Proposal for a Large Family.* Yeast, 1997. **13**(11): p. 1053-1058.
42. Harata, M., et al., *Multiple actin-related proteins of Saccharomyces cerevisiae are present in the nucleus.* J Biochem, 2000. **128**(4): p. 665-71.
43. Wu, X., et al., *Regulation of RNA-polymerase-II-dependent transcription by N-WASP and its nuclear-binding partners.* Nat Cell Biol, 2006. **8**(7): p. 756-63.
44. Yoo, Y., X. Wu, and J.L. Guan, *A novel role of the actin-nucleating Arp2/3 complex in the regulation of RNA polymerase II-dependent transcription.* J Biol Chem, 2007. **282**(10): p. 7616-23.

45. Peterson, C.L., Y. Zhao, and B.T. Chait, *Subunits of the Yeast SWI/SNF Complex Are Members of the Actin-related Protein (ARP) Family.* Journal of Biological Chemistry, 1998. **273**(37): p. 23641-23644.
46. Cairns, B.R., et al., *Two Actin-Related Proteins Are Shared Functional Components of the Chromatin-Remodeling Complexes RSC and SWI/SNF.* Molecular Cell, 1998. **2**(5): p. 639-651.
47. Galarneau, L., et al., *Multiple Links between the NuA4 Histone Acetyltransferase Complex and Epigenetic Control of Transcription.* Molecular Cell, 2000. **5**(6): p. 927-937.
48. Dion, V., K. Shimada, and S.M. Gasser, *Actin-related proteins in the nucleus: life beyond chromatin remodelers.* Current Opinion in Cell Biology, 2010. **22**(3): p. 383-391.
49. Muller, J., et al., *Sequence and comparative genomic analysis of actin-related proteins.* Mol Biol Cell, 2005. **16**(12): p. 5736-48.
50. van Attikum, H., et al., *Recruitment of the INO80 Complex by H2A Phosphorylation Links ATP-Dependent Chromatin Remodeling with DNA Double-Strand Break Repair.* Cell, 2004. **119**(6): p. 777-788.
51. van Attikum, H., O. Fritsch, and S.M. Gasser, *Distinct roles for SWR1 and INO80 chromatin remodeling complexes at chromosomal double-strand breaks.* EMBO J, 2007. **26**(18): p. 4113-4125.
52. Kawashima, S., et al., *The INO80 complex is required for damage-induced recombination.* Biochemical and Biophysical Research Communications, 2007. **355**(3): p. 835-841.
53. Downs, J.A., et al., *Binding of Chromatin-Modifying Activities to Phosphorylated Histone H2A at DNA Damage Sites.* Molecular Cell, 2004. **16**(6): p. 979-990.
54. Morrison, A.J., et al., *INO80 and γ-H2AX Interaction Links ATP-Dependent Chromatin Remodeling to DNA Damage Repair.* Cell, 2004. **119**(6): p. 767-775.
55. Kashiwaba, S.-i., et al., *The mammalian INO80 complex is recruited to DNA damage sites in an ARP8 dependent manner.* Biochemical and Biophysical Research Communications, 2010. **402**(4): p. 619-625.
56. Klopf, E., et al., *Cooperation between the INO80 Complex and Histone Chaperones Determines Adaptation of Stress Gene Transcription in the Yeast Saccharomyces cerevisiae.* Molecular and Cellular Biology, 2009. **29**(18): p. 4994-5007.
57. Chen, M. and X. Shen, *Nuclear actin and actin-related proteins in chromatin dynamics.* Current Opinion in Cell Biology, 2007. **19**(3): p. 326-330.
58. Aoyama, N., et al., *The actin-related protein hArp8 accumulates on the mitotic chromosomes and functions in chromosome alignment.* Experimental Cell Research, 2008. **314**(4): p. 859-868.
59. Fenn, S., et al., *Structural biochemistry of nuclear actin-related proteins 4 and 8 reveals their interaction with actin.* EMBO J, 2011. **30**(11): p. 2153-2166.
60. McDonald, D., et al., *Nucleoplasmic β-actin exists in a dynamic equilibrium between low-mobility polymeric species and rapidly diffusing populations.* The Journal of Cell Biology, 2006. **172**(4): p. 541-552.
61. Straub, B.F. and A. Szent-Györgyi, *Studies on Muscle.* Acta Physiol Scandinav 1945. **9 (Suppl): 25.**
62. Schleicher, M. and B. Jockusch, *Actin: its cumbersome pilgrimage through cellular compartments.* Histochemistry and Cell Biology, 2008. **129**(6): p. 695-704.
63. Sotiropoulos, A., et al., *Signal-Regulated Activation of Serum Response Factor Is Mediated by Changes in Actin Dynamics.* Cell, 1999. **98**(2): p. 159-169.
64. Astbury, W.T., et al., *An electron microscope and X-ray study of actin: I. Electron microscope.* Biochimica et Biophysica Acta, 1947. **1**(0): p. 379-392.
65. Sheterline, P., J. Clayton, and J. Sparrow, *Actin.* Protein Profile, 1995. **2**(1): p. 1-103.
66. Galkin, V.E., et al., *A New Internal Mode in F-Actin Helps Explain the Remarkable Evolutionary Conservation of Actin's Sequence and Structure.* Current biology : CB, 2002. **12**(7): p. 570-575.

67. Reisler, E. and E.H. Egelman, *Actin Structure and Function: What We Still Do Not Understand.* Journal of Biological Chemistry, 2007. **282**(50): p. 36133-36137.
68. Kabsch, W., et al., *Atomic structure of the actin: DNase I complex.* Nature, 1990. **347**(6288): p. 37-44.
69. Oda, T., et al., *The nature of the globular- to fibrous-actin transition.* Nature, 2009. **457**(7228): p. 441-5.
70. Millonig, R., H. Salvo, and U. Aebi, *Probing actin polymerization by intermolecular cross-linking.* J Cell Biol, 1988. **106**(3): p. 785-96.
71. Hesterkamp, T., A.G. Weeds, and H.G. Mannherz, *The actin monomers in the ternary gelsolin: 2 actin complex are in an antiparallel orientation.* European Journal of Biochemistry, 1993. **218**(2): p. 507-513.
72. Campellone, K.G. and M.D. Welch, *A nucleator arms race: cellular control of actin assembly.* Nat Rev Mol Cell Biol, 2010. **11**(4): p. 237-251.
73. Nagy, B. and H. Strzelecka-Golaszewska, *Optical rotatory dispersion and circular dichroic spectra of G-actin.* Arch Biochem Biophys, 1972. **150**(2): p. 428-35.
74. Blanchoin, L. and T.D. Pollard, *Hydrolysis of ATP by Polymerized Actin Depends on the Bound Divalent Cation but Not Profilin†.* Biochemistry, 2001. **41**(2): p. 597-602.
75. Rickard, J.E. and P. Sheterline, *Cytoplasmic concentrations of inorganic phosphate affect the critical concentration for assembly of actin in the presence of cytochalasin D or ADP.* Journal of Molecular Biology, 1986. **191**(2): p. 273-280.
76. Sept, D. and J.A. McCammon, *Thermodynamics and Kinetics of Actin Filament Nucleation.* Biophysical journal, 2001. **81**(2): p. 667-674.
77. Nishimoto, N., et al., *Heterocomplex Formation by Arp4 and β-Actin Involved in Integrity of the Brg1 Chromatin Remodeling Complex.* Journal of Cell Science, 2012.
78. Philimonenko, V.V., et al., *Nuclear actin and myosin I are required for RNA polymerase I transcription.* Nat Cell Biol, 2004. **6**(12): p. 1165-72.
79. Ye, J., et al., *Nuclear myosin I acts in concert with polymeric actin to drive RNA polymerase I transcription.* Genes Dev, 2008. **22**(3): p. 322-30.
80. Hu, P., S. Wu, and N. Hernandez, *A role for beta-actin in RNA polymerase III transcription.* Genes Dev, 2004. **18**(24): p. 3010-5.
81. Yoo, Y., X. Wu, and J.-L. Guan, *A Novel Role of the Actin-nucleating Arp2/3 Complex in the Regulation of RNA Polymerase II-dependent Transcription.* Journal of Biological Chemistry, 2007. **282**(10): p. 7616-7623.
82. Miyamoto, K., et al., *Nuclear actin polymerization is required for transcriptional reprogramming of Oct4 by oocytes.* Genes & Development, 2011. **25**(9): p. 946-958.
83. Chuang, C.-H., et al., *Long-Range Directional Movement of an Interphase Chromosome Site.* Current Biology, 2006. **16**(8): p. 825-831.
84. Taddei, A., et al., *Nuclear pore association confers optimal expression levels for an inducible yeast gene.* Nature, 2006. **441**(7094): p. 774-778.
85. Kalocsay, M., N.J. Hiller, and S. Jentsch, *Chromosome-wide Rad51 Spreading and SUMO-H2A.Z-Dependent Chromosome Fixation in Response to a Persistent DNA Double-Strand Break.* Molecular Cell, 2009. **33**(3): p. 335-343.
86. Simon, D.N., M.S. Zastrow, and K.L. Wilson, *Direct actin binding to A- and B-type lamin tails and actin filament bundling by the lamin A tail.* Nucleus, 2010. **1**(3): p. 264-72.
87. Mislow, J.M.K., et al., *Nesprin-1α self-associates and binds directly to emerin and lamin A in vitro.* FEBS Letters, 2002. **525**(1–3): p. 135-140.
88. Sosa, Brian A., et al., *LINC Complexes Form by Binding of Three KASH Peptides to Domain Interfaces of Trimeric SUN Proteins.* Cell, 2012. **149**(5): p. 1035-1047.

89. Crisp, M., et al., *Coupling of the nucleus and cytoplasm.* The Journal of Cell Biology, 2006. **172**(1): p. 41-53.
90. Holaska, J.M., A.K. Kowalski, and K.L. Wilson, *Emerin Caps the Pointed End of Actin Filaments: Evidence for an Actin Cortical Network at the Nuclear Inner Membrane.* PLoS Biol, 2004. **2**(9): p. e231.
91. Simon, D.N. and K.L. Wilson, *The nucleoskeleton as a genome-associated dynamic 'network of networks'.* Nat Rev Mol Cell Biol, 2011. **12**(11): p. 695-708.
92. Berger, I., D.J. Fitzgerald, and T.J. Richmond, *Baculovirus expression system for heterologous multiprotein complexes.* Nat Biotech, 2004. **22**(12): p. 1583-1587.
93. Hanahan, D., J. Jessee, and F.R. Bloom, *[4] Plasmid transformation of Escherichia coli and other bacteria*, in *Methods Enzymol*, H.M. Jeffrey, Editor 1991, Academic Press. p. 63-113.
94. Sambrook, J., D.W. Russell, and C.S.H. Laboratory., *Molecular cloning : a laboratory manual / Joseph Sambrook, David W. Russell*. 3rd. ed. ed2001, Cold Spring Harbor, N.Y. :: Cold Spring Harbor Laboratory. 3 v. :.
95. Sambrook, J., *Molecular cloning : a laboratory manual / Joseph Sambrook, David W. Russell*, ed. D.W. Russell and L. Cold Spring Harbor2001, Cold Spring Harbor, N.Y. :: Cold Spring Harbor Laboratory.
96. Fitzgerald, D.J., et al., *Protein complex expression by using multigene baculoviral vectors.* Nat Meth, 2006. **3**(12): p. 1021-1032.
97. Fenn, S., *Structural biochemistry of the INO80 chromatin remodeler reveals an unexpected function of its two subunits Arp4 and Arp8*, in *Fakultät Chemie und Pharmazie*2011, LMU München.
98. Drenth, J. and J. Mesters, *Principles of protein x-ray crystallography*. 3rd ed2007, New York: Springer. xiv, 332 p.
99. Rhodes, G., *Crystallography made crystal clear : a guide for users of macromolecular models*. 3rd ed. Complementary science series2006, Amsterdam ; Boston: Elsevier/Academic Press. xxv, 306 p.
100. Bergfors, T.M., *Protein crystallization*. IUL biotechnology series2009, La Jolla, Calif.: International University Line. xxvii, 474 p.
101. Engh, R.A. and R. Huber, *Accurate bond and angle parameters for X-ray protein structure refinement.* Acta Crystallographica Section A, 1991. **47**(4): p. 392-400.
102. Kabsch, W., *Xds.* Acta Crystallogr D Biol Crystallogr, 2010. **66**(Pt 2): p. 125-32.
103. Stein, N., *CHAINSAW: a program for mutating pdb files used as templates in molecular replacement.* Journal of Applied Crystallography, 2008. **41**(3): p. 641-643.
104. McCoy, A.J., et al., *Phaser crystallographic software.* Journal of Applied Crystallography, 2007. **40**(4): p. 658-674.
105. Langer, G., et al., *Automated macromolecular model building for X-ray crystallography using ARP/wARP version 7.* Nat. Protocols, 2008. **3**(7): p. 1171-1179.
106. Cowtan, K., *The Buccaneer software for automated model building. 1. Tracing protein chains.* Acta Crystallographica Section D, 2006. **62**(9): p. 1002-1011.
107. Bailey, S., *The Ccp4 suite[mdash]programs for protein crystallography.* Acta Crystallogr D, 1994. **50**: p. 760-763.
108. Emsley, P., et al., *Features and development of Coot.* Acta Crystallogr D Biol Crystallogr, 2010. **66**: p. 486-501.
109. Adams, P.D., et al., *The Phenix software for automated determination of macromolecular structures.* Methods, 2011. **55**(1): p. 94-106.
110. Brunger, A.T., et al., *Crystallography & NMR System: A New Software Suite for Macromolecular Structure Determination.* Acta Crystallographica Section D, 1998. **54**(5): p. 905-921.

111. Brunger, A.T., *Version 1.2 of the Crystallography and NMR system.* Nat. Protocols, 2007. **2**(11): p. 2728-2733.
112. DeLano, W.L., *The PyMOL Molecular Graphics System, Version 1.5.0.1 Schrödinger, LLC.* 2010.
113. Pettersen, E.F., et al., *UCSF Chimera—A visualization system for exploratory research and analysis.* Journal of Computational Chemistry, 2004. **25**(13): p. 1605-1612.
114. Putnam, C.D., et al., *X-ray solution scattering (SAXS) combined with crystallography and computation: defining accurate macromolecular structures, conformations and assemblies in solution.* Q Rev Biophys, 2007. **40**(3): p. 191-285.
115. Koch, M.H., P. Vachette, and D.I. Svergun, *Small-angle scattering: a view on the properties, structures and structural changes of biological macromolecules in solution.* Q Rev Biophys, 2003. **36**(2): p. 147-227.
116. Putnam, C.D., et al., *X-ray solution scattering (SAXS) combined with crystallography and computation: defining accurate macromolecular structures, conformations and assemblies in solution.* Quarterly Reviews of Biophysics, 2007. **40**(03): p. 191-285.
117. Konarev, P.V., et al., *ATSAS 2.1, a program package for small-angle scattering data analysis.* Journal of Applied Crystallography, 2006. **39**(2): p. 277-286.
118. Söderberg, C.A.G., et al., *Oligomerization Propensity and Flexibility of Yeast Frataxin Studied by X-ray Crystallography and Small-Angle X-ray Scattering.* Journal of Molecular Biology, 2011. **414**(5): p. 783-797.
119. Wriggers, W. and P. Chacon, *Using Situs for the registration of protein structures with low-resolution bead models from X-ray solution scattering.* Journal of Applied Crystallography, 2001. **34**(6): p. 773-776.
120. Svergun, D., C. Barberato, and M.H.J. Koch, *CRYSOL - a Program to Evaluate X-ray Solution Scattering of Biological Macromolecules from Atomic Coordinates.* Journal of Applied Crystallography, 1995. **28**(6): p. 768-773.
121. Hertzog, M. and M.F. Carlier, *Functional characterization of proteins regulating actin assembly.* Curr Protoc Cell Biol, 2005. **Chapter 13**: p. Unit 13 6.
122. Breitsprecher, D., et al., *Analysis of actin assembly by in vitro TIRF microscopy.* Methods Mol Biol, 2009. **571**: p. 401-15.
123. Fenn, S., et al., *Structural biochemistry of nuclear actin-related proteins 4 and 8 reveals their interaction with actin.* EMBO J, 2011. **30**(11): p. 2153-66.
124. Aloy, P., M. Pichaud, and R.B. Russell, *Protein complexes: structure prediction challenges for the 21st century.* Current Opinion in Structural Biology, 2005. **15**(1): p. 15-22.
125. Leitner, A., et al., *Probing Native Protein Structures by Chemical Cross-linking, Mass Spectrometry, and Bioinformatics.* Molecular & Cellular Proteomics, 2010. **9**(8): p. 1634-1649.
126. Herzog, F., et al., *Structural Probing of a Protein Phosphatase 2A Network by Chemical Cross-Linking and Mass Spectrometry.* Science, 2012. **337**(6100): p. 1348-1352.
127. Cory, J.G., et al., *Inhibition of ribonucleotide reductase and L1210 cell growth by N-hydroxy-N'-aminoguanidine derivatives.* Biochemical Pharmacology, 1985. **34**(15): p. 2645-2650.
128. Lundin, C., et al., *Methyl methanesulfonate (MMS) produces heat-labile DNA damage but no detectable in vivo DNA double-strand breaks.* Nucleic Acids Research, 2005. **33**(12): p. 3799-3811.
129. Tomicic, M.T. and B. Kaina, *Topoisomerase degradation, DSB repair, p53 and IAPs in cancer cell resistance to camptothecin-like topoisomerase I inhibitors.* Biochimica et Biophysica Acta (BBA) - Reviews on Cancer, 2013. **1835**(1): p. 11-27.
130. Li, C., L.-E. Wang, and Q. Wei, *DNA repair phenotype and cancer susceptibility—A mini review.* International Journal of Cancer, 2009. **124**(5): p. 999-1007.

131. Grigorieff, N. and S.C. Harrison, *Near-atomic resolution reconstructions of icosahedral viruses from electron cryo-microscopy.* Current Opinion in Structural Biology, 2011. **21**(2): p. 265-273.
132. De Carlo, S. and J.R. Harris, *Negative staining and cryo-negative staining of macromolecules and viruses for TEM.* Micron, 2011. **42**(2): p. 117-131.
133. Hainfeld, J.F., et al., *Ni–NTA–Gold Clusters Target His-Tagged Proteins.* Journal of Structural Biology, 1999. **127**(2): p. 185-198.
134. Harata, M., et al., *The Nuclear Actin-related Protein of Saccharomyces cerevisiae, Act3p/Arp4, Interacts with Core Histones.* Mol. Biol. Cell, 1999. **10**(8): p. 2595-2605.
135. Anderson, B.J., et al., *Using fluorophore-labeled oligonucleotides to measure affinities of protein-DNA interactions.* Methods Enzymol, 2008. **450**: p. 253-72.
136. Winkler, D.D., K. Luger, and A.R. Hieb, *Quantifiying chromatin associated interactions: the HI-FI System.* Methods Enzymol., 2012. **in press**.
137. Andrews, A.J., et al., *A thermodynamic model for Nap1-histone interactions.* J Biol Chem, 2008. **283**(47): p. 32412-8.
138. Dominguez, R. and K.C. Holmes, *Actin structure and function.* Annu Rev Biophys, 2011. **40**: p. 169-86.
139. David T, J., *Protein secondary structure prediction based on position-specific scoring matrices.* Journal of Molecular Biology, 1999. **292**(2): p. 195-202.
140. Dosztányi, Z., et al., *The Pairwise Energy Content Estimated from Amino Acid Composition Discriminates between Folded and Intrinsically Unstructured Proteins.* Journal of Molecular Biology, 2005. **347**(4): p. 827-839.
141. Krissinel, E., *Crystal contacts as nature's docking solutions.* Journal of Computational Chemistry, 2010. **31**(1): p. 133-143.
142. Otterbein, L.R., P. Graceffa, and R. Dominguez, *The crystal structure of uncomplexed actin in the ADP state.* Science, 2001. **293**(5530): p. 708-11.
143. Graceffa, P. and R. Dominguez, *Crystal Structure of Monomeric Actin in the ATP State.* Journal of Biological Chemistry, 2003. **278**(36): p. 34172-34180.
144. Pfaendtner, J., et al., *Nucleotide-dependent conformational states of actin.* Proceedings of the National Academy of Sciences, 2009. **106**(31): p. 12723-12728.
145. Iwasa, M., et al., *Dual roles of Gln137 of actin revealed by recombinant human cardiac muscle alpha-actin mutants.* J Biol Chem, 2008. **283**(30): p. 21045-53.
146. Fujii, T., et al., *Direct visualization of secondary structures of F-actin by electron cryomicroscopy.* Nature, 2010. **467**(7316): p. 724-728.
147. Cooper, J.A., S.B. Walker, and T.D. Pollard, *Pyrene actin: documentation of the validity of a sensitive assay for actin polymerization.* Journal of Muscle Research and Cell Motility, 1983. **4**(2): p. 253-262.
148. Cooper, J.A. and T.D. Pollard, *[19] Methods to measure actin polymerization*, in *Methods Enzymol*, L.W.C. Dixie W. Frederiksen, Editor 1982, Academic Press. p. 182-210.
149. Posern, G., A. Sotiropoulos, and R. Treisman, *Mutant Actins Demonstrate a Role for Unpolymerized Actin in Control of Transcription by Serum Response Factor.* Molecular Biology of the Cell, 2002. **13**(12): p. 4167-4178.
150. Bakshi, R., et al., *Characterization of a human SWI2/SNF2 like protein hINO80: Demonstration of catalytic and DNA binding activity.* Biochemical and Biophysical Research Communications, 2006. **339**(1): p. 313-320.
151. Volkmann, N., et al., *Structure of Arp2/3 complex in its activated state and in actin filament branch junctions.* Science, 2001. **293**(5539): p. 2456-9.
152. Robinson, R.C., et al., *Crystal structure of Arp2/3 complex.* Science, 2001. **294**(5547): p. 1679-84.

153. Marchand, J.-B., et al., *Interaction of WASP/Scar proteins with actin and vertebrate Arp2/3 complex.* Nat Cell Biol, 2001. **3**(1): p. 76-82.
154. Hofmann, W.A., et al., *Actin is part of pre-initiation complexes and is necessary for transcription by RNA polymerase II.* Nat Cell Biol, 2004. **6**(11): p. 1094-1101.
155. Franke, W.W., *Actin's many actions start at the genes.* Nat Cell Biol, 2004. **6**(11): p. 1013-1014.
156. Dundr, M., et al., *Actin-dependent intranuclear repositioning of an active gene locus in vivo.* The Journal of Cell Biology, 2007. **179**(6): p. 1095-1103.
157. Neumann, F.R., et al., *Targeted INO80 enhances subnuclear chromatin movement and ectopic homologous recombination.* Genes & Development, 2012. **26**(4): p. 369-383.
158. Chesarone, M.A. and B.L. Goode, *Actin nucleation and elongation factors: mechanisms and interplay.* Current Opinion in Cell Biology, 2009. **21**(1): p. 28-37.
159. Quinlan, M.E., et al., *Drosophila Spire is an actin nucleation factor.* Nature, 2005. **433**(7024): p. 382-388.
160. Bosch, M., et al., *Analysis of the Function of Spire in Actin Assembly and Its Synergy with Formin and Profilin.* Molecular Cell, 2007. **28**(4): p. 555-568.
161. Gieni, R.S. and M.J. Hendzel, *Actin dynamics and functions in the interphase nucleus: moving toward an understanding of nuclear polymeric actinThis paper is one of a selection of papers published in this Special Issue, entitled 29th Annual International Asilomar Chromatin and Chromosomes Conference, and has undergone the Journal's usual peer review process.* Biochemistry and Cell Biology, 2009. **87**(1): p. 283-306.
162. Gonsior, S., et al., *Conformational difference between nuclear and cytoplasmic actin as detected by a monoclonal antibody.* J Cell Sci, 1999. **112**(6): p. 797-809.
163. Gerhold, C.B., et al., *Structure of Actin-related protein 8 and its contribution to nucleosome binding.* Nucleic Acids Research, 2012.
164. Sunada, R., et al., *The nuclear actin-related protein Act3p/Arp4p is involved in the dynamics of chromatin-modulating complexes.* Yeast, 2005. **22**(10): p. 753-768.
165. Morrison, A.J., et al., *Mec1/Tel1 Phosphorylation of the INO80 Chromatin Remodeling Complex Influences DNA Damage Checkpoint Responses.* Cell, 2007. **130**(3): p. 499-511.
166. Fenn, S., C.B. Gerhold, and K.P. Hopfner, *Nuclear actin-related proteins take shape.* Bioarchitecture, 2011. **1**(4): p. 192-195.
167. Zhao, K., et al., *Rapid and Phosphoinositol-Dependent Binding of the SWI/SNF-like BAF Complex to Chromatin after T Lymphocyte Receptor Signaling.* Cell, 1998. **95**(5): p. 625-636.
168. Rando, O.J., et al., *Phosphatidylinositol-dependent actin filament binding by the SWI/SNF-like BAF chromatin remodeling complex.* Proceedings of the National Academy of Sciences, 2002. **99**(5): p. 2824-2829.
169. Machesky, L.M., et al., *Purification of a cortical complex containing two unconventional actins from Acanthamoeba by affinity chromatography on profilin-agarose.* The Journal of Cell Biology, 1994. **127**(1): p. 107-115.
170. Dyche Mullins, R. and T.D. Pollard, *Structure and function of the Arp2/3 complex.* Current Opinion in Structural Biology, 1999. **9**(2): p. 244-249.
171. Machesky, L.M. and R.H. Insall, *Scar1 and the related Wiskott–Aldrich syndrome protein, WASP, regulate the actin cytoskeleton through the Arp2/3 complex.* Current Biology, 1998. **8**(25): p. 1347-1356.
172. Machesky, L.M., et al., *Scar, a WASp-related protein, activates nucleation of actin filaments by the Arp2/3 complex.* Proc Natl Acad Sci U S A, 1999. **96**(7): p. 3739-44.
173. Rottner, K., J. Hänisch, and K.G. Campellone, *WASH, WHAMM and JMY: regulation of Arp2/3 complex and beyond.* Trends in Cell Biology, 2010. **20**(11): p. 650-661.

174. Higgs, H.N. and T.D. Pollard, *Regulation of Actin Polymerization by Arp2/3 Complex and WASp/Scar Proteins.* Journal of Biological Chemistry, 1999. **274**(46): p. 32531-32534.
175. Meagher, R.B., et al., *Chapter 5 Nuclear Actin-Related Proteins in Epigenetic Control*, in *International Review of Cell and Molecular Biology*, W.J. Kwang, Editor 2009, Academic Press. p. 157-215.
176. Harata, M., et al., *The Nuclear Actin-related Protein of Saccharomyces cerevisiae, Act3p/Arp4, Interacts with Core Histones.* Molecular Biology of the Cell, 1999. **10**(8): p. 2595-2605.
177. Killian, J.L., et al., *Recent advances in single molecule studies of nucleosomes.* Current Opinion in Structural Biology, 2012. **22**(1): p. 80-87.
178. Luger, K., M.L. Dechassa, and D.J. Tremethick, *New insights into nucleosome and chromatin structure: an ordered state or a disordered affair?* Nat Rev Mol Cell Biol, 2012. **13**(7): p. 436-447.
179. Billon, P. and J. Côté, *Precise deposition of histone H2A.Z in chromatin for genome expression and maintenance.* Biochimica et Biophysica Acta (BBA) - Gene Regulatory Mechanisms, 2012. **1819**(3–4): p. 290-302.
180. Winkler, D.D., et al., *Histone Chaperone FACT Coordinates Nucleosome Interaction through Multiple Synergistic Binding Events.* Journal of Biological Chemistry, 2011. **286**(48): p. 41883-41892.
181. Udugama, M., A. Sabri, and B. Bartholomew, *The INO80 ATP-Dependent Chromatin Remodeling Complex Is a Nucleosome Spacing Factor.* Molecular and Cellular Biology, 2011. **31**(4): p. 662-673.
182. Bengtsson, L. and K.L. Wilson, *Multiple and surprising new functions for emerin, a nuclear membrane protein.* Current Opinion in Cell Biology, 2004. **16**(1): p. 73-79.
183. Kumaran, R.I. and D.L. Spector, *A genetic locus targeted to the nuclear periphery in living cells maintains its transcriptional competence.* The Journal of Cell Biology, 2008. **180**(1): p. 51-65.
184. Cremer, T. and C. Cremer, *Chromosome territories, nuclear architecture and gene regulation in mammalian cells.* Nat Rev Genet, 2001. **2**(4): p. 292-301.
185. Yoshida, T., et al., *Actin-Related Protein Arp6 Influences H2A.Z-Dependent and -Independent Gene Expression and Links Ribosomal Protein Genes to Nuclear Pores.* PLoS Genet, 2010. **6**(4): p. e1000910.
186. Maruyama, E.O., et al., *The actin family member Arp6 and the histone variant H2A.Z are required for spatial positioning of chromatin in chicken cell nuclei.* Journal of Cell Science, 2012. **125**(16): p. 3739-3743.
187. Teixeira, M.T., B. Dujon, and E. Fabre, *Genome-wide Nuclear Morphology Screen Identifies Novel Genes Involved in Nuclear Architecture and Gene-silencing in Saccharomyces cerevisiae.* Journal of Molecular Biology, 2002. **321**(4): p. 551-561.
188. Guttman, M., et al., *Chromatin signature reveals over a thousand highly conserved large non-coding RNAs in mammals.* Nature, 2009. **458**(7235): p. 223-227.
189. Zhang, R., L. Zhang, and W. Yu, *Genome-wide expression of non-coding RNA and global chromatin modification.* Acta Biochimica et Biophysica Sinica, 2012. **44**(1): p. 40-47.
190. Bertone, P., et al., *Global Identification of Human Transcribed Sequences with Genome Tiling Arrays.* Science, 2004. **306**(5705): p. 2242-2246.
191. Tsai, M.-C., et al., *Long Noncoding RNA as Modular Scaffold of Histone Modification Complexes.* Science, 2010. **329**(5992): p. 689-693.
192. Khalil, A.M., et al., *Many human large intergenic noncoding RNAs associate with chromatin-modifying complexes and affect gene expression.* Proceedings of the National Academy of Sciences, 2009. **106**(28): p. 11667-11672.
193. Wang, X., et al., *Induced ncRNAs allosterically modify RNA-binding proteins in cis to inhibit transcription.* Nature, 2008. **454**(7200): p. 126-130.

194. Morris, K.V., et al., *Small Interfering RNA-Induced Transcriptional Gene Silencing in Human Cells.* Science, 2004. **305**(5688): p. 1289-1292.
195. Watanabe, T., et al., *Role for piRNAs and Noncoding RNA in de Novo DNA Methylation of the Imprinted Mouse Rasgrf1 Locus.* Science, 2011. **332**(6031): p. 848-852.
196. Hotchkiss, R.D., *THE QUANTITATIVE SEPARATION OF PURINES, PYRIMIDINES, AND NUCLEOSIDES BY PAPER CHROMATOGRAPHY.* Journal of Biological Chemistry, 1948. **175**(1): p. 315-332.
197. Holliday, R. and J. Pugh, *DNA modification mechanisms and gene activity during development.* Science, 1975. **187**(4173): p. 226-232.
198. Bird, A., *DNA methylation patterns and epigenetic memory.* Genes Dev, 2002. **16**: p. 6-21.
199. Moore, L.D., T. Le, and G. Fan, *DNA Methylation and Its Basic Function.* Neuropsychopharmacology, 2012.
200. Prendergast, G.C. and E.B. Ziff, *Methylation-sensitive sequence-specific DNA binding by the c-Myc basic region.* Science, 1991. **251**(4990): p. 186-9.
201. Watt, F. and P.L. Molloy, *Cytosine methylation prevents binding to DNA of a HeLa cell transcription factor required for optimal expression of the adenovirus major late promoter.* Genes & Development, 1988. **2**(9): p. 1136-1143.
202. Nan, X., et al., *Transcriptional repression by the methyl-CpG-binding protein MeCP2 involves a histone deacetylase complex.* Nature, 1998. **393**(6683): p. 386-389.
203. Jones, P.L., et al., *Methylated DNA and MeCP2 recruit histone deacetylase to repress transcription.* Nat Genet, 1998. **19**(2): p. 187-191.
204. Rakyan, V.K., et al., *DNA Methylation Profiling of the Human Major Histocompatibility Complex: A Pilot Study for the Human Epigenome Project.* PLoS Biol, 2004. **2**(12): p. e405.
205. Maunakea, A.K., et al., *Conserved role of intragenic DNA methylation in regulating alternative promoters.* Nature, 2010. **466**(7303): p. 253-257.
206. Irizarry, R.A., et al., *The human colon cancer methylome shows similar hypo- and hypermethylation at conserved tissue-specific CpG island shores.* Nat Genet, 2009. **41**(2): p. 178-186.
207. Brandeis, M., et al., *Spl elements protect a CpG island from de novo methylation.* Nature, 1994. **371**(6496): p. 435-438.
208. Brenet, F., et al., *DNA Methylation of the First Exon Is Tightly Linked to Transcriptional Silencing.* PLoS ONE, 2011. **6**(1): p. e14524.
209. Hellman, A. and A. Chess, *Gene Body-Specific Methylation on the Active X Chromosome.* Science, 2007. **315**(5815): p. 1141-1143.
210. Aran, D., et al., *Replication timing-related and gene body-specific methylation of active human genes.* Human Molecular Genetics, 2011. **20**(4): p. 670-680.
211. Pradhan, S., et al., *Recombinant Human DNA (Cytosine-5) Methyltransferase.* Journal of Biological Chemistry, 1999. **274**(46): p. 33002-33010.
212. Leonhardt, H., et al., *A targeting sequence directs DNA methyltransferase to sites of DNA replication in mammalian nuclei.* Cell, 1992. **71**(5): p. 865-873.
213. Okano, M., et al., *DNA Methyltransferases Dnmt3a and Dnmt3b Are Essential for De Novo Methylation and Mammalian Development.* Cell, 1999. **99**(3): p. 247-257.
214. Filion, G.J.P., et al., *A Family of Human Zinc Finger Proteins That Bind Methylated DNA and Repress Transcription.* Molecular and Cellular Biology, 2006. **26**(1): p. 169-181.
215. Bostick, M., et al., *UHRF1 Plays a Role in Maintaining DNA Methylation in Mammalian Cells.* Science, 2007. **317**(5845): p. 1760-1764.
216. Sharif, J., et al., *The SRA protein Np95 mediates epigenetic inheritance by recruiting Dnmt1 to methylated DNA.* Nature, 2007. **450**(7171): p. 908-912.

217. Tahiliani, M., et al., *Conversion of 5-Methylcytosine to 5-Hydroxymethylcytosine in Mammalian DNA by MLL Partner TET1.* Science, 2009. **324**(5929): p. 930-935.
218. Pastor, W.A., et al., *Genome-wide mapping of 5-hydroxymethylcytosine in embryonic stem cells.* Nature, 2011. **473**(7347): p. 394-397.
219. Fuks, F., et al., *The DNA methyltransferases associate with HP1 and the SUV39H1 histone methyltransferase.* Nucleic Acids Research, 2003. **31**(9): p. 2305-2312.
220. Luger, K., et al., *Crystal structure of the nucleosome core particle at 2.8[thinsp]A resolution.* Nature, 1997. **389**: p. 251-260.
221. Oudet, P., M. Gross-Bellard, and P. Chambon, *Electron microscopic and biochemical evidence that chromatin structure is a repeating unit.* Cell, 1975. **4**(4): p. 281-300.
222. Bhaumik, S.R., E. Smith, and A. Shilatifard, *Covalent modifications of histones during development and disease pathogenesis.* Nat Struct Mol Biol, 2007. **14**(11): p. 1008-1016.
223. Tan, M., et al., *Identification of 67 Histone Marks and Histone Lysine Crotonylation as a New Type of Histone Modification.* Cell, 2011. **146**(6): p. 1016-1028.
224. Bannister, A.J. and T. Kouzarides, *The CBP co-activator is a histone acetyltransferase.* Nature, 1996. **384**(6610): p. 641-643.
225. Xue, Y., et al., *NURD, a Novel Complex with Both ATP-Dependent Chromatin-Remodeling and Histone Deacetylase Activities.* Molecular Cell, 1998. **2**(6): p. 851-861.
226. Metzger, E., et al., *Phosphorylation of histone H3T6 by PKC[bgr]I controls demethylation at histone H3K4.* Nature, 2010. **464**(7289): p. 792-796.
227. Xu, D., et al., *Covalent modifications of histones during mitosis and meiosis.* Cell Cycle, 2009. **8**(22): p. 3688-3694.
228. Bao, Y., *Chromatin response to DNA double-strand break damage.* Epigenomics, 2011. **3**(3): p. 307-321.
229. Banerjee, T. and D. Chakravarti, *A Peek into the Complex Realm of Histone Phosphorylation.* Molecular and Cellular Biology, 2011. **31**(24): p. 4858-4873.
230. Goldknopf, I.L., et al., *Isolation and characterization of protein A24, a "histone-like" non-histone chromosomal protein.* J Biol Chem, 1975. **250**(18): p. 7182-7.
231. West, M.H.P. and W.M. Bonner, *Histone 2B can be modified by the attachment of ubiquitin.* Nucleic Acids Research, 1980. **8**(20): p. 4671-4680.
232. Wang, H., et al., *Histone H3 and H4 Ubiquitylation by the CUL4-DDB-ROC1 Ubiquitin Ligase Facilitates Cellular Response to DNA Damage.* Molecular Cell, 2006. **22**(3): p. 383-394.
233. Cao, J. and Q. Yan, *Histone ubiquitination and deubiquitination in transcription, DNA damage response, and cancer.* Frontiers in Oncology, 2012. **2**.
234. Chen, A., et al., *Autoubiquitination of the BRCA1·BARD1 RING Ubiquitin Ligase.* Journal of Biological Chemistry, 2002. **277**(24): p. 22085-22092.
235. Nakagawa, T., et al., *Deubiquitylation of histone H2A activates transcriptional initiation via trans-histone cross-talk with H3K4 di- and trimethylation.* Genes & Development, 2008. **22**(1): p. 37-49.
236. Joo, H.-Y., et al., *Regulation of cell cycle progression and gene expression by H2A deubiquitination.* Nature, 2007. **449**(7165): p. 1068-1072.
237. Minsky, N., et al., *Monoubiquitinated H2B is associated with the transcribed region of highly expressed genes in human cells.* Nat Cell Biol, 2008. **10**(4): p. 483-488.
238. Sun, Z.-W. and C.D. Allis, *Ubiquitination of histone H2B regulates H3 methylation and gene silencing in yeast.* Nature, 2002. **418**(6893): p. 104-108.
239. Pavri, R., et al., *Histone H2B Monoubiquitination Functions Cooperatively with FACT to Regulate Elongation by RNA Polymerase II.* Cell, 2006. **125**(4): p. 703-717.

240. Xiao, T., et al., *Histone H2B Ubiquitylation Is Associated with Elongating RNA Polymerase II.* Molecular and Cellular Biology, 2005. **25**(2): p. 637-651.
241. Zhang, X.-Y., et al., *The Putative Cancer Stem Cell Marker USP22 Is a Subunit of the Human SAGA Complex Required for Activated Transcription and Cell-Cycle Progression.* Molecular Cell, 2008. **29**(1): p. 102-111.
242. Zhao, Y., et al., *A TFTC/STAGA Module Mediates Histone H2A and H2B Deubiquitination, Coactivates Nuclear Receptors, and Counteracts Heterochromatin Silencing.* Molecular Cell, 2008. **29**(1): p. 92-101.
243. Henry, K.W., et al., *Transcriptional activation via sequential histone H2B ubiquitylation and deubiquitylation, mediated by SAGA-associated Ubp8.* Genes & Development, 2003. **17**(21): p. 2648-2663.
244. Fierz, B., et al., *Histone H2B ubiquitylation disrupts local and higher-order chromatin compaction.* Nat Chem Biol, 2011. **7**(2): p. 113-119.
245. Shi, Y., et al., *Histone Demethylation Mediated by the Nuclear Amine Oxidase Homolog LSD1.* Cell, 2004. **119**(7): p. 941-953.
246. Greer, E.L. and Y. Shi, *Histone methylation: a dynamic mark in health, disease and inheritance.* Nat Rev Genet, 2012. **13**(5): p. 343-357.
247. Gershey, E.L., et al., *Chemical studies of histone methylation. Evidence for the occurrence of 3-methylhistidine in avian erythrocyte histone fractions.* J Biol Chem, 1969. **244**(18): p. 4871-7.
248. Shilatifard, A., *Chromatin Modifications by Methylation and Ubiquitination: Implications in the Regulation of Gene Expression.* Annual Review of Biochemistry, 2006. **75**(1): p. 243-269.
249. Whetstine, J.R., et al., *Reversal of Histone Lysine Trimethylation by the JMJD2 Family of Histone Demethylases.* Cell, 2006. **125**(3): p. 467-481.
250. Stassen, M.J., et al., *The Drosophila trithorax proteins contain a novel variant of the nuclear receptor type DNA binding domain and an ancient conserved motif found in other chromosomal proteins.* Mech Dev, 1995. **52**(2-3): p. 209-23.
251. Lachner, M., et al., *Methylation of histone H3 lysine 9 creates a binding site for HP1 proteins.* Nature, 2001. **410**(6824): p. 116-120.
252. Noma, K.-i., C.D. Allis, and S.I.S. Grewal, *Transitions in Distinct Histone H3 Methylation Patterns at the Heterochromatin Domain Boundaries.* Science, 2001. **293**(5532): p. 1150-1155.
253. Miller, T., et al., *COMPASS: A complex of proteins associated with a trithorax-related SET domain protein.* Proceedings of the National Academy of Sciences, 2001. **98**(23): p. 12902-12907.
254. Schaft, D., et al., *The histone 3 lysine 36 methyltransferase, SET2, is involved in transcriptional elongation.* Nucleic Acids Research, 2003. **31**(10): p. 2475-2482.
255. Shiio, Y. and R.N. Eisenman, *Histone sumoylation is associated with transcriptional repression.* Proceedings of the National Academy of Sciences, 2003. **100**(23): p. 13225-13230.
256. Nathan, D., et al., *Histone sumoylation is a negative regulator in Saccharomyces cerevisiae and shows dynamic interplay with positive-acting histone modifications.* Genes & Development, 2006. **20**(8): p. 966-976.
257. Hottiger, M.O., et al., *Toward a unified nomenclature for mammalian ADP-ribosyltransferases.* Trends in Biochemical Sciences, 2010. **35**(4): p. 208-219.
258. Koch-Nolte, F., et al., *Mammalian ADP-ribosyltransferases and ADP-ribosylhydrolases.* Front Biosci, 2008. **13**: p. 6716-29.
259. Messner, S. and M.O. Hottiger, *Histone ADP-ribosylation in DNA repair, replication and transcription.* Trends in Cell Biology, 2011. **21**(9): p. 534-542.
260. de Murcia, G., A. Huletsky, and G.G. Poirier, *Modulation of chromatin structure by poly(ADP-ribosyl)ation.* Biochem Cell Biol, 1988. **66**(6): p. 626-35.

261. R J Aubin, A.F., G de Murcia, P Mandel, A Lord, G Grondin, and G G Poirier, *Correlation between endogenous nucleosomal hyper(ADP-ribosyl)ation of histone H1 and the induction of chromatin relaxation.* EMBO Journal, 1983. **2**(10): p. 1685–1693.
262. Martinez-Zamudio, R. and H.C. Ha, *Histone ADP-Ribosylation Facilitates Gene Transcription by Directly Remodeling Nucleosomes.* Molecular and Cellular Biology, 2012. **32**(13): p. 2490-2502.
263. Messner, S., et al., *PARP1 ADP-ribosylates lysine residues of the core histone tails.* Nucleic Acids Research, 2010. **38**(19): p. 6350-6362.
264. Duan, Q., et al., *Phosphorylation of H3S10 Blocks the Access of H3K9 by Specific Antibodies and Histone Methyltransferase.* Journal of Biological Chemistry, 2008. **283**(48): p. 33585-33590.
265. Fischle, W., et al., *Regulation of HP1-chromatin binding by histone H3 methylation and phosphorylation.* Nature, 2005. **438**(7071): p. 1116-1122.
266. Sarma, K. and D. Reinberg, *Histone variants meet their match.* Nat Rev Mol Cell Biol, 2005. **6**(2): p. 139-149.
267. Jin, J., et al., *In and out: histone variant exchange in chromatin.* Trends in Biochemical Sciences, 2005. **30**(12): p. 680-687.
268. Henikoff, S. and K. Ahmad, *ASSEMBLY OF VARIANT HISTONES INTO CHROMATIN.* Annual Review of Cell and Developmental Biology, 2005. **21**(1): p. 133-153.
269. Tagami, H., et al., *Histone H3.1 and H3.3 Complexes Mediate Nucleosome Assembly Pathways Dependent or Independent of DNA Synthesis.* Cell, 2004. **116**(1): p. 51-61.
270. Talbert, P.B. and S. Henikoff, *Histone variants [mdash] ancient wrap artists of the epigenome.* Nat Rev Mol Cell Biol, 2010. **11**(4): p. 264-275.
271. Malik, H.S. and S. Henikoff, *Phylogenomics of the nucleosome.* Nat Struct Mol Biol, 2003. **10**(11): p. 882-891.
272. Wieland, G., et al., *Functional Complementation of Human Centromere Protein A (CENP-A) by Cse4p from Saccharomyces cerevisiae.* Molecular and Cellular Biology, 2004. **24**(15): p. 6620-6630.
273. Dalal, Y., et al., *Structure, dynamics, and evolution of centromeric nucleosomes.* Proceedings of the National Academy of Sciences, 2007. **104**(41): p. 15974-15981.
274. Furuyama, T. and S. Henikoff, *Centromeric Nucleosomes Induce Positive DNA Supercoils.* Cell, 2009. **138**(1): p. 104-113.
275. Santaguida, S. and A. Musacchio, *The life and miracles of kinetochores.* EMBO J, 2009. **28**(17): p. 2511-2531.
276. Cui, B., Y. Liu, and M.A. Gorovsky, *Deposition and Function of Histone H3 Variants in Tetrahymena thermophila.* Molecular and Cellular Biology, 2006. **26**(20): p. 7719-7730.
277. Sakai, A., et al., *Transcriptional and Developmental Functions of the H3.3 Histone Variant in Drosophila.* Current Biology, 2009. **19**(21): p. 1816-1820.
278. Schwartz, B.E. and K. Ahmad, *Transcriptional activation triggers deposition and removal of the histone variant H3.3.* Genes & Development, 2005. **19**(7): p. 804-814.
279. Ng, R.K. and J.B. Gurdon, *Epigenetic memory of an active gene state depends on histone H3.3 incorporation into chromatin in the absence of transcription.* Nat Cell Biol, 2008. **10**(1): p. 102-109.
280. Redon, C., et al., *Histone H2A variants H2AX and H2AZ.* Current Opinion in Genetics & Development, 2002. **12**(2): p. 162-169.
281. Chadwick, B.P. and H.F. Willard, *A Novel Chromatin Protein, Distantly Related to Histone H2a, Is Largely Excluded from the Inactive X Chromosome.* The Journal of Cell Biology, 2001. **152**(2): p. 375-384.

282. Eirín-López, J.M., T. Ishibashi, and J. Ausió, *H2A.Bbd: a quickly evolving hypervariable mammalian histone that destabilizes nucleosomes in an acetylation-independent way.* The FASEB Journal, 2008. **22**(1): p. 316-326.
283. Bao, Y., et al., *Nucleosomes containing the histone variant H2A.Bbd organize only 118 base pairs of DNA.* EMBO J, 2004. **23**(16): p. 3314-3324.
284. González-Romero, R., et al., *Quickly evolving histones, nucleosome stability and chromatin folding: All about histone H2A.Bbd.* Gene, 2008. **413**(1–2): p. 1-7.
285. Zhou, J., et al., *The nucleosome surface regulates chromatin compaction and couples it with transcriptional repression.* Nat Struct Mol Biol, 2007. **14**(11): p. 1070-1076.
286. Gautier, T., et al., *Histone variant H2ABbd confers lower stability to the nucleosome.* EMBO Rep, 2004. **5**(7): p. 715-720.
287. Doyen, C.-M., et al., *Dissection of the unusual structural and functional properties of the variant H2A.Bbd nucleosome.* EMBO J, 2006. **25**(18): p. 4234-4244.
288. Angelov, D., et al., *SWI/SNF remodeling and p300-dependent transcription of histone variant H2ABbd nucleosomal arrays.* EMBO J, 2004. **23**(19): p. 3815-3824.
289. Chadwick, B.P. and H.F. Willard, *Histone H2A variants and the inactive X chromosome: identification of a second macroH2A variant.* Human Molecular Genetics, 2001. **10**(10): p. 1101-1113.
290. Chakravarthy, S., et al., *Structural Characterization of the Histone Variant macroH2A.* Molecular and Cellular Biology, 2005. **25**(17): p. 7616-7624.
291. Doyen, C.-M., et al., *Mechanism of Polymerase II Transcription Repression by the Histone Variant macroH2A.* Molecular and Cellular Biology, 2006. **26**(3): p. 1156-1164.
292. Abbott, D.W., et al., *Beyond the Xi.* Journal of Biological Chemistry, 2005. **280**(16): p. 16437-16445.
293. Nusinow, D.A., et al., *Poly(ADP-ribose) Polymerase 1 Is Inhibited by a Histone H2A Variant, MacroH2A, and Contributes to Silencing of the Inactive X Chromosome.* Journal of Biological Chemistry, 2007. **282**(17): p. 12851-12859.
294. Timinszky, G., et al., *A macrodomain-containing histone rearranges chromatin upon sensing PARP1 activation.* Nat Struct Mol Biol, 2009. **16**(9): p. 923-929.
295. Ouararhni, K., et al., *The histone variant mH2A1.1 interferes with transcription by down-regulating PARP-1 enzymatic activity.* Genes & Development, 2006. **20**(23): p. 3324-3336.
296. Buschbeck, M., et al., *The histone variant macroH2A is an epigenetic regulator of key developmental genes.* Nat Struct Mol Biol, 2009. **16**(10): p. 1074-1079.
297. Rogakou, E.P., et al., *DNA Double-stranded Breaks Induce Histone H2AX Phosphorylation on Serine 139.* Journal of Biological Chemistry, 1998. **273**(10): p. 5858-5868.
298. Fernandez-Capetillo, O., et al., *H2AX: the histone guardian of the genome.* DNA Repair, 2004. **3**(8–9): p. 959-967.
299. Shiloh, Y., *ATM and related protein kinases: safeguarding genome integrity.* Nat Rev Cancer, 2003. **3**(3): p. 155-168.
300. Shroff, R., et al., *Distribution and Dynamics of Chromatin Modification Induced by a Defined DNA Double-Strand Break.* Current Biology, 2004. **14**(19): p. 1703-1711.
301. Rogakou, E.P., et al., *Megabase Chromatin Domains Involved in DNA Double-Strand Breaks in Vivo.* The Journal of Cell Biology, 1999. **146**(5): p. 905-916.
302. Celeste, A., et al., *Histone H2AX phosphorylation is dispensable for the initial recognition of DNA breaks.* Nat Cell Biol, 2003. **5**(7): p. 675-679.
303. Ismail, I.H. and M.J. Hendzel, *The γ-H2A.X: Is it just a surrogate marker of double-strand breaks or much more?* Environmental and Molecular Mutagenesis, 2008. **49**(1): p. 73-82.

304. Celeste, A., et al., *Genomic Instability in Mice Lacking Histone H2AX.* Science, 2002. **296**(5569): p. 922-927.
305. Zlatanova, J. and A. Thakar, *H2A.Z: View from the Top.* Structure, 2008. **16**(2): p. 166-179.
306. Ishibashi, T., et al., *Acetylation of Vertebrate H2A.Z and Its Effect on the Structure of the Nucleosome.* Biochemistry, 2009. **48**(22): p. 5007-5017.
307. Abbott, D.W., et al., *Characterization of the Stability and Folding of H2A.Z Chromatin Particles.* Journal of Biological Chemistry, 2001. **276**(45): p. 41945-41949.
308. Park, Y.-J., et al., *A New Fluorescence Resonance Energy Transfer Approach Demonstrates That the Histone Variant H2AZ Stabilizes the Histone Octamer within the Nucleosome.* Journal of Biological Chemistry, 2004. **279**(23): p. 24274-24282.
309. Rangasamy, D., et al., *Pericentric heterochromatin becomes enriched with H2A.Z during early mammalian development.* EMBO J, 2003. **22**(7): p. 1599-1607.
310. Fan, J.Y., et al., *H2A.Z Alters the Nucleosome Surface to Promote HP1α-Mediated Chromatin Fiber Folding.* Molecular Cell, 2004. **16**(4): p. 655-661.
311. Meneghini, M.D., M. Wu, and H.D. Madhani, *Conserved Histone Variant H2A.Z Protects Euchromatin from the Ectopic Spread of Silent Heterochromatin.* Cell, 2003. **112**(5): p. 725-736.
312. Zhang, H., D.N. Roberts, and B.R. Cairns, *Genome-Wide Dynamics of Htz1, a Histone H2A Variant that Poises Repressed/Basal Promoters for Activation through Histone Loss.* Cell, 2005. **123**(2): p. 219-231.
313. Sarcinella, E., et al., *Monoubiquitylation of H2A.Z Distinguishes Its Association with Euchromatin or Facultative Heterochromatin.* Molecular and Cellular Biology, 2007. **27**(18): p. 6457-6468.
314. Hardy, S., et al., *The Euchromatic and Heterochromatic Landscapes Are Shaped by Antagonizing Effects of Transcription on H2A.Z Deposition.* PLoS Genet, 2009. **5**(10): p. e1000687.
315. Altaf, M., et al., *Connection between histone H2A variants and chromatin remodeling complexesThis paper is one of a selection of papers published in this Special Issue, entitled CSBMCB's 51st Annual Meeting – Epigenetics and Chromatin Dynamics, and has undergone the Journal's usual peer review process.* Biochemistry and Cell Biology, 2009. **87**(1): p. 35-50.
316. Bönisch, C., et al., *H2A.Z.2.2 is an alternatively spliced histone H2A.Z variant that causes severe nucleosome destabilization.* Nucleic Acids Research, 2012. **40**(13): p. 5951-5964.
317. Goldman, J.A., J.D. Garlick, and R.E. Kingston, *Chromatin Remodeling by Imitation Switch (ISWI) Class ATP-dependent Remodelers Is Stimulated by Histone Variant H2A.Z.* Journal of Biological Chemistry, 2010. **285**(7): p. 4645-4651.

7. Attachment

7.1 Overview of the current literature of epigenetics

7.1.1 Epigenetic readouts

Three of the four main regulatory mechanisms that inter-dependently modulate the state of chromatin are discussed here. Please find a brief summary of the current literature on DNA methylation, post-translational modification of histones and large intervening non-coding RNAs (ncRNAs) attached to this thesis, while , ATP-dependent chromatin remodeling is described in the introductory chapter.

7.1.1.1 non-coding RNAs

Non-coding RNAs have recently been described to appoint conserved signatures to chromatin [188] and it has been proposed that these long intergenic non coding RNAs (lincRNAs) are suitable candidates to bridge DNA and chromatin modifying complexes due to their ability to form secondary structures that can be recognized by proteins as well as their aptitude to base pair with complementary DNA sequences [189]. Indeed, it has been shown that transcription of intergenic DNA occurs [190], and the corresponding lincRNAs can act as modular scaffolds for chromatin modifying complexes [191]. Moreover, many lincRNAs are tightly associated with chromatin modifying complexes and alter gene expression [192]. A putatively uniform mechanism could then be an allosterical modulation of RNA-binding co-regulators by signal-induced ncRNAs that are localized to regulatory regions of transcription as it has been shown for TLS (for translocated in liposarcoma) that specifically binds and inhibits CBP (CREB-binding protein) and p300 histone acetyltransferase activities on *cyclin D1* (*CCND1*) upon RNA binding [193].

Other non-coding RNA such as small interfering RNA (siRNA) or microRNA silence genes associated with DNA methylation of the targeted sequence [194] and in a more recent study PIWI-interacting RNA (piRNA) pathway has been found to be required for de novo methylation leading to a model in which piRNAs and a target RNA orchestrate the sequence-specific methylation of DNA [195].

7.1.1.2 DNA methylation and hydroxymethylation

DNA methylation is the most extensively studied epigenetic mark. First described in 1948 [196] it became clear that this DNA modification plays a role in differential gene expression in the 1970s [197].

DNA methylation primarily takes place at position 5 of cytosine within CpG dimers that are prevalently organized in so called CpG island which are located in regions of large repetitive DNA sequences or gene promotor regions [198]. DNA methylation is the most extensively studied epigenetic modification and is implicated in gene silencing by either promoting or preventing the binding of regulatory proteins [199].

For instance, binding of transcription factors such as c-myc or MLTF (major late transcription factor) is impaired by methylated DNA [200, 201], while regulatory proteins such as MeCP2 (methyl CpG binding protein 2) are recruited to methylated CpG islands and subsequently target Histone Deacetylases to their chromatin substrate [202, 203]. Recently however, it has been shown that CpG islands seldom display tissue-specific methylation patterns, which would have been expected for the control of differential gene expression [204, 205]. Instead, so called CpG island shores, situated up to 2 kb away from CpG islands, show conserved and tissue-specific methylation patterns that reduce gene expression [206]. It appears that transcription factor binding to CpG islands prevents DNA methylation at these loci [207]. Interestingly, methylation in intra-genic regions can stimulate as well as repress expression. While methylation in the first exon of the gene results in gene silencing [208], methylation of the remainder of the gene sequence stimulates expression in fast dividing cells [209] but not in slowly dividing cells [210]. This phenomenon coined the term gene body, which is the open reading frame except the first exon.

The responsible enzymes for methylating DNA were identified to be the DNA (cytosine-5)-methyltransferases Dnmt1, Dnmt3a and Dnmt3b. Dnmt1 preferentially methylates hemimethylated DNA [211] and coherently associates with the replication machinery [212]. On the contrary, Dnmt3a and Dnmt3b are *de novo* DNA methyltransfersases, which show no preference for hemimethylated DNA strands [213].

So far, three different protein families have been found to recognize methylated DNA: MBD (methyl-CpG-binding domain) proteins, UHRF (human ubiquitin-like containing PHD and RING finger) proteins and zinc-finger proteins. Binding of these protein families to methylated DNA usually aids in the inhibition of transcription factor recruitment and hence in the repression of expression [214]. UHRF1 however, guides Dnmt1 to hemimethylated DNA during replication and therefore plays a role in the maintenance of genomic methylation patterns during cell division [215, 216].

Enzymes that directly demethylate 5-methyl cytosine remain elusive. Instead, a series of enzymatic reactions involving deamination and potentially oxidation transform 5-methyl cytosine into products that are then repaired by the BER (base excision repair) pathway.

One possible intermediate within the removal of methylation marks is 5-hydroxymethyl cytosine (5hmC), which is the product of 5m-cytosine oxidation by the TET (ten-eleven translocation) family of

proteins [217]. Interestingly, 5hmC has been shown to be a distinct epigenetic marker on its own, which is enriched at poised promoters that bear the dual histone modification histone 3 lysine 27 trimethylation (H3K27me3) and histone 3 lysine 4 trimethylation (H3K4me3) [218], suggesting crosstalk between epigenetic marks on DNA as well as on histones.

Indeed, it has been shown that enzymes involved in DNA methylation are tightly connected to histone modifications and to enzymes that govern this additional important epigenetic mark. Dnmts work together with histone modifying enzymes to maintain or enforce transcriptional repression on specific gene loci. For instance, Dnmt1 and Dnmt3 bind to SUV39H1 (suppressor of variegation 3-9 homolog), which is a histone methyltransferase that methylates H3K9 to also repress gene transcription [219].

7.1.1.3 Histone modifications

The packaging of DNA is mostly accomplished by nucleosomes, in which approximately 146 base pairs of DNA are wrapped around a histone octamer [220]. These nucleosomes resemble a beads (histones) on a string (DNA) model [221] that assembles into higher ordered structures, whose exact conformations are still under debate [178].

Nonetheless it is now clear, that post-translational modifications of the core histones or the exchange of canonical histones with certain variants have a stark impact on the structure of chromatin and hence the accessibility of its DNA content.

Defined residues of the flexible N-terminal tail of histones as well as some amino acids of the globular domain can be subjected to modifications such as acetylation, phosphorylation, ubiquitination, methylation, sumoylation as well as ADP-ribosylation [222]. A rather newly identified modification is the crotonylation of histones [223]. In the following section all modifications will be briefly described.

Acetylation

All four canonical histones can undergo acetylation, where HATs (histone acetyltransferases) use acetyl-coenzyme A to transfer the acetyl moiety to the ε-amine of lysines, which neutralizes the positive charge and thereby usually weakens histone-DNA interactions. As a consequence, acetylated chromatin adopts a relaxed conformation, which is more accessible to transcription. Consistently, transcriptional activators, such as p300/CBP (CREB binding protein), frequently have intrinsic HAT activity [224]. In contrast to DNA methylation, histone acetylation can be enzymatically removed in a single step reaction

by HDACs (histone deacetylases), which often are subunits of transcriptional co-repressors like NURD/Mi-2 [225].

Therefore the interplay between HATs and HDACs governs the cellular acetylation levels of histones and majorly contributes to the accessibility of DNA within chromatin.

Very recently histone lysine crotonylation (Kcr) has been discovered, which is mechanistically and functionally different from lysine acetylation (Kac). Nonetheless, Kcr putatively affects chromatin structure to facilitate histone replacement and thus transcription similar to Kac. The distinct chemical properties of the crotonyl moiety however might orchestrate the reorganization of chromatin after histone exchange in a manner distinct from Kac marks [223].

Phosphorylation

Even though histone phosphorylation can also influence transcription via cross-talk to other histone modifications [226], it is generally involved in signaling pathways important for mitosis [227] or DNA damage repair [228]. While the Kinases responsible for histone phosphorylation of all canonical histones and the histone variant H2A.X are mostly identified, many proteins that recognize phosphorylated histones have yet to be discovered [229]. The MRN (Mre11 Rad50 Nbs1) and INO80 (inositol requiring 80) complexes are notable exceptions, since it has been shown that these protein complexes read the phosphorylated histone code in context of DNA damage repair.

Ubiquitination

Ubiquitination has been discovered to take place at all canonical histones [230-232]. H3 and H4 become polyubiquitinated upon UV irradiation but the consequences of these modifications are not well understood. On the other hand, H2A and H2B are two of the most abundantly monoubiquitinated proteins within the nucleus. The according E2 and E3 ligases and DUBs (deubiquitinating enzymes) have recently been reviewed [233]. For example, BRCA1 (breast cancer susceptibility gene 1) is a potential E3 ubiquitin ligase for H2A and H2A.X that covalently attaches ubiquitin to lysine 119 of the histones in vertebrates [234].

Interestingly, H2Aub and H2Bub seem to have opposing effects in transcriptional regulation. Ubiquitinated H2A is implicated in gene silencing since it prevents the establishment of H3K4me2 and H3K4me3 that mark actively transcribed chromatin [235] and H2Aub DUBs are necessary for gene activation [236].

In contrast, H2ABub was found to be enriched in highly transcribed genes [237] and monoubiquitinated H2B unidirectionally leads to the methylation of H3K4 [238]. Moreover, H2Bub stimulates PolII (RNA Polymerase II) elongation via the enhanced replacement of H2A-H2B dimers [239] and mutations in the H2B ubiquitination pathway result in transcriptional elongation defects [240].

Interestingly, H2Bub DUBs are found in co-activator complexes with histone acetyltransferase activity such as SAGA (Spt–Ada–Gcn5–acetyltransferase) or TFTC/STAGA (TBP-free TAFII complex/*Spt*3-TAFII31-*Gcn*5-L-acetyltransferase) suggesting that also the deubiquitination of H2B seems to be important for gene transcription [241, 242].

In fact, the full ubiquitination and deubiquitination cycle of H2B is necessary for the activation of PolII RNA transcription [243], possibly via the enhanced mobilization of H2A-H2B dimers.

Like H2Aub, H2Bub also undergoes cross-talk with accompanying histone modifications as it interacts with acetylated H4 to disrupt chromatin structures for increased accessibility [244] and it reciprocally influences H3K4 methylation compared to H2Aub as it specifically promotes H3K4 trimethylation [243].

Methylation

Histone methylation like ubiquitination is linked to transcriptional activation as well as repression depending on the context of the modification. All canonical histones including H1 can be methylated but so far only methylation marks at H3 and H4 have been further characterized in detail with respect to their biological function. Even though histone methylation was long thought to be an irreversible enzymatic reaction similar to DNA methylation, the identification of the first histone demethylase proved that histone methylation is a changeable modification within the epigenetic code [245]. Today, many histone methyltransferases and demethylases are known that specifically alter the histone code and thus the transcriptional landscape [246]. Three distinct families of methyltransferases use SAM (S-adenosylmethionine) to specifically transfer the methyl group onto histones. SET-domain containing proteins (Su(var)3-9, Enhancer of zeste and trithorax) and DOT1-like proteins (disruptor of telomeric silencing 1) modify lysines, while PMRTs (protein arginine N-methyltransferases) methylate arginines. In lysines, the ε-amine group can be mono- (me1), di- (me2) or trimethylated (me3) and arginine guanidinyl groups are either monomethylated (me1) or dimethylated, which can be either symmetrical (me2s) or asymmetrical (me2a).

Also monomethylated histidines have been reported but have not been further described [247].

Histone demethylases belong to either the family of amine oxidases or jumonji C domain containing, iron-dependent dioxygenases. Despite presence of these demethylases, histone methylation, especially trimethylation is considered to be a more persistent mark compared to other modifications [248] and an enzyme that demethylates trimethylated lysines has only recently been discovered [249]. The turnover of trimethylated lysines however seems to be important as mutations of the specific demethylase triggers p53-dependent germline apoptosis.

Remarkably, the methylation pattern of histones can result in transcriptional activation or repression according to the modification of specific residues. Both, the gene activating TrxG (trithorax group) and silencing PcG (Polycomb group) families of proteins contain a histone methyltransferase SET domain [250].

PcG proteins mediate the methylation of H3K9, which is recognized by of HP1 (heterochromatin protein 1) via its chromodomain [251]. HP1 in turn propagates heterochromatin spreading by recruiting further HP1 molecules as well as additional H3K9 methyltransferases and prevents H3K4 methylation, which is a mark of transcriptional activation [252].

This transcription inducing methylation mark is implemented into chromatin by COMPASS (complex proteins associated with SET1), which belongs to TrxG proteins [253]. COMPASS associates with RNA PolII in the early phase of gene transcription. Likewise, methylation mark H3K36 mediated by SET2 [254] also promotes active gene transcription.

SUMOylation

SUMOylation covalently links the small SUMO protein (small ubiquitin-like modifier) of 12 kDa onto other proteins similar to ubiquitination. In 2003 the SUMOylation of histones has been described [255]. All four core histones can be SUMOylated and multi-site SUMOylation or poly-SUMO chain formation has been suggested. The abundance of SUMO-histones is relatively low and even decreased for the histone variant H2A.Z. Since most of the SUMO target lysines can also be acetylated, SUMOylation seems to antagonize histone acetylation and represses gene transcription [256].

ADP-ribosylation

ADP-ribosylation is the transfer of an ADP-ribose moiety onto a substrate protein using NAD^+ as a donor. The range of potential acceptor amino acids is wide and comprises lysine, arginine, phospho-serine,

aspartate, asparagine, glutamate and cysteine residues. Furthermore, ATP-ribosylated proteins can accept further moieties to yield a protein linked to PAR (poly ADP-ribose) [257].

All histones and linker histone H1 can be subjected to mono or poly ADP-ribosylation by ARTDs (ADP-ribosyltransferases diphtheria toxin-like) and possibly to deribosylation by ARHs (ADP-ribosylation hydrolases) or by PARGs (poly ADP-ribosylation glycohydrolases) [258]. ARTDs are also known as PARPs (poly ADP-ribosyl polymerases) in the literature.

In general, poly ADP-ribosylated histones account only for a few percent of the total histones and H2A, H3 and H4 are only marginally modified. H1 on the other hand appears to be the best PAR acceptor followed by H2B [259].

Poly ADP-ribosylated histones are more accessible to antibodies and also nucleases than in native chromatin, suggesting a more open chromatin structure [260]. Poly-ADP ribosylated H1 promotes chromatin unwinding since gradual loss of H1 affinity to DNA upon the addition of several ADP-ribosyl moieties putatively prevents the formation of higher-order heterochromatin structures [261].

In line with this, the finding that histone ADP-ribosylation via chromatin-associated poly(ADP-ribose) polymerase1 (PARP-1) enables gene transcription through elevated promoter accessibility [262] corroborates the assumption that PAR modifications exert chromatin relaxation.

7.1.2 Epigenetic Cross-talk

Distinct histone and DNA modifications alter the structure of chromatin and hence transcription levels, significantly. Herby, the same mark at different residues of histones might result in distinct transcriptional regulations. For example, H3K4 methylation marks an increased transcription rate, while H3K27 is implicated in gene silencing.

The interplay between these modifications adds additional layers of complexity to epigenetics and the riddle of the so called histone code is far from being solved.

A synergistic effect can also be monitored in the interplay between the transcription activating marks H2B ubiquitination and H4K16 acetylation that together severely hamper the formation of higher-ordered chromatin [244].

In some cases however, distinct epigenetic marks with similar outcomes compete with one another. Poly(ADP-ribosyl)ation generally relaxes the structure of chromatin but ADP-ribosylated H4K16 prevents this residue from being acetylated, which also confers transcriptional activation [263].

It has also been observed, that specific histone marks preserve other modifications but alter their effects. For instance H3S10 and H3S28 phosphorylation are both detected in strongly condensed chromosomes in mitosis and H3S10 phosphorylation maintains the silencing mark H3K9 trimethylation during cell division, while di- and monomethylation are significantly reduced [264]. The HP1 binding of trimethylated H3K9 however, is hampered by the phosphorylation mark of the neighboring serine until dephosphorylation occurs [265].

It is also possible that distinct modifications that mark the formation of heterochromatin are mutually exclusive. Ubiquitination of H2A, which is implicated in transcriptional silencing, needs to be removed in order to enable H3S10 and H3S28 phosphorylation by the Aurora B kinase. Otherwise no proper chromosomal condensation and M-phase progression occurs [236]. This intricate network of interdependency is also referred to as the histone code, which is additionally extended by the incorporation of certain histone variants with altered chemical properties that also influence chromatin structure.

7.1.3 Histone variants

Besides via post-translational modifications to histones, the structure of chromatin can be altered by the incorporation of H3 and H2A histone variants, which show distinct differences in the primary amino acid sequence compared to canonical histones H3 and H2A.

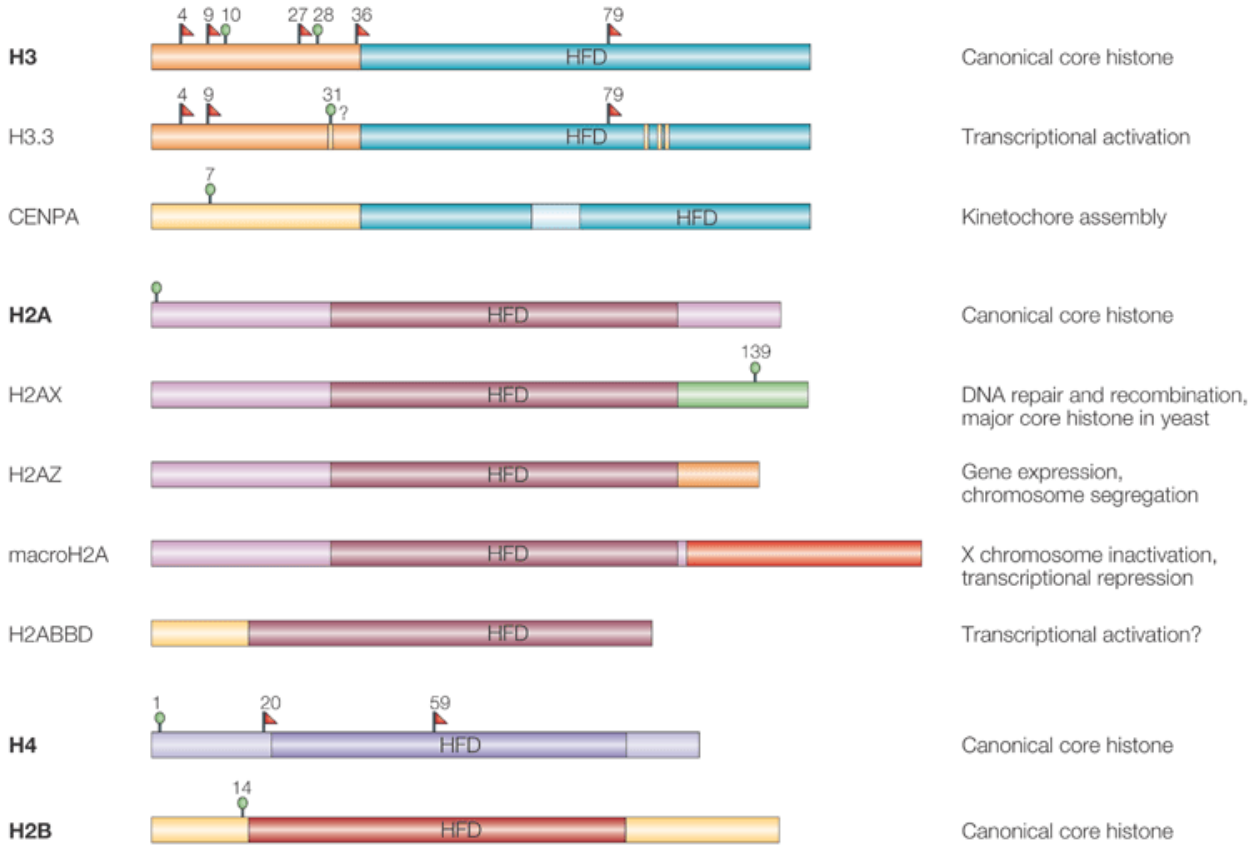

Figure 38: Overview of different histone variants
Adapted from Sarma *et al.* [266]

H2A.Z for example (Htz1 in yeast), has an approximate 60% sequence identity as compared to H2A [267], but Histone H3.3 differs from H3.1 at only four amino acid positions [268].

Interestingly, the two H2A like the H3 molecules in the nucleosome interact with one another, whereas invariant H2B and H4 do not.

The 'canonical' histones of animals are encoded in genes that cluster in repeat arrays and their expression is intertwined with DNA replication. In contrast, histone variants are usually encoded once in the genome and constitutively expressed [269]. While canonical histones principally function in genome

packaging as well as gene regulation, the portfolio of variants includes additional roles in DNA repair, meiotic recombination, chromosome segregation, transcription initiation and termination, sex chromosome condensation as well as sperm chromatin packaging [270].

Several eukaryotic histone variants like centromeric histone variant H3 (CenH3; chromosome segregation protein 4 (Cse4) in *Saccharomyces cerevisiae*), H3.3, H2A.Z and H2A.X are found in most eukaryotic organisms, suggesting that they were present in a common ancestor [271]. The universal and replication independent variants CenH3, H3.3, H2A.Z and H2A.X might have even preceded the replication dependent canonical histones [270], as for example H2A.X but not canonical H2A is present in fungi.

7.1.3.1 H3 variants

CenH3

CenH3s have only approximately 50–60% identity with canonical H3s in their HFD (histone fold domain) and the N-terminal tails are not conserved at all.

Also, a considerable sequence divergence is found among CenH3 paralogues from different species. Nonetheless, Cse4 from *S. cerevisiae* can substitute for human CENP-A [272], suggesting structural conservation.

The nucleosome core structure undergoes profound structural changes that are different compared to the octamer, if CenH3 is present. It seems that CenH3 promotes the formation of hemisomes containing only one histone copy of CenH3, H4, H2A and H2B [273]. These differences then induce right-handed DNA supercoils, whereas canonical nucleosomes are wrapped by DNA left-handedly [274].

These positively supercoiled CenH3 containing tetrameric structures seem to withstand mitotic chromatin condensation and herby they provide an assymetric surface recognized by kinetochore proteins that assemble at the centromer. This is corroborated by the findings that centromere specific histone variants are indispensable for kinetochore assembly [275].

H3.3

As stated above, H3.3 differs only marginally from H3 in humans. In yeast and some other unicellular organisms no such histone variant exists and the functional overlap of H3 and H3.3 has been shown in the ciliate *Tetrahymena thermophila*, where H3s are dispensable if H3.3s are overexpressed [276].

Moreover, H3.3 mutants in other organisms are also not always lethal, but result in infertility due to meiotic defects in chromosome condensation and segregation in *D. melanogaster* spermatocytes, arguing for a role of H3.3. in germline-specific chromatin remodeling [277].

In somatic cells, H3.3 is deposited into transcribed genes upon induction of transcription and seems to facilitate transcriptional elongation due to a more rapid turnover as compared to canonical H3 nucleosomes [278]. Hence, H3.3 contributes to chromatin accessibility. Moreover, H3.3 but not H3 plays a role in maintaining the epigenetically activated transcription state of a gene that depends on H3.3K4 methylation during several rounds of cell division, which implies a role in epigenetic memory [279].

7.1.3.2 H2A variants

The histone H2A family involves the greatest diversity of variants among core histones which can substitute canonical H2A [266, 271, 280]. The variety is putatively based on the more labile interface of the H2A–H2B dimer with the tetramer and DNA within the core particle [220].

H2A.Bbd

H2A Barr body-deficient (H2A.Bbd) is a mammalian specific, fast evolving variant that shares only 48% sequence identity with canonical H2A.

This variant is according to its name deficient on inactivated X-chromosomes and coincides with acetylated H4 but seems to alter nucleosome structures independent of acetylation [281, 282].

H2A.Bbd lacks the lysines involved in H2A PTMs and hence must be regulated differently. A shorter C-terminus and a truncated docking domain lead to H2A.Bbd nucleosomes that organize only 118 base pairs of DNA. Nonetheless, this DNA is a prerequisite for nucleosome formation as the interface between H2A.Bbd-H2B and the $(H3\text{-}H4)_2$ tetramer is destabilized [283]. H2A.Bbd also lacks the acidic patch due to mutations and nucleosomes containing this variant are incapable of forming the 30nm chromatin fiber [284, 285]. In line with the destabilizing properties, H2A.Bbd is exchanged more quickly than H2A in the nucleosome [286] and therefore makes chromatin more accessible and transcriptionally active.

Moreover, H2A.Bbd nucleosomes cannot be mobilized by either SWI/SNF (Switch Imitating / sucrose non fermenting) or ACF (ATP-utilising chromatin remodeling and assembly Factor) enzymes, which can

be attributed to the altered docking domain of the variant [287, 288]. A specific function for H2A.Bbd beyond the formation of accessible chromatin remains enigmatic.

macroH2A

In contrast to H2A.Bbd variants, the MacroH2As (mH2As) paralogues are highly conserved. In addition to the HFD, which has a 64% sequence identity to canonical H2A, macroH2As harbor a long C-terminal non-histone domain with a basic region and as well as a 'macrodomain'. So far, two genes that encode for MacroH2A are known in vertebrates and the corresponding proteins (mH2A1 and mH2A2) share 80% sequence identity. Both macroH2A variants act are enriched on the inactivated X-chromosome of female mammals, hinting towards a role in transcriptional silencing [289].

Indeed, hybrid nucleosomes with one macroH2a and one canonical H2A, which are preferentially formed, show increased salt stability and are resistant to H2A-H2B dimer exchange [290]. Additionally, mH2A interferes with histone acetylation and blocks SWI/SNF and ACF remodeling of nucleosomes thereby repressing gene transcription [291].

The exact mechanisms that underlie this silencing effect are still under debate. It has been shown that mH2A and H1 act mutually exclusive and show functional redundancy in silencing. Also, the macrodomain may become ADP-ribosylated [292], even though the non-histone domain (NHD) of mH2A interacts with PARP-1 and inhibits its ADP-ribosylation activity [293] ADP-ribosylation, however, seems to play a dual role in transcriptional regulation, as PARP-1 can also participate in the maintenance of gene silencing. Upon PARP-activation during DNA damage, mH2A is recruited to the sites of DNA damage and transiently compacts DNA around the lesions. This effect is only mediated by mH2A1.1 but not by its alternatively spliced variant mH2A1.2 even though both variants like mH2A2 are able to bind and inhibit PARP-1 activity *in vitro* [294]. The presence of three different mH2A variants with apparently distinct functions complicates research on macroH2A significantly.

The complex interplay between macroH2A and PARP-1 in transcriptional regulation also gives leeway for a fast response to external stimuli. MacroH2A variants silence inducible genes such as *Hsp70.1 and Hsp70.2* (heat shock protein 70) due to chromatin compaction, but also recruit PARP-1 to these sites. Upon heat-shock PARP-1 is released and poly ADP-ribosylates adjacent targets, leading to HSP70 expression [295].

The conditional silencing and activation of genes is a prerequisite in development and indeed mH2A1 and mH2A2 are enriched in promoters of developmental genes coinciding with H3K27 trimethylation ,

which is a repression mark mediated by the Polycomb repressive complex 2. The role in directing developmental transcription is further corroborated by developmental defects of mH2A2 deficient zebrafish [296].

H2A.X

H2A.X is very similar to canonical H2A in the histone fold domain (HFD) except for the C-terminal motif Ser-Gln-(Glu/Asp)-Φ, in which Φ represents a hydrophobic residue [271]. It is a relatively abundant variant as it constitutes up to 25% of mammalian H2A and in contrast to H2A.Bbd and macroH2A it can be found in almost all eukaryotic species.

Due to its similarity to canonical H2A, H2A.X putatively gets incorporated into chromatin after replication and therefore is evenly distributed throughout the genome. Its most prominent role is the function in DNA repair, where the serine of the C- terminal motif becomes phosphorylated to yield γ-H2A.X at the site of DNA double-strand breaks [297]. The kinases involved in this process are phosphoinositide 3-kinase-like kinases, ataxia telangiectasia mutated (ATM), ataxia telangiectasia and RAD3-related (ATR) and DNA-dependent protein kinase (DNA-PK) [298, 299].

Upon phosphorylation γ-H2A.X triggers the additional deposition of H2A.X variants to the site of DNA damage, which subsequently become phosphorylated in order to spread a phosphorylation mark that stretches approximately 40 kbp around the lesion in yeast [300] and up to several mega base pairs in humans [301].

Interestingly, γ-H2A.X does not seem to be essential for the recruitment for important DNA repair factors, including Nbs1 (Nijmegen breakage syndrome 1), 53BP1 (p53 binding protein) and Brca1 (breast cancer 1), but the phosphorylated histone variant retains these proteins at the site of damage and therefore enriches the repair machinery at double strand breaks [302].

Moreover, γH2A.X plays undefined roles distinct from double strand break repair. Putatively, γH2A.X might poise specific regions for chromatin remodeling, which include the Barr body Xi [303].

Despite its important functions, especially in the repair of DNA lesions, H2A.X is not essential as *C. elegans* has no gene for H2A.X and mice are viable without the variant. However, mice lacking H2AX show strong phenotypes including radiation sensitivity, growth retardation, immune deficiency and infertility [304]. *Drosophila melanogaster* has a specific Histone variant H2Av that combines H2A.X and another important and universal variant H2A.Z [280].

H2A.Z

H2A.Z differs from H2A and H2A.X in the C-terminal 'docking domain' that contacts H3 [271]. The sequence identity to H2A is approximately 60% but 90% between H2A.Z paralogues. This omnipresent eukaryotic histone variant is essential in many species [305].

Homotypic nucleosomes contain two H2A.Z histones and seem to be more stable than hybrid nucleosomes harboring one H2A.Z, which in turn show slightly more salt stability than canonical nucleosomes, if H2A.Z is acetylated. Unmodified homotypic and hybrid nucleosomes on the other hand appear to be equally more salt-stable than H2A only nucleosomes [306], even though the structure of the H2A.Z nucleosome suggests a subtle destabilization in the H2A.Z/H3 interaction due to loss of three hydrogen bonds [305]. In fact, divergent experimental data in the literature report destabilizing properties [307] of H2A.Z or support the finding of more stable H2A.Z nucleosome [308].

H2A.Z/H2B dimers provide an extension of the acidic patch on the nucleosomal surface, which potentially could interact with the H4 N-terminal tail of a neighboring nucleosome. This might aid in chromatin compaction and in line with this structural feature, it has been shown that H2A.Z colocalizes with Hp1 (heterochromatin protein 1) in mammals [309] and both protein cooperate in heterochromatin formation [310].

In yeast, Htz1 is enriched at the boundaries between hetero- and euchromatin and antagonizes Sir dependent silencing and thus heterochromatin formation, which seems to be in stark contrast to mammalian H2A.Z [311].

In the same line of evidence, yeast H2A.Z (Htz1) is mobilized more easily from purified chromatin *in vitro*, which suggests that H2A.Z might facilitate transcriptional induction of repressed genes [312].

More recent work suggests, that mammalian H2A.Z is associated with euchromatin as well and that monoubiqitination is required for H2A.Z to be a specific marker for heterochromatin as for example on the inactivated X-chromosome [313]. More specifically, H2A.Z seems to be randomly and actively placed into the genome and active transcription first mobilizes H2A.Z nucleosomes and then hampers the reincorporation of H2A.Z, thus enriching this variant in heterochromatic regions [314].

The apparent contradictory roles of H2A.Z has apparently contradictory roles in transcription, nucleosome stability and turnover as well as DNA repair [305, 315] could at least be in part explained by PTMs or additional (splicing) variants of H2A.Z [316]. Moreover, nucleosomes, especially H2A.Z containing ones are inextricably linked to chromatin remodeling [317].

7.2 List of the inter-protein cross-links in subcomplex I

7.2.1 Cross-links sorted according to the ID score

Lysine protein 1		Lysine protein 2		Id score
Arp8	210	HSA (Ino80 462-685)	62	37,64
Arp8	144	HSA (Ino80 462-685)	44	36,95
Arp8	211	HSA (Ino80 462-685)	65	36,57
Arp8	172	HSA (Ino80 462-685)	44	35,94
HSA (Ino80 462-685)	17	ARP4	323	35,2
Arp8	132	HSA (Ino80 462-685)	44	35,17
Arp8	165	HSA (Ino80 462-685)	44	34,12
Arp8	211	HSA (Ino80 462-685)	62	33,84
HSA (Ino80 462-685)	44	Arp8	176	33,13
Arp8	158	HSA (Ino80 462-685)	44	32,03
Arp8	149	HSA (Ino80 462-685)	44	31,63
Arp8	688	actin	328	31,59
Arp8	284	HSA (Ino80 462-685)	84	31,38
Arp8	165	HSA (Ino80 462-685)	26	30,37
Arp8	158	HSA (Ino80 462-685)	44	30,28
Arp8	165	ARP4	436	29,81
Arp8	150	HSA (Ino80 462-685)	65	29,78
Arp8	158	HSA (Ino80 462-685)	22	29,57
Arp8	150	HSA (Ino80 462-685)	44	29,36
Arp8	211	HSA (Ino80 462-685)	62	29,25
Arp8	284	HSA (Ino80 462-685)	95	29,12
Arp8	284	HSA (Ino80 462-685)	84	28,76
Arp8	688	actin	328	28,68
Arp8	775	HSA (Ino80 462-685)	44	28,21
Arp8	132	HSA (Ino80 462-685)	65	28,2
Arp8	136	HSA (Ino80 462-685)	44	27,72
Arp8	144	HSA (Ino80 462-685)	44	27,38
Arp8	158	HSA (Ino80 462-685)	65	27,11
Arp8	158	HSA (Ino80 462-685)	44	26,84
Arp8	158	HSA (Ino80 462-685)	26	26,52
Arp8	172	HSA (Ino80 462-685)	44	26,37
Arp8	202	HSA (Ino80 462-685)	44	24,37
Arp4	267	Arp8	132	24,33
Arp8	787	HSA (Ino80 462-685)	62	24,15
Arp8	139	HSA (Ino80 462-685)	44	23,11
Arp8	787	HSA (Ino80 462-685)	44	21,99
HSA (Ino80 462-685)	114	Arp4	213	20,15
Arp8	210	HSA (Ino80 462-685)	44	19,31
Arp4	259	HSA (Ino80 462-685)	111	18,7
actin	326	Arp4	218	18,6

7.2.1 Cross-links lysines sorted according to their locations within the proteins

Lysine N-terminus Arp8		Lysine HSA domain		Id score
Arp8	132	HSA (Ino80 462-685)	44	35,17
Arp8	132	HSA (Ino80 462-685)	65	28,2
Arp8	136	HSA (Ino80 462-685)	44	27,72
Arp8	139	HSA (Ino80 462-685)	44	23,11
Arp8	144	HSA (Ino80 462-685)	44	36,95
Arp8	149	HSA (Ino80 462-685)	44	31,63
Arp8	150	HSA (Ino80 462-685)	65	29,78
Arp8	150	HSA (Ino80 462-685)	44	29,36
Arp8	158	HSA (Ino80 462-685)	44	32,03
Arp8	158	HSA (Ino80 462-685)	22	29,57
Arp8	158	HSA (Ino80 462-685)	65	27,11
Arp8	158	HSA (Ino80 462-685)	44	26,84
Arp8	158	HSA (Ino80 462-685)	26	26,52
Arp8	165	HSA (Ino80 462-685)	44	34,12
Arp8	165	HSA (Ino80 462-685)	26	30,37
Arp8	172	HSA (Ino80 462-685)	44	35,94
Arp8	202	HSA (Ino80 462-685)	44	24,37
Arp8	210	HSA (Ino80 462-685)	62	37,64
Arp8	210	HSA (Ino80 462-685)	44	19,31
Arp8	211	HSA (Ino80 462-685)	65	36,57
Arp8	211	HSA (Ino80 462-685)	62	33,84
Lysines subdomain 1 of Arp8		Lysines HSA domain		
Arp8	284	HSA (Ino80 462-685)	95	29,12
Arp8	284	HSA (Ino80 462-685)	84	28,76
Lysines subdomain 3 of Arp 8		Lysines HSA domain		
Arp8	775	HSA (Ino80 462-685)	44	28,21
Arp8	787	HSA (Ino80 462-685)	62	24,15
Arp8	787	HSA (Ino80 462-685)	44	21,99
Lysine Arp8 N-terminus		Lysine subdomain 4 Arp4		
Arp8	132	Arp4	267	24,33
Lysine Arp8 N-terminus		Lysine subdomain 3 Arp4		
Arp8	165	Arp4	436	29,81

Arp8 insertion IV		actin subdomain 3		Id score
Arp8	688	actin	328	28,68

subdomain 4 of Arp4		HSA domain		
Arp4	259	HSA (Ino80 462-685)	111	18,7

Arp4 insertion I pointed end				
Arp4	213	HSA (Ino80 462-685)	114	20,15

Arp4 insertion II barbed end				
Arp4	323	HSA (Ino80 462-685)	17	35,2

Arp4 insertion I		actin subdomain 3		
Arp4	218	actin	326	18,6

7.3 Sequence alignment of *S. cerevisiae* and *H. sapiens* Arp8

```
ScArp8 MSQEEAESSIIYEEPIDIPLEDDDDEDELEEENSVPLSSQADQENAENESDDSVDNVVGS 60
HsArp8 ------------------------------------------------------------

ScArp8 ETPRSVTGLSVDPRDVADEEDEDEEGEDEDEDEDDNDVDNEDENDNDNANENENELGSSR 120
HsArp8 -------------------MTQAEKGDTE--------------NGKEKGGEKEKEQRGVK 27
                           : *:*: *              *.:::..*:*:*  . :

ScArp8 DKRAPPAVQTSKRYKKYPKLDPAKAPPGKKVPLHLLEKRRLGRIKAAEEFAKTLKKIGIE 180
HsArp8 RPIVPALVPES---------------------------------------------- 38
          .*. *  *

ScArp8 KVETTTLPATGLFQPLMLINQKNYSSDYLKKDDQIFALRDRKFLRNNNTSQISSTNTPDV 240
HsArp8 ------------------------------------------------------------

ScArp8 IDLKSLPHSEASAAPLNDEIDLNDPTATIVIHPGSNSIKIGFPKDDHPVVVPNCVAVPKK 300
HsArp8 ---------------LQEQIQSN---FIIVIHPGSTTLRIGRATDTLPASIPHVIARRHK 80
                     *:::*: *     *******.:::** ..*  *. :*: :*  :*

ScArp8 WLD--LENSEHVENVCLQREQSEE--FNNIKSEMEKNFRERMRYYKRKVPGNAHEQVVSF 356
HsArp8 QQGQPLYKDSWLLREGLNKPESNEQRQNGLKMVDQAIWSKKMSNGTRRIP-VSPEQARSY 139
         .  * :.. : .  *:: :*:*   *.:*   :  : ::*   .*::*  : **. *:

ScArp8 NENSKPEIISEKNDPSPIEWIFDDSKLYYGSDALRCVDEKFVIRKPFRGGSFNVKSPYYK 416
HsArp8 NKQMRPAILDHCSGNKWTNTSHHPEYLVGEEALYVNPLDCYNIHWPIRRGQLNIHPGPGG 199
       *:: :* *:.. .. .  :  .. . *   .       : : *: *:* *.:*::.

ScArp8 SLAELISDVTKLLEHALNSETLNVKPTKFNQYKVVLVIPDIFKKSHVETFIRVLLTELQF 476
HsArp8 SLTAVLADIEVIWSHAIQ-KYLEIPLKDLKYYRCILLIPDIYNKQHVKELVNMILMKMGF 258
       **: :::*:  : .**:: : *::  ..:: *: :*:****::*.**: ::.::* :: *

ScArp8 QAVAIIQESLATCYGAGISTSTCVVNIGAAETRIACVDEGTVLEHSAITLDYGGDDITRL 536
HsArp8 SGIVVHQESVCATYGSGLSS-TCIVDVGDQKTSVCCVEDGVSHRNTRLCLAYGGSDVSRC 317
       ..:.: ***:.: **:*:*: **:*::*  :* :.**::*.  .:: : * ***.*::*

ScArp8 FALFLLQSDFPLQDWKIDSKHGWLLAERLKKNFTTFQDADVAVQLYNFMNRSPNQPTEKY 596
HsArp8 FYWLMQRAGFPYRECQLTNKMDCLLLQHLKETFCHLDQDISGLQDHEFQIRHPDSPALLY 377
       *  :: ::.** :: :: .* . ** ::**:.*  :::   .:* ::*  * *:.*:  *

ScArp8 EFKLFDEVMLAPLALFFPQIFKLIRTSSHKNSSLEFQLPESRDLFTNELNDWNSLSQFES 656
HsArp8 QFRLGDEKLQAPMALFYPATFGIVG---QKMTTLQHRSQGD----PEDPHDEHYLLATQS 430
       :*:* ** : **:***:*  * ::    :* ::*:.:   .    .:: :* : *   :*

ScArp8 KEGNLYCDLNDDLKILNRILDAHNIIDQLQDKPENYGNTLKENFAPLEKAIVQSIANASI 716
HsArp8 KQEQSAKATAD---------------RKSASKPIGFEGDLRGQSSDLPERLHSQEVDLGS 475
       *: :      *               :  .** .: . *: : : * : : .. .: .

ScArp8 TADVTRMNSFYSNILIVGGSSKIPALDFILTDRINIWRPSLLSSASFPQFYKKLTKEIKD 776
HsArp8 AQGDGLMAGNDSEEALTALMSRKTAISLFEGKALGLDKAILHS----IDCCSSDDTKKKM 531
       : .   * .  *:  :..  *: .*:.::  . :.: :. * *     :  ..  .: *
```

```
ScArp8 LEGHYVNAPDKTEDENKQILQAQIKEKIVEELEEQHQNIEHQNGNEHIFPVSIIPPPRDM 836
HsArp8 YSSILVVGGGLMFHKAQEFLQHRILNKMPPSFRRIIENVD------------VITRPKDM 579
        ..  * . .   .: :::** :* :*:  .:..  :*::            :*. *:**

ScArp8 NPALIIWKGASVLAQIKLVEELFITNSDWDVHGSRILQYKCIFTY 881
HsArp8 DPRLIAWKGGAVLACLDTTQELWIYQREWQRFGVRMLRERAAFVW 624
       :* ** ***.:*** :. .:**:* : :*: .* *:*: :. *.:
```

8. Acknowledgements

I would like to express my gratitude to everybody who has contributed to the work in this thesis. The first one to name is my supervisor Prof. Karl-Peter Hopfner for providing much appreciated support and scientific input. Furthermore, he is mainly responsible for a generally very positive and optimistic attitude in his research group. In my opinion, this is essential for the work on particularly challenging projects such as research on chromatin remodeling.

All group members of the whole Hopfner lab contributed to a friendly and enjoyable atmosphere and I would like to thank everyone for this. Here, I would like to especially point out all researchers dealing with INO80 during the time of my PhD: Kristina Lakomek, Sebastian Fenn, Gregor Witte, Florian Seifert, Alessandro Tosi and Brigitte Keßler. Thank you very much for help, advice and discussions on our work. I believe that we together were able to push the project to a higher level and our work has acquired quite some recognition in the international chromatin community, despite starting from scratch just a few years ago.

I would also like to thank the many collaborators I worked with during this Graduate Thesis. Dennis Breitsprecher and Jan Faix have helped a great deal in tackling the question on how nuclear Arps are involved in actin dynamics. Without Duane Winkler and Karolin Luger the quantitative analysis of Arp-histone binding would not have been possible. Alessandro Tosi, Franz Herzog and Ruedi Abersold kindly provided me with the X-link / mass spec data.

Even though no results in this respect have been mentioned in the thesis, I would like to acknowledge the collaboration with Kei Miyamoto and John Gurdon on Arps and reprogramming. All collaborators really contributed a great deal to our understanding of the extremely versatile properties of Actin-related proteins and I hope that these collaborations will go on, because I feel that there are yet many surprises to be unveiled.

I would also like to thank my parents, siblings, parents-in-law and siblings-in-law for all encouragement during the past time and you certainly also helped me to finish the thesis. I would also like to thank my grandparents for their generosity during the last few years.

During this work I started my own family with my fantastic wife, Heike and we are very grateful for our two sons Noah Christopher and Jonas Benedikt. Even though I have to admit that the boys were not quite contributing to the successful completion of the work, I would like to thank them for being the way they are and for making me proud as a father.

I was receiving invaluable backing by my great wife Heike, who despite her own doctoral work devoted so much time to raise our children and to support me as good as she could. Thank you so much!
My apologies to other contributors whom I didn't mentioned by name. My gratitude is with you as well.